Dynamic phase transitions in biased ensembles of particle systems with repulsive interactions

Thompson, Ian

Award date:
2015

Awarding institution:
University of Bath

Dynamic phase transitions in biased ensembles of particle systems with repulsive interactions

Ian Richard Thompson

A thesis submitted for the degree of Doctor of Philosophy

University of Bath
Department of Physics

July 2015

☕☕📚📖💻🎶😓💻🔨🍺☕📖🎓

Thanks to 👩 and 🐵 for the 😄 and ❤️, I know there's been 😤, 😱 and 😓 along the way. Thanks for the ⬛ sense of 😂🐵, I'll say it now because you won't be here by 🎄. Thanks 👩 for everything else.

👦💍👩 &🐴👍 on the 🏚, the 🐝 and the 👨‍👩‍👧.

👸 enjoy Amsterdam 😋. Bonne chance et félicitations 🎓 😊.

Thanks to #lads 😎.

Thank you to 🔢4.5 and 👦🕶.

Saz you're an 😇, I'll always have a 🍷 for you 😉.

Looks like I'm staying in 🛁 for a little while longer 😊. Come on Inter ⚽.

Now I need a 🍺 or 🍻 before this all goes 📉💩.

One paper was published during the course of this PhD with Dr. Robert Jack and Dr. Peter Sollich, "Hyperuniformity and Phase Separation in Biased Ensembles of Trajectories for Diffusive Systems", PRL 114, 060601 (2015). It contained results for the constant volume one dimensional system's dynamic phase transition and structural measurements of the different dynamic phases.

Two other papers will be submitted and published resulting from the work in this thesis. One paper for the dynamic phase transition in the one dimensional system and a second paper for the dynamic phase transition and jamming properties of the three dimensional system.

Contents

List of Figures

Abstract

We study dynamic phase transitions in the constant-volume and constant-pressure ensembles of two different systems: a one-dimensional system of diffusive hard particles and a three-dimensional glass-former of nearly-hard repulsive particles. The dynamic transitions are observed using ensembles of trajectories biased with respect to their dynamic activity, biasing to greater or lower activities than equilibrium allows us to sample different dynamic phases. We perform finite-size scaling of the transitions with respect to system size and observation time, and compare them to first-order phase transitions. The two ensembles are not equivalent in the one-dimensional model. We compare our results to analytic predictions for diffusive systems in both the active and inactive phases, there are structural signatures for both dynamic regimes. The active phases show hyperuniform ordering and the inactive regimes show jamming behaviour, local jamming in the constant-volume ensemble is achieved through phase separation. In the three-dimensional system we observe a dynamic transition to a glassy inactive phase, there is no obvious structural change and the structural relaxation time increases significantly. We take configurations from the active and inactive phases and subject them to a jamming protocol in order to compare the final density of the jammed packings. Previous work shows that the inactive phase of glass-forming systems have a different distribution of vibrational modes and a higher compressibility, this suggests that the jamming behaviour should differ between the two phases. We show that jammed packings generated from inactive configurations are denser than those generated from active configurations.

Chapter 1

Introduction

States with long structural relaxation times in the absence of static ordering are a hallmark of glassy behaviour[1]. The nature of the transition between a supercooled fluid and a glass is an open, and controversial, question in physics. Although this hasn't slowed the adoption and development of glasses in technology, (smart phone screens alone represent small fortunes in material science research and development,) it is still an outstanding question which may have significant practical implications. There is no single, accepted theory of the glass transition and no single theory supports all of the experimentally observed phenomena[2]. The underlying observation of dynamical arrest without structural order defies an obvious description or quantification, should one consider the dynamics that aren't happening or the structure that hasn't changed?

The theoretical picture is made more complicated by possible links to jamming behaviour and wider questions around amorphous-order and stability[3, 4]. The glass transition has made an appearance in many areas of condensed matter physics; without a comprehensive theory for the transition it is not known where the boundaries are or what the relationship is between glassy physics and other phenomena. Jamming describes the arrest of an entire system due to geometric constraints without structural ordering, it is a transition driven by an increase in density. Jamming is the closest phenomena to the glass transition, particle motion ceases and there is no clear thermodynamic transition. There have been a number of proposals about the

relationship between jamming and the glass transition, the common principle being that jamming could be the zero temperature manifestation of the glass transition[5, 6]. The two transitions can be identified by two diverging measurements, the structural relaxation time diverges at the glass transition and pressure diverges at the jamming point[7].

Upon cooling, simple fluids at equilibrium crystallise, adopting an ordered structure, becoming rigid and qualitatively changing their response to stress, shear and vibration. The first order phase transition occurs at the melting temperature T_m and the translational invariance of particle positions is broken in favour of long range periodicity. If cooled quickly enough the liquid can be supercooled below T_m and still behave as the equilibrium fluid with properties that can be extrapolated from the equilibrium liquid. The supercooled liquid is not the equilibrium phase of the system, the crystal has lower total energy, and the liquid is metastable.

Some materials do not crystallise, instead they freeze in their liquid structure: the particles no longer move freely and vibrate about their positions. The system has entered the glass phase: microscopically a fluid with extremely long relaxation times but with the macroscopic properties of a solid. The structural relaxation time of a glass is much longer than the supercooled fluid, and can exhibit a number of different scaling relationships with temperature, "strong" glasses scale with Arrhenius behaviour while the relaxation of "fragile" glasses is super-Arrhenius[8]. There is no phase transition in any structural observable such as the density, or even in more complex structural measurements regarding periodicity[2]. The entropy of the glass is equal to that of the supercooled liquid, there is no latent heat released in the transition.

Having the entropy of a liquid means that there are exponentially many degenerate configurations where particles vibrate about stable positions. In this simple context the glass transition could be a kinetic effect of rapid cooling, the particles are trapped in energy basins and thermal fluctuations are weak enough that relaxation times become extremely long.

Static theories of the glass transition attempt to describe glassy phenomenology as the consequence of a system exploring a complex configurational energy landscape. In these theories the structure of energy minima

and their distribution on a complex energy surface define the glass phase, the slow relaxation and mechanical properties of glasses can be rationalised by considering configurations exploring this surface[9]. However an energy landscape description cannot predict the behaviour of dynamics and assumes that dynamic behaviour would be homogeneous in space. Configurational theories of the glass transition were significantly weakened by the experimental observation of dynamic heterogeneity[10, 4] in supercooled glass-formers. Particles in fast regions of the system moved orders of magnitude faster than those in slow regions.

This discovery prompted a change to considering glassy behaviour in real-space and the idea that dynamics are the cause of the glass transition, not merely a symptom. In 2002 Garrahan & Chandler described a model of glassy behaviour that was entirely dominated by dynamic constraints, the configuration space of the model is trivial and structural relaxation times are dominated by interactions in trajectory space[11]. The nature of the constraints determined the scaling of the relaxation time with respect to temperature. In 2005 Merolle et al.[12] observed non-Gaussian tails in the distribution of a dynamic observable in glass-forming systems, caused by an order-disorder transition in trajectory space. This dynamic transition was identified as a kind of glass transition. They suggested that the glass transition could be an entirely dynamic phenomena, a phase transition in an observable that is extensive in time as well as space, while there is no transition in a static observable.

By using a space-time order parameter that quantifies structural relaxation, it is possible to show a phase transition between equilibrium and metastable states of an atomistic glass-forming system[13]. The transition is described as being between dynamically active and inactive states and is driven by a finite dynamic bias, the field s. The inactive phase exhibits many properties of a glass and the transition has been suggested as a general model for the glass transition. The dynamically inactive phase exhibits long relaxation times and no obvious structural change compared to the equilibrium system. The phase transition has been well studied in the Kob-Andersen (KA) mixture[14], a glass-forming system with Lennard-Jones interactions, and is robust to several selections of dynamic order parameter and simulation

methodology[13, 15, 16, 17, 18].

All of the previous work on dynamic phase transitions in atomistic systems have focussed on a soft system with Lennard-Jones pair-wise interactions. To extend dynamic phase transitions in atomistic models we will study a glass-forming system with short-range, purely repulsive harmonic interactions in chapters 5 and 6. The nature of the particle interactions means that the low temperature limit is equivalent to a hard-sphere system. Work on harmonic sphere mixtures has shown that the glass transition can be driven by an increase in packing fraction at constant-temperature. The contact-only nature of the interaction means that the potential energy of the system is dominated by the local density of the system and jamming behaviour is easily quantifiable in terms of the low-temperature limit.

Berthier & Witten showed finite-temperature glassy behaviour in a system of harmonic particles and were able to make a strong comparison to the hard sphere case as a low temperature limit of the system[19]. This included rapid compression of hard spheres and the finite-temperature system with a view to measuring the divergence of the structural relaxation time and pressure. They showed that the relaxation time appears to diverge at a lower density than the pressure and so the glass transition density is not the same as the jamming density, at least using their compression protocol. We will study the system in a context that allows the density to fluctuate, in order to investigate whether the inactive phase spontaneously exhibits a higher density.

As the glass and jamming transitions are very sensitive to changes in density[7] we will explicitly consider two ensembles in chapter 5: the isothermal, constant-number, constant-volume (constant-NVT) ensemble and the isothermal, isobaric, constant-number (constant-NPT ensemble). The constant-volume ensemble is at fixed global density and can support fluctuations in the local density. Constant-pressure ensemble systems can vary their volume and hence the global density. At equilibrium they can be considered as subsystems of a larger constant-volume system, exchanging local volume with the larger system.

In equilibrium systems there is equivalence between different ensembles, static phase transitions occur at the same point in parameter space regard-

less of the ensemble. It has been observed that non-equilibrium systems can break ensemble equivalence when different processes occur on widely separated timescales[20]. The inequivalence was only observed when the timescale associated with the grand-canonical process was well separated from the diffusive timescale. The issue of multiple relaxation processes and their associated timescales, and the effect on ensemble equivalence, in dynamic transitions has not been addressed.

Before considering the three-dimensional atomistic system we will study dynamic phase transitions and ensemble equivalence in a one-dimensional model in chapter 4. To gain an understanding of dynamic behaviour in the constant-pressure ensemble we will study a simple one-dimensional model of diffusing particles. The particles are of finite length and cannot interpenetrate or move past one another, the equilibrium configuration space of the system can be described by density. The dynamics of the individual particles are described by a Langevin equation, the constant-pressure ensemble introduces a second coupled Langevin equation to describe the motion of the system volume. This system can be coarse-grained on long length scales and described hydrodynamically, dynamic studies have show these systems undergo a dynamic phase transition characterised by phase separation[21]. We will use the one-dimensional model to investigate the issue of ensemble equivalence and the role of separate timescales in the system.

In chapter 6 we will characterise the inactive phase of the atomistic ensembles. In three-dimensional glass-forming systems there is no equivalent to phase separation, the inactive phase corresponds to a glass, despite a lack of obvious structural change[1] a more subtle change has been identified. Jack et al. measured the relaxation of states drawn from the inactive phase of the s-ensemble back to active, equilibrium behaviour. They found that there was no short timescale relaxation of particle vibrations[22], only a slow relaxation process consistent with structural relaxation between different energy basins. This finding was interpreted as the inactive phase occupying a region of configuration space, and inherent structure[23], that was typical of a lower temperature but with equilibrium-like behaviour of particle vibrations.

[1] Here we refer to pair correlation measurements.

Measuring the energy contributions due to thermal vibrations and the inherent structural energy showed that the active and inactive phases had equal vibrational energy but very different structural energies. A more thorough investigation of the vibrational density of states found that in the inactive state there was a suppression of both the highest and lowest frequency modes, that is the stiffest modes of the system became softer, while the softest modes became stiffer[16]. Hence the inactive phase was more stable, long-range structural relaxation along the soft modes was suppressed, short-range rapid vibration leading to local density fluctuations and instabilities was suppressed, the system was more stable on all length scales.

The suppression of the stiffest modes corresponds to a shallower energy landscape with respect to short-range motion, particles have more freedom to make small displacements and explore their local environment. Short-range translation freedom means that small compressions can occur and any particle overlaps can be resolved easily, the number of particles involved in a relaxation is small. This means the system should be more compressible, configurations can move along the stiff directions more easily before reaching a configuration that cannot be compressed further. We will investigate the relationship between the active-inactive dynamic transition, the change in vibrational modes and jamming behaviour by submitting active and inactive configurations to a jamming protocol.

Chapter 2

Theoretical concepts

We are interested in the dynamic behaviour of glasses, systems that exhibit long structural relaxation times and the role of dynamic arrest in creating metastable states of the system.

Glasses are mechanically stable, like a crystal the static shear modulus G_0 is non-zero: they can sustain an external shear without flowing. Ergodicity is broken for systems with $G_0 \neq 0$, symmetry breaking in the crystal means that ergodicity, too, is broken. However in the glass there is no symmetry breaking transition, the glass retains the symmetry of the amorphous liquid, it is a liquid that cannot flow. The rigidity of the system is caused by a large energy barrier preventing rearrangement of particles. In strong glasses such as SiO_2 this is understood as a microscopic effect, the interaction between particles is very strong and the viscosity follows an Arrhenius law $\eta \sim \mathrm{e}^{\beta \Delta E}$, where $\beta = (k_\mathrm{B} T)^{-1}$ is the inverse temperature and ΔE is the energy barrier for particle motion. However in fragile glasses the microscopic interactions are much weaker and experiments show that the energy barrier grows in a super-Arrhenius manner as temperature is decreased. This suggests that rearrangement involves many particles moving collectively, requiring a short-range amorphous order that increases in strength and/or range upon cooling.

It is difficult to define the glass transition temperature, T_G for a liquid in the absence of a sharp transition. Practically it is defined as the temperature where an observable either exceeds a fixed limit, e.g. the viscosity, or when there is a kink or step in a property, e.g. the heat capacity, as the liquid is

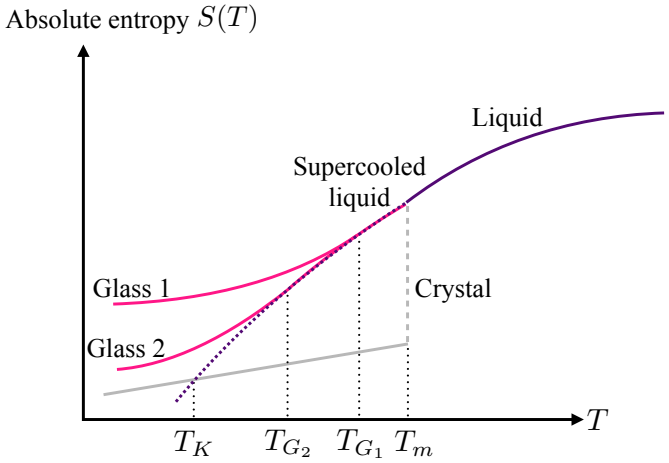

Figure 2.1: A schematic phase diagram for a glass-forming liquid, the glass transition temperature can vary depending upon the rate of cooling. Latent heat is released in the transition to a crystal, but in supercooling and the glass transition involves no such discontinuity. Instead the properties of the supercooled fluid can be extrapolated from the equilibrium liquid along the dotted purple line.

cooled at a constant rate. Frequently the caloric glass transition temperature is used, the heat capacity of the system is measured as a function of temperature and there is a kink at T_G. The transition temperature depends upon the rate of cooling, with slower cooling reducing T_G. Furthermore two samples of a glass prepared using different cooling rates have different properties even at the same temperature $T < T_G$. Due to the long timescales involved, experimental measurements and simulations often concern themselves with the supercooled liquid phase just above T_G.

If one imagines cooling further, and avoiding the glass transition, then the extrapolated entropy of the supercooled liquid would be equal to that of the crystal at the Kauzmann temperature T_K (see figure 2.1 or similar figures in e.g.[9]). Named after Walter Kauzmann this temperature raises a paradox where the supercooled liquid cannot exist below T_K and there must be a phase transition before reaching T_K. Kauzmann himself simply

postulated that all liquids must crystallise before T_K, however some cite this as evidence that there is a true thermodynamic transition to the glass phase, known as the ideal glass transition at $T_{IG} > T_K$. In that scenario the observed glass transition is controlled by an avoided critical point at T_{IG} and if cooled sufficiently there would be an observed thermodynamic phase transition with a static order parameter.

It is also known that approaching the glass transition the dynamics of particles are increasingly heterogeneous in space and intermittent in time[24]. Both fluids and glasses have disordered structures so all particles experience varying microscopic environments. However in the fluid relaxation is fast enough that bulk properties such as viscosity can be related to the diffusion rates of particles. The same is not true of glasses, the presence of dynamic heterogeneities[4] means that microscopic relaxation is a collective process and hence no relation between microscopic and bulk properties. It has also been observed that mobile particles cluster in space, the typical size and separation of these clusters are a means of quantifying the degree of dynamic heterogeneity in the system[24].

The length scales associated with dynamic phenomena grow approaching the glass transition, for example the decay length that describes the effect of local density fluctuations grows upon cooling[25]. Dynamic heterogeneity means that glassy behaviour cannot be thought of as a purely local phenomenon, concerned only with microscopic energy barriers and local free volume. Instead these growing length scales mean that there is a larger collective behaviour in the system, dictating the dynamics and thus the relaxation. A successful theory of the glass transition must explain the mechanical stability of configurations so very similar to the flowing liquid: the collective nature of relaxation in fragile glasses: the absence of change in any observable static length scale: and the non-local behaviour of dynamic heterogeneity.

Random first order transition (RFOT) theory describes a complex energy landscape where the large number of amorphous metastable configurations lead to long relaxation times[26]. As the temperature is reduced the number of energy minima in the landscape reduces upon cooling until it becomes non-exponential with respect to system size, this equates to the configura-

tional entropy of the system vanishing at T_{IG} and the system at entering the ideal glass phase at equilibrium. The temperature region of observed glassy behaviour is caused by the system breaking up into a mosaic of sub-systems, each with their own amorphous order. Sub-systems with a spatial extent less than a length scale ℓ^* behave like glasses and cannot relax, effectively being below T_{IG}. Those with a size greater than ℓ^* behave like the supercooled liquid. The length ℓ^* is set by thermodynamics alone and diverges as $T \to T_{IG}$.

Although there is evidence in favour of RFOT theory, it is not conclusive and there remain open problems and unexplained phenomena, for an overview of RFOT see [26].

Mode coupling theory (MCT) was developed in the 1970s to describe the behaviour of dense, simple fluids. It was successful in describing viscous fluids and the dynamic behaviour of simple fluids nearing T_m in terms of the density autocorrelation function. Bengtzelius, Götze and Sjölander showed that, with a few low temperature approximations, the time dependent solution to the mode coupling equations exhibited a discontinuous change below a critical temperature T_{MCT}[27]. The discontinuity is tied to a divergence in the structural relaxation time and so was suggested as a description of the glass transition. The extreme slowdown of dynamics approaching T_{MCT} is consistent with the increase of relaxation time in supercooled glass-formers. Although MCT has some similarities to the glass transition it does not accurately predict T_G, $T_{\mathrm{MCT}} > T_G$, nor dynamic heterogeneity. For more on MCT and the glass transition see[28].

In 1952 Sir Charles Frank suggested that the glass transition was caused by the formation of locally preferred structures that could not fill space[29]. The local structures would be stable and would not relax so the system as a whole would consist of multiple locally stable regions. Although local ordering has not been observed experimentally the concept of locally stable phenomena being frustrated in the larger system remains relevant. Sir Charles suggested the local structure would be icosahedral, work since then has examined a series of different preferred local structures that may vary from system to system. More recent work on local structure across the glass transition used a dynamic bias to promote the formation of local clusters[18],

this work is discussed further below.

The wealth of dynamic phenomena across the glass transition has motivated theories that address the dynamics directly, there is no structural transition and no related correlations emerge in configuration space. Instead one must consider a dynamic order parameter that quantifies the behaviour of the system through time as well as across space. In this dynamic space interactions and correlations emerge that can dominate the behaviour of the system[30].

Both glassy and jamming behaviour have been observed in ensembles of trajectories that are biased with respect to a time-integrated observable[31, 32, 21]. By considering an observable that is extensive in time as well as space it is possible to quantify the dynamic evolution of a system and distinguish between configurations that produce a lot of dynamic activity and configurations that evolve very slowly. Dynamic phase transitions describe the phase behaviour of these time-integrated observables[33]. Although the phase transition is only observable in a dynamic context there can be a structural difference between different dynamic phases.

2.1 The importance of dynamics

Considering the role of dynamics in defining glassy behaviour was first motivated by experimental observations of dynamic heterogeneity in glass-forming supercooled liquids. Fast regions of a system can move or rotate several orders of magnitude faster than slow regions. This heterogeneity is present in the dynamics only, structurally the regions are very similar. Although fast and slow regions cannot be identified by static structure the dynamic heterogeneity is reproducible from the same initial conditions[34]. Widmer-Cooper et al. coined the idea of "dynamic propensity" to describe the typical dynamics that propagate from a given local structure. The relationship between a static configuration and the dynamic propensity of the configuration mean that the relaxation time can be related to its structure.

Dynamic heterogeneities in glass-forming systems cannot be explained by homogeneous thermodynamic theories that only consider static configurations. In 2002 Garrahan & Chandler showed that dynamic heterogeneity

can be interpreted as a consequence of dynamic constraints in the system[11]. They studied two stochastic dynamic models that exhibited dynamic heterogeneity and have a trivial distribution of static configurations: the East model (see below) and the FA-model[35] with super-Arrhenius and Arrhenius relaxation times respectively. They used the concept of a trajectory as a history of the system evolving through time with an extent in space N, and a duration in time, the observation time t_{obs}. Within trajectories there are space-time domains where the system is slow-relaxing and dynamics are suppressed.

By considering an ensemble of trajectories they found non-trivial structure emerge over time and the existence of spatial interactions that acted in trajectory space only. The dynamic behaviour of the domains in space-time is equivalent to the static behaviour of dense non-interpenetrating mixtures in $d + 1$ dimensions. Over an ensemble the relation between temperature and relaxation time can be described in terms of interfaces between the fast and slow dynamic domains. In this manner Garrahan & Chandler suggested that dynamic heterogeneities in a system were a sign of internal kinetic constraints, and that the behaviour of these systems may be best studied in trajectory space.

Both of the models studied were conceived as examples of dynamic facilitation and are members of a class of models called kinetically constrained models (KCM). The East model[36] is a one-dimensional spin-$\frac{1}{2}$ Ising model with modified dynamics where a spin i can only flip if its left-hand neighbour $i+1$ is in the "spin-up" state. In this model particles are "active" or "frozen" depending upon the state of their neighbouring spin and dynamic activity is measured by counting the number of spin flips over time. Fast domains will exhibit more spin flips in a given time than slow domains. The dynamics of the system can be described in terms of the number of spin-up sites as a function of time, i.e. sites that facilitate motion and hence create activity. In this context inactive domains of the system are "empty", clusters of down-spins with no excitations allowing them to flip – the domain is defined by up-spins at each end and must relax from the left.

In 2005 Merolle et al.[12] measured the dynamic action, an observable that is extensive in time and space, in the FA and East models. They mea-

sured long exponential tails in the low-action probability distribution, indicative of a system approaching phase coexistence with an inactive system in trajectory space. Trajectories with an action that falls in the exponential tails have entropy that is non-extensive in time. On a timescale τ_{tails} the exponential tails become statistically negligible. The existence of the tails means that the system cannot equilibrate on timescales $t_{\text{obs}} < \tau_{\text{tails}}$. Hence the fact that glass-formers fall out of equilibrium on finite, albeit long, timescales agrees with the exponential distribution of low-action trajectories. They suggested that the glass transition is a disorder-order dynamic phase transition in trajectory space, there is a qualitative change in the distribution of trajectories between the two phases. All of the configurations within trajectories are drawn from equilibrium and the evolution from one configuration to another is governed by equilibrium processes, only the time-integrated properties of the trajectory change. The trajectories exhibited dynamic heterogeneity and "bubbles" of inactive behaviour formed with trajectories. In the models studied inactive regions consist of a spatial extent of the system that contains no excitations for a sustained length of time[30].

The idea that systems with trivial static behaviour can have non-trivial dynamics that lead to interactions and structure over time is the key concept of dynamic facilitation. The partition function of trajectories and the master equation of the East model can be expressed analytically, the simple structure and kinetic constraints mean that the dynamic behaviour can be explored mathematically[37]. With regard to glassy behaviour the sudden change in dynamics, and consistent structural properties, across the transition are a strong motivation to study the behaviour of glasses in trajectory space.

The dynamics of particle systems are more complex and cannot be explored analytically, instead trajectory space must be explored numerically. The glass phase is characterised by little particle movement and slow structural relaxation, defining a dynamic order parameter that measures particle movement that contributes to relaxation can distinguish a dynamic transition to the glass. The dynamic activity is a general term used to describe the amount of structural relaxation that occurs in a system, in discrete systems it simply counts the number of configuration changes. In particle systems the choice of definition for the activity is more nuanced and free to the inves-

tigator with the proviso that the time integral of the quantity is monotonic. To study the dynamic behaviour of a system we need to define a framework which describes the properties of trajectories and the fluctuations of the activity.

2.2 Thermodynamics of histories

We are interested in the fluctuations of dynamic observables in glassy systems. Classical thermodynamics is concerned with the statistical properties of extensive observables, the mean and fluctuations about the mean, in ensembles of configurations. The ensembles are classified by the constraints placed on the system, the microcanonical ensemble constrains the number of particles, the volume and the energy of the system and the canonical ensemble imposes a constant number of particles, volume and temperature of the system. The two ensembles are equivalent for an appropriate choice of the energy and temperature respectively. Temperature is the intensive field that controls the average value of the extensive energy, that is temperature is the conjugate field to energy.

We follow the explanation laid out in [38]. Thermodynamics describes the probability distribution of configurations of large systems through the counting factor:

$$\Omega(E, N) = \text{Number of configurations of size } N \text{ with energy } E \tag{2.1}$$

where we are considering an extensive observable, here the energy E.

As $N \to \infty$ we consider the energy density $e = \frac{E}{N}$ and we introduce the entropy density:

$$s(e) = \lim_{N\to\infty} \frac{1}{N} \ln \left[\Omega(eN, N)\right] \tag{2.2}$$

Moving from a microcanonical approach to a canonical one we define a partition function:

$$Z(T, N) = \sum_{E} \Omega(E, N) \mathrm{e}^{-\frac{E}{k_\mathrm{B}T}} \tag{2.3}$$

which describes the probability of different values of the energy at temperature T. (Note it is convenient here to use the inverse temperature β.) The

probability of a configuration $\mathcal{C}$ with given energy E occurring in an ensemble defined by $Z(\beta, N)$ is simply:

$$\boldsymbol{P}(\mathcal{C}, N) = \frac{\mathrm{e}^{-\beta E(\mathcal{C})}}{Z(\beta, N)} \tag{2.4}$$

where $\boldsymbol{P}$ denotes a probability distribution, this notation will be continued throughout.

The intensive free energy $f(\beta)$ of the ensemble is:

$$f(\beta) = \lim_{N\to\infty} \frac{-1}{\beta N} \ln\left[Z(\beta, N)\right] \tag{2.5}$$

Singularities in $f(\beta)$ indicate phase transitions between two or more phases with a discontinuity in an associated order parameter. For example there is a first-order discontinuity in the density at the gas-liquid phase transition at the boiling point T_b.

Static thermodynamics imposes constraints upon a system that apply at all times, equivalent to minimising the free energy with respect to those constraints. By applying constraints to time-integrated observables we can minimise the "dynamical free energy", in effect the power required to maintain the constraints for the duration of integration[39]. To minimise this power the system will enter states with long relaxation times, even in the presence of a large energy barrier to first establish the state. In one-dimension this means that there can exist phase transitions in space-time at finite temperature, despite a lack of static phase transitions.

Moving to dynamic observables let the observable A be extensive in time, e.g. the average of the mean squared displacements over a fixed time interval. From a system moving through time draw a set of histories of duration t, starting from some time t' measure A until time $t' + t$. We can define a dynamical counting factor:

$$\Omega_{\mathrm{dyn}}(A, t) = \text{Fraction of histories of duration } t \text{ with given value of } A \tag{2.6}$$

and by introducing a field conjugate to A we can define a dynamical partition function:

$$Z_A(s, t) = \sum_A \Omega_{\mathrm{dyn}}(A, t)\mathrm{e}^{-sA} \tag{2.7}$$

and the probability of observing a history of duration t, denoted by $\mathcal{C}(t)$, with a given value of A in the s-ensemble of histories is:

$$\boldsymbol{P}[\mathcal{C}(t), t] = \frac{\mathrm{e}^{-sA[\mathcal{C}(t)]}}{Z_A(s,t)} \tag{2.8}$$

This defines the s-ensemble and describes the statistical properties of fluctuating dynamic observables in histories of fixed duration. At long times we require that the system and the observable satisfy $\lim_{t\to\infty} \frac{1}{t} \ln [\Omega_{\mathrm{dyn}}(at, t)]$ is finite, where $a = \frac{A}{t}$, for the thermodynamic extension to dynamic observables to hold true.

There is an associated intensive 'dynamical free energy' in the ensemble of histories defined as:

$$\psi(s) = \lim_{t\to\infty} \frac{-1}{t} \ln [Z(s,t)] \tag{2.9}$$

Dynamic phase transitions occur at values of the field s when $\psi(s)$ exhibits a singularity[40].

If a static system has macroscopic constraints placed upon it one can realise the corresponding macrostate by minimising the free energy of the system subject to the constraints. This corresponds to minimising the amount of work required to apply the constraints microscopically, it is clear that this defines the macrostate. If a dynamic constraint is placed upon the system then we should minimise the dynamic free energy to find the macrostate of the constrained system. This corresponds to minimising the power required to maintain the constraints over time against thermal fluctuations[39].

For a given constraint, minimising the dissipated power is not equivalent to minimising the work of every configuration. Creating a state with a long relaxation time can mean less power is dissipated even if the work required to create the initial state is high[41]. Hence constraints on dynamic variables are a natural way to address metastable states and slow relaxation processes. Ensembles of particle systems which have been created using conditioned dynamics have been suggested as models for glassy behaviour: the dynamically inactive state is the same as the glassy state and exhibits slow relaxation back to the equilibrium behaviour of the unconstrained system[22].

To further illustrate the generality of thermodynamics applied to ensembles of histories we briefly describe another dynamical ensemble. Instead of

the observable A fluctuating in histories with fixed duration t, consider the time required for the measured observable to equal a given value of A. This fluctuating time observable has been described by Garrahan et al.[42] and dubbed the X-ensemble with a partition function:

$$Z(X, A) = \sum_t \Omega_{\mathrm{dyn}}(t, A)\mathrm{e}^{-Xt} \tag{2.10}$$

where X is the field conjugate to the duration. The general concept of fixing one constraint while allowing the conjugate variable to fluctuate under the constraint can be extended into dynamic systems.

2.2.1 The s-ensemble

Subject to the requirement on the long-time limit and monotonicity, the choice of dynamic observable is free to be suited to the investigation. The observable should contain information about the particular physical process one is interested in, for example the total number of particles that flow through a system connected to two reservoirs. We are interested in metastable configurations with long relaxation times and their relation to glassy behaviour, as such we define an observable that measures the extent of structural relaxation in time.

To quantify structural relaxation we measure the amount of movement on length scales that contribute to relaxation. We study particle systems with repulsive pairwise interactions evolving through time with stochastic dynamics. The extensive activity K of a trajectory is a sum of the total squared displacement of all particles measured over a coarse graining time Δt:

$$K\left[x(t)\right] = \sum_{j=1}^{M}\sum_{i}^{N} \left|\hat{\boldsymbol{r}}_i(t_j) - \hat{\boldsymbol{r}}_i(t_{j-1})\right|^2 \tag{2.11}$$

in accordance with [13], where $t_j = j\Delta t$ and $[x(t)]$ represents a trajectory: a single realisation of a given system evolving in time.

$\hat{\boldsymbol{r}}_i$ is the position of particle i relative to the centre of mass $\overline{\boldsymbol{r}}$:

$$\hat{\boldsymbol{r}}_i(t) = \boldsymbol{r}_i(t) - \frac{1}{N}\sum_{j}^{N} \boldsymbol{r}_j(t) \tag{2.12}$$

assuming all particles have the same mass.

We want to measure motion that is significant in terms of structural relaxation and brings about a qualitative change in structure, rapid vibrational motion about fixed positions should be ignored. Hence the coarse graining time Δt should be chosen to be roughly equal to τ_β, the timescale for particles to explore their local environments through thermal vibration, this means that K cannot measure processes that occur on timescales less than τ_β.

The activity is a space-time observable, it is not defined for a single configuration and will exhibit finite size effects both in time and space. As K is extensive in space and time, we define an intensive activity k that we expect to satisfy a finite limit when $Nt_{\text{obs}} \to \infty$:

$$k = \frac{K}{Nt_{\text{obs}}} \tag{2.13}$$

To investigate trajectories with atypical values of the activity we define a biased ensemble that depends on a field s that couples to the activity[38]. The ensemble at $s = 0$ is typical of equilibrium behaviour and the distribution of the activity has a "normal" mean and variance. The ensemble is defined through the probability of observing a trajectory $x(t)$ with activity $K[x(t)]$:

$$\boldsymbol{P}_s[x(t)] = \frac{\boldsymbol{P}_0[x(t)]\mathrm{e}^{-sK[x(t)]}}{Z_K(s,t)} \tag{2.14}$$

Recalling the definition of the free energy on Equation 2.9 the average activity in the biased ensemble is:

$$\langle K \rangle_s = \mathrm{e}^{\psi(s)Nt_{\text{obs}}} \left\langle K\mathrm{e}^{-sK} \right\rangle_0 \tag{2.15}$$

where the subscripted 0 indicates the average is taken from the unbiased, equilibrium system. For sufficiently large Nt_{obs} the statistical properties of trajectories from the biased ensemble at fixed s are equivalent to those of trajectories where K is constrained. We can exploit this numerically and study a constrained system by using established biased sampling techniques[43].

By measuring the probability distribution $\boldsymbol{P}_s(K)$ for different values of s we can reconstruct the equilibrium distribution $\boldsymbol{P}_0(K)$ for atypical values of K. The sampling under bias is used to investigate behaviour that would be very rare in the equilibrium distribution but effects a qualitative change

in the properties of the system. If there is a dynamic phase transition at a finite bias, s^*, the reconstructed distribution $\boldsymbol{P}_0(K)$ exhibits non-Gaussian behaviour away from typical values of the activity. The s-ensemble is a means of estimating just how rare rare events are and investigating the processes responsible for the change in behaviour.

The counting factor $\Omega_{\rm dyn}(K,t)$ cannot be obtained numerically and instead we sample a finite number of histories and estimate the partition function as:

$$Z_K(s,t) \simeq \frac{\sum_{\rm traj} {\rm e}^{-sK[x(t)]}}{N_{\rm traj}} = \left\langle {\rm e}^{-sK} \right\rangle_0 \tag{2.16}$$

Using this we can estimate the dynamic free energy:

$$\psi(s) = -\frac{\ln Z_K(s,t)}{N t_{\rm obs}} \tag{2.17}$$

The s-ensemble has been used to study low activity glassy states in kinetically constrained models[44, 32], lattice models[21] and particle systems[17]. Different models use different definitions of the activity, in discrete systems the activity can be a function that counts configurational changes, for example spin flips. In all cases the activity was chosen to measure structural relaxation and so the low activity phases exhibited long relaxation times and glassy behaviour. Although these metastable states may occur very rarely in equilibrium systems their long lifetime means that they can play a disproportionately large role in the behaviour of the system.

2.3 Dynamic phase transitions in model systems

The s-ensemble is a natural way to study a system in trajectory space and can be used to investigate dynamic phase behaviour. In kinetically constrained models there is a dynamic phase transition between active and inactive phases, this corresponds to the active and inactive domains of the system (as discussed above) expanding to dominate the system.

The dynamic behaviour of KCMs can be predicted by considering properties of a static configuration. Let $\nu(\mathcal{C})$ be the total escape rate from configuration $\mathcal{C}$. If we find that:

$$\lim_{N\to\infty} \frac{1}{N} \min_{\mathcal{C}} \nu(\mathcal{C}) = 0 \tag{2.18}$$

then in the thermodynamic limit there exists a state with a sub-extensive escape rate. If there exists a state with a sub-extensive escape rate then there is a dynamic transition between equilibrium states and metastable states with no applied bias to the system (at $s = 0$)[38]. These metastable states correspond to the inactive phase of KCMs where, due to the discrete nature of the activity, $k = 0$. The transition is defined by the change in the dynamic order parameter, but there is an accompanying structural change.

Another class of simple models that have been used to investigate dynamic phase transitions are exclusion processes. The simple symmetric exclusion process (SSEP)[45] consists of a one-dimensional periodic lattice of L sites with N hard particles, a maximum of one particle is allowed on each lattice site. A given configuration can be described by the occupation numbers n_j, where $0 \leq j < L$ denotes a lattice site and $n_j = 1$ for an occupied site, and 0 otherwise. The distribution of configurations can be described just using the parameter $\phi = N/L$, with particles distributed randomly as an ideal lattice gas. Dynamically particles can hop to their neighbouring sites, with equal rates for left and right hops, provided the target site is unoccupied. The dynamic activity is defined by counting the number of hops in a fixed observation time.

The dynamic phase behaviour of this model can be solved analytically in several ways. Fluctuating hydrodynamics can be used to describe the dynamics of the system as a continuous distribution of particles on large length scales. By defining a continuous local density $\rho(x, t)$ and considering the diffusive dynamics of the density according to the conserving Langevin equation[40]:

$$\frac{\partial}{\partial t}\rho - D\frac{\partial^2}{\partial x^2}\rho - \frac{1}{L}\frac{\partial}{\partial x}\sqrt{\sigma(\rho)}\eta = 0 \tag{2.19}$$

where $D(\rho) = 1$ is the macroscopic diffusion constant of ρ, $\sigma(\rho) = 2\rho(1-\rho)$ is a function that describes the macroscopic dynamics of the SSEP and η is a Gaussian white noise with correlations $\langle \eta(x,t)\eta(x',t')\rangle = \delta(x-x')\delta(t-t')$.

The activity is then written as an integral of $\sigma(\rho)$ over x and t, considering any relevant rescalings of time and position. It is then possible to consider the large deviations of the activity by writing the generating function of the activity, $G(s, L, t, \rho_0)$ as a path integral (see[40] for more details). This can

produce an expression for the optimal density profile for a given $\langle K \rangle$ and s. Appert et al.[21] showed that the large deviation function of the activity could also be expressed analytically.

As the activity is a dynamic observable it is extensive in space and time. The phase behaviour of the system can be considered using space-time bubbles of the non-dominant phase[30]. In a finite trajectory of the active phase there are small bubbles of the inactive phase that present as rare fluctuations. From the active phase as $s \to s^*$ the typical size and lifetime of the bubbles increase until at s^* there is coexistence between the active and inactive phases.

There is a first-order dynamic transition to an inactive phase that corresponds to a kink in the density profile and phase separation of particles into a single dense cluster. A phase separated configuration of the SSEP satisfies the condition in Equation 2.18, the structure cannot relax and breaks ergodicity for the system. Only the two end particles can move, thus the escape rate for the block configuration is reduced to the 2 possible moves out of the $2N$ total moves, the escape rate vanishes in the large system limit. However the energy of the phase separated configuration is the same as any other configuration, there is no static thermodynamic transition between the fluid and the phase-separated state.

A common component of simple dynamic models is the hard nature of the constraints. Hard constraints mean that, once formed, dynamically inactive systems do not relax back on a finite timescale and so can exist at equilibrium. However if the constraints are softened then the inactive phase can always relax at finite temperature and the activity does not fall completely to 0. Elmatad et al.showed that softening the constraints in a kinetically constrained model causes the lifetime of the inactive state to become finite and the first-order transition to the inactive phase occurs at a finite value of the dynamic field[32]. Furthermore the transition line in soft systems ends in a finite temperature critical point, Figure 2.2 shows the schematic phase diagrams for systems with hard and soft dynamic constraints.

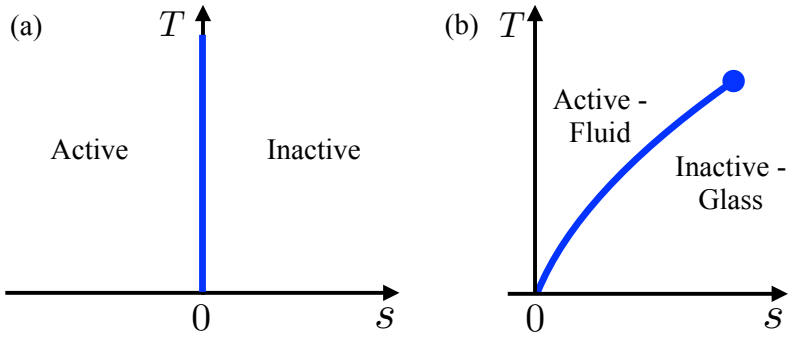

Figure 2.2: Generic phase diagrams for biased ensembles of trajectories, equilibrium behaviour is found along the $s = 0$ axis. Filled circles represent finite-temperature critical points, lines represent dynamic phase transitions. (a) Represents the phase diagram for KCMs with hard constraints, e.g. facilitated spin models like the East model, the coexistence between active and inactive states remains at $s = 0$ for all temperatures. (b) Represents the phase diagram for systems with soft constraints such as thermal glass-formers, there is a critical point at finite temperature above which dynamic facilitation is weak compared to fluctuations and no transition occurs. At sufficiently low temperatures there is a dynamic transition at finite bias with finite-size scaling analogous to a first-order phase transition.[32]

2.3.1 First-order phase transitions

The dynamic transitions discussed above are first-order with respect to the activity. A phase transition is defined in terms of an order parameter and a control field, the order parameter is an observable that can characterise the phase of the system uniquely, the transition leads to a change in the order parameter. The control field is thermodynamic field that can cause a a transition between one phase and another. For a liquid-vapour transition the density, ρ of a system is an order parameter that can distinguish the phases, the temperature or the pressure of the system can control the transition. First-order phase transitions are defined by a discontinuity in the first derivative of the order parameter with respect to the control parameter, for example $\frac{\partial \rho}{\partial T} = \infty$ for the liquid-vapour transition.

For an equilibrium thermodynamic system characterised by the order parameter M the ensemble mean can be written as $\langle M \rangle (h, N)$, where h is the conjugate field to the observable M. The intensive order parameter is defined as $m = M/N$. We can define a partition function $Z_M(T, h)$ and an associated free energy $F(T, h) = -k_{\mathrm{B}} T \ln Z_M(T, h)$. The probability distribution of M under the field h is given by[46]:

$$\boldsymbol{P}_h(M) = \frac{\Omega(M) \mathrm{e}^{-hM}}{Z_M} \tag{2.20}$$

where $\Omega(M)$ is a counting factor that counts the number of microstates with the order parameter equal to M. The distribution of M in a single phase system is Gaussian around the mean $\langle M \rangle (h, N)$, and the variance is:

$$\mathrm{Var}[M(h, N)] = \left\langle M^2 \right\rangle (h, N) - \langle M \rangle^2 (h, N) \tag{2.21}$$

The variance of the extensive observable is proportional to N due to the central limit theorem[47]. The variance of the intensive observable obeys $\mathrm{Var}[m(h)] = \frac{1}{N^2} \mathrm{Var}[M(h, N)]$, hence $\mathrm{Var}[m(h)] \propto N^{-1}$ in a single phase system.

The susceptibility $\chi(h)$ is defined as:

$$\chi(h) = -\frac{\mathrm{d}}{\mathrm{d}h} m(h) = \frac{\mathrm{Var}[M(h, N)]}{N k_{\mathrm{B}} T} \tag{2.22}$$

thus $\chi(h)$ is a constant with respect to N. Hence in a single phase the susceptibility is a constant and the mean intensive order parameter varies smoothly with the field h.

Fluctuations in the order parameter can be related to the partition function by:

$$Z_M(T,h) = \int \Omega(M)\mathrm{e}^{-hM}.\,\mathrm{d}h \tag{2.23}$$

$$\frac{\partial \ln Z_M}{\partial h} = \frac{\int \Omega(M)\mathrm{e}^{-hM}(-M).dh}{Z_M} \tag{2.24}$$

note that this is equal to $-\langle M\rangle(h,N)$ by definition of $\boldsymbol{P}_h(M)$. The derivative of the mean is given by:

$$-\frac{\partial \langle M\rangle(h,N)}{\partial h} = \frac{\partial^2 \ln Z_M}{\partial h^2} \tag{2.25}$$

$$\frac{\partial^2 \ln Z_M}{\partial h^2} = \frac{\int \Omega(M)\mathrm{e}^{-hM}M^2.dh}{Z_M} - \frac{\int \Omega(M)\mathrm{e}^{-hM}(-M).dh}{Z_M^2}\frac{\partial Z_M}{\partial h} \tag{2.26}$$

$$\frac{\partial^2 \ln Z_M}{\partial h^2} = \left\langle M^2\right\rangle - \langle M\rangle^2 \tag{2.27}$$

hence $\mathrm{Var}[M(h,N)] = -\frac{\partial\langle M\rangle(h,N)}{\partial h}$. Thus the mean and the variance of the order parameter are related to the derivatives of the partition function.

If the system contains a region of a second phase then the total order parameter is $M = (N-n)m_a + nm_b$ where n is the size of the subsystem that is in phase b and m_i is the intensive order parameter of phase i. The probability of a subsystem of size n to be in a different phase is proportional to the difference in the corresponding bulk free energy and the surface tension between the two phases. We define an intensive free energy per particle $f = F/N$. At constant temperature:

$$\boldsymbol{P}_{b|a}(n) \propto \mathrm{e}^{-[(N-n)f_a(T,h)+nf_b(T,h)+\gamma A_{ab}]} \tag{2.28}$$

where f_a is the bulk free energy of phase a and f_b of phase b, γ is the surface tension between the two phases and A_{ab} is the interfacial surface area. In a system of phase a then phase b is metastable and $f_b > f_a$, thus the probability of a subsystem of phase b decays exponentially with the size of the subsystem. As $N \to \infty$ at constant h the ratio $n/N \to 0$ and the total intensive order parameter $m = m_a - \frac{n}{N}(m_a - m_b)$ tends to m_a. In the thermodynamic limit

the typical size of fluctuations becomes vanishingly small compared to N and the system is in a single phase with order parameter $M = Nm_a$, and the variance in M reduces as N^{-1}.

At a first-order phase transition the scaling with system size fundamentally changes due to the coexistence of two phases. If h^* is the critical field for a transition from phase a to phase b with a change $\Delta M = M_a - M_b$, then the distribution of M at h^* is bimodal with two peaks at M_a and M_b respectively. The variance of a bimodal distribution $\boldsymbol{P}_{h*}(M)$, with equal weights in each peak, is[48]:

$$\mathrm{Var}[M(h^*, N)] = \frac{1}{2}\left(\chi_a + \left(\frac{N\Delta m}{2}\right)^2\right) + \frac{1}{2}\left(\chi_b + \left(\frac{-N\Delta m}{2}\right)^2\right) \quad (2.29)$$

where χ_i is the susceptibility of phase i and the mean of the bimodal distribution is $\langle M_a \rangle + \frac{\Delta M}{2}$.

Hence $\mathrm{Var}[M(h^*, N)] \propto N^2$ and so $\chi_a^* \propto N$. In the thermodynamic limit $N \to \infty$ the susceptibility diverges at h^* and M becomes discontinuous. The average intensive order parameters (m_a and m_b), and the variance of the bimodal distribution $\mathrm{Var}[m(h^*)]$, remain fixed with respect to N. At the transition $f(T, h^*) = f_a(T, h^*) = f_b(T, h^*)$ and so the probability of phase fluctuations depends only on the interfacial area between the two phases A_{ab}.

However the probability ratio of the entire system being in either phase is:

$$\frac{\boldsymbol{P}_a}{\boldsymbol{P}_b} \propto \frac{\mathrm{e}^{-f_a(T,h^*)}}{\mathrm{e}^{-f_b(T,h^*)}} = 1 \quad (2.30)$$

Both phases are equally likely (as shown by the bimodal histogram) but the probability of an interface between phases is still proportional to $\mathrm{e}^{-\gamma A_{ab}}$. The probability of the system spontaneously switching from one phase to another at coexistence requires a subsystem of $n \sim N/2$ to nucleate in the opposite phase. If the second phase has density ρ_b then a spherical region of the system of size n has a surface area $A_{ab} = 3n/\rho_b r$ and radius r. At h^* the probability of a subsystem of size n changing phase is proportional to $\mathrm{e}^{-\gamma 3n/2\rho_b r}$.

As $N \to \infty$ the variance of the total distribution $\boldsymbol{P}_{h^*}(m)$ remains constant but the variance of each unimodal distribution reduces as N^{-1}. Hence

as system size increases the two peaks become a narrower and the overlap of distributions reduces.

For dynamic phase transitions there is a similar scaling of the transition but the order parameter is extensive in time as well as space and fluctuations of a second phase have a lifetime τ as well as a size n. This means that equation 2.28 becomes:

$$\boldsymbol{P}_{b|a}(n,\tau) \propto \mathrm{e}^{-((N-n)\tau F_a(T,h)+n\tau F_b(T,h)+\gamma\tau A_{ab})} \tag{2.31}$$

where the energy required to maintain the surface A_{ab} becomes the work required to maintain the boundary over the time τ. Hence for dynamic phase transitions one expects that the susceptibility scales as $\chi^*_{\mathrm{dyn}} \propto Nt_{\mathrm{obs}}$, where t_{obs} is the duration of trajectories and $\chi_{\mathrm{dyn}} = -\frac{\mathrm{d}k}{\mathrm{d}s}$.

2.4 Dynamic phase transitions in atomistic systems

In the last decade there has been an increasing body of work that focussed on the dynamic behaviour of soft particle systems across the glass transition[13, 18, 15]. In this context the glass corresponds to the dynamically inactive phase of the system with soft constraints imposed by the inter-particle potential and $s^* > 0$. As $s \to s^*$ the typical space-time bubbles of the inactive phase become larger in space and time, this causes the dynamic heterogeneities seen in glass formers approaching T_G.

Previous studies of a three-dimensional Kob-Andersen (KA) glass forming system[14], subjected to dynamic bias using the s-ensemble formalism described above, found a first-order dynamic transition[13] to an inactive state at finite s^*. The KA mixture is a binary mixture of particles with a diameter ratio of $1 : 0.8$ and a number ratio of $80 : 20$, the mixture is known to frustrate crystallisation. The system did not crystallise nor phase separate, unlike kinetically constrained models there was no obvious structural difference between the active and inactive phase. Configurations drawn from the inactive phase had long relaxation times and a lower potential energy compared to the active phase. They found that the inactive state had a structure characteristic of a lower temperature system, although the thermal vibrations of particles were equivalent to equilibrium.

The separation between the two phases of the bimodal distribution $\boldsymbol{P}_{s^*}(k)$ increased with t_{obs} in accordance with a first-order transition as discussed above. The transition between a supercooled fluid and a glassy inactive phase in the KA mixture has been observed using a number of different dynamic order parameters; the mean squared displacement of particles as in Equation 2.11; the number density of active particles[17]; the number of particles in $11A$ structural clusters[18]. The $11A$ cluster is a cluster of 11 particles in a bicapped square antiprism configuration with a low potential energy, measurements of the glass phase have shown an increase in the number of $11A$ clusters. All of these investigations have found a dynamic transition at finite bias and the same qualitative glassy properties of the inactive phase.

In 2003 Garrahan & Chandler used the number density of dynamic excitations to explain dynamic heterogeneities and glassy behaviour in a coarse-grained glass-former[49]. They deconstructed the system into a lattice and described cells as either mobile or immobile, the density of mobile cells can distinguish between strong and fragile behaviour of the glass-former. In 2012 Speck & Chandler used the number density of mobile particles in the KA mixture as an order parameter to measure the dynamic phase transition[17]. Coupling the dynamic field s to the density of mobile particles showed a first-order dynamic transition equivalent to the transition in the activity. In general the density of localised excitations in a glass-forming system defines the dynamic behaviour of the system, suppressing the density of excitations results in an inactive metastable phase.

The transition can also be driven by a dynamic structural bias as in[18] but if a static chemical potential is applied to the system then no transition is observed. Thus the structure of the system at a given moment affects the future dynamics and relaxation properties, e.g. through the vibrational density of states, but the transition only occurs in the context of dynamic observables and biases. This principle is one of the chief results that links the transitions in KCMs to those in particle systems, they cannot be driven by static order parameters. There are concomitant changes in static observables in particle systems, for example the potential energy of the system[13], but these observables cannot be used to drive the transition.

The definition of the activity is obviously important and by describing

different processes they can reveal new information about the underlying phase transition. In studies of the KA glass-former two different definitions of the activity were found to be anti-correlated: one measured movement on short length and time scales, we will call it K_{alt}. The other observable measured movement as in equation 2.11. The transition in K_{alt} occurred at negative s_{alt} and was between equilibrium and a phase with a higher value ofK_{alt}, and more short range, vibrational motion. The transition in K, at $s^* > 0$, was to a phase with lower K, trajectories with less motion on timescales comparable to τ_α. The transition in both cases is between equilibrium behaviour and slow relaxing metastable behaviour and it is robust to different measures of the dynamic activity. Consideration of the energy landscape showed that for both definitions of K the inactive phase had a qualitatively different Hessian eigenvalue distribution from equilibrium[16].

2.5 The inactive phase of atomistic systems

An analysis of the inactive phase of the KA system was performed by Jack et al.[22] in order to clarify what structural properties, if any, lead to configurations with low dynamic propensity. They considered the potential energy of configurations as a sum of an inherent structural energy, $E_{IS}(\mathcal{C})$[23], and "vibrational" contributions from the motion of particles about that inherent structure (IS), $E_{vib}(\mathcal{C})$. They found that for configurations drawn from the inactive phase $E_{IS}(\mathcal{C})$ was much lower than equilibrium configurations at the same temperature. The value of E_{IS} was typical of equilibrium configurations at much lower temperatures, the inactive phase occupies a lower energy basin in the potential landscape. The value for the vibrational energy was equal in both dynamic phases, and agreed with the theoretical prediction that the particles undergo harmonic fluctuations about the IS with energy $E_{vib} = \frac{3}{2}Nk_{\mathrm{B}}T$.

Jack et al. also measured the vibrational density of states, an approach that was expanded upon by Fullerton & Jack[16]. Fullerton showed that the differences in the potential across the transition could be described in terms of structural modes[50]. There was a suppression in both the lowest and highest eigenfrequency modes of inactive configurations relative to equilib-

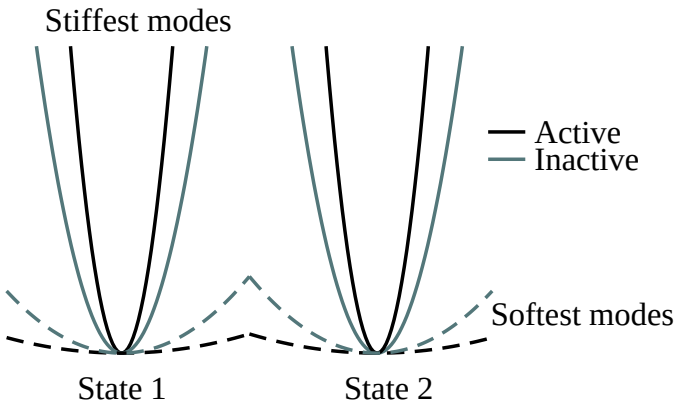

Figure 2.3: The difference in the energy landscape of the equilibrium and inactive phases. In the inactive phase the stiff modes relax and become typical of a lower temperature system, the strongly curving direction of the energy landscape is shallower and so local motion is easier. The soft modes are suppressed and the long-range motion between inherent structures has a larger energy barrier.

rium configurations. This was interpreted in terms of the typical excited stiff and soft modes. The stiff modes of the system correspond to rapid vibrations on short length scales about fixed positions, by suppressing the highest frequencies of the system the available stiff modes become softer. Alternately the low-frequency soft-modes of the system correspond to large scale structural relaxation and so the suppression of these modes is consistent with the inactive phase occupying a region of the energy landscape typical of lower temperatures. The dearth of soft modes leads to structural stability and frustrates structural relaxation, hence the metastable nature of the inactive phase. Figure 2.3 illustrates the difference in vibrational modes (a similar figure is shown in [16]).

Allowing the inactive phase of the KA mixture to melt back to equilibrium showed not only a long relaxation time for inactive configurations but also a different mechanism for relaxation[22]. For an equilibrium configuration melting from a lower to a higher temperature there are two stages to the melting process in the potential energy. Firstly there is a rapid thermalisation

of fast vibrational motion along the stiff modes of the system to behaviour typical of the new temperature. Then there is a second slower relaxation in the structure to an equilibrium state of the new temperature, this corresponds to the system relaxing along soft modes of the system. However if a configuration is taken from the inactive phase and then melted back to $s = 0$ under equilibrium dynamics there is only one step in the melting. There is no short-time thermalisation of the stiff modes, only a slow relaxation of the structure along the soft modes. The vibrational energy of the inactive state is equal to that of equilibrium so no relaxation of short time particle vibration is required, this agrees with the inactive phase adopting a lower energy inherent structure while maintaining equilibrium thermal vibrations.

2.6 Jamming

Consider a system of repulsive particles at low density, there is almost no pressure in the system as the particles interact rarely. Upon rapid isotropic compression particles will collide and there will be finite forces in the system as particles move relative to one another to resolve interparticle forces. Eventually at high densities the particles will be unable to resolve forces through movement, the pressure will diverge as the system has jammed. Jamming is defined as the point where a system develops a yield stress in the disordered state[51]. If the compression is slow enough the system will instead crystallise, although the crystal packing shares the mechanical properties of the jammed state it possesses structural order not found in jammed packings.

As a system is compressed it explores a series of packings closely related in configuration space, although there may be many equal configurations at given ϕ the system cannot explore them due to geometric constraints. This creates a disjointed set of "clusters" in configuration space, each corresponding to a closely related group of configurations that a system can explore[52]. As density increases each cluster contracts around a single jammed state, hence there are many possible jammed states but transitions from one to another are forbidden.

The jammed state is mechanically stable and can support external forces up to the yield stress, particles are prevented from moving by contacts with

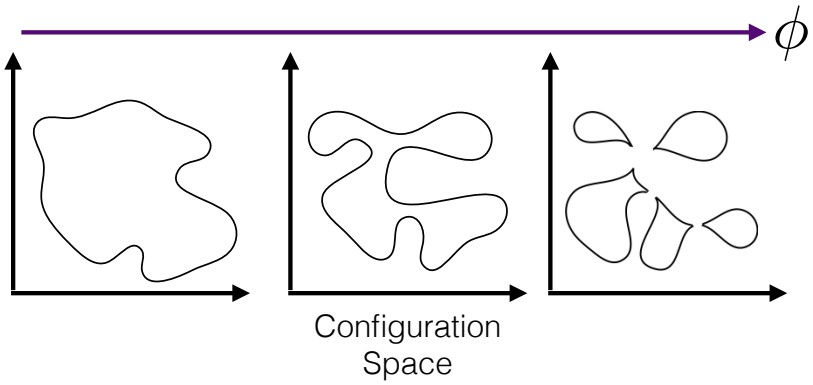

Figure 2.4: The decomposition of a high dimension configuration space as density increases. The possible configuration space collapses about a small number of high-density packings. In the first panel there are a large number of available configurations in the system. In the middle panel the number of possible configurations has reduced and structural relaxation between clusters of closely-related configurations are rare, relying on a small number of kinetic pathways. In the final panel the regions are completely separated as the system cannot move between all possible configurations.

their neighbours. Hence the particle coordination number is a critical metric for jamming and is a more sensitive measure of jamming than the packing fraction[53]. The distribution of the coordination number can distinguish between disordered jammed states and the crystal packing. For a given system at finite N there is no single well-defined packing fraction where the system jams, ϕ_J. Instead ϕ_J occurs over a range of packing fractions and is dependent upon the initial configuration and the protocol that is used to produce the jammed packing[52]. By changing the algorithm or tuning parameters in the jamming protocol, the average jammed packing fraction $\langle\phi_J\rangle$ can be changed by as much as 8%[54]. Typically jamming protocols use a parameter γ that describes the rate of change of ϕ in the system, this can be varied by many orders of magnitude and the chosen value of γ can have a large effect on the resultant distribution of ϕ_J.

The extreme slow down of dynamics, with structural relaxation times exceeding experimentally accessible timescale, and the fragmentation of phase space into a very complex, heavily pitted landscape, brings about comparisons to the glass transition. The jamming picture described above is more severe than glassy behaviour: in glasses the structure can still relax and explore phase space, albeit extremely slowly, and there are no constraints on the pressure or coordination numbers. It is possible that the two transitions are related and that the structural arrest of the glass means that the jammed states are simply not seen, although they may be the final state that the system relaxes toward.

Figure 2.5 shows possible phase diagrams for jamming (similar to the one first suggested in[5]) which separates ergodic, flowing states from glassy states that are kinetically trapped and jammed states that are geometrically trapped in phase space. The point $\boldsymbol{G}$ represents the point where the structural relaxation time τ_α diverges for hard spheres, and point $\boldsymbol{J}$ represents the point where the pressure diverges at zero temperature[7]. In the dynamic facilitation model there is no static glass transition so that there is no phase diagram in the $T-\phi$ plane.

At finite temperature the possibility of an ideal glass transition makes the phase diagram more complicated. If it exists then ergodicity is lost before the pressure diverges and so point $\boldsymbol{G}$ is separate from $\boldsymbol{J}$, as in Fig-

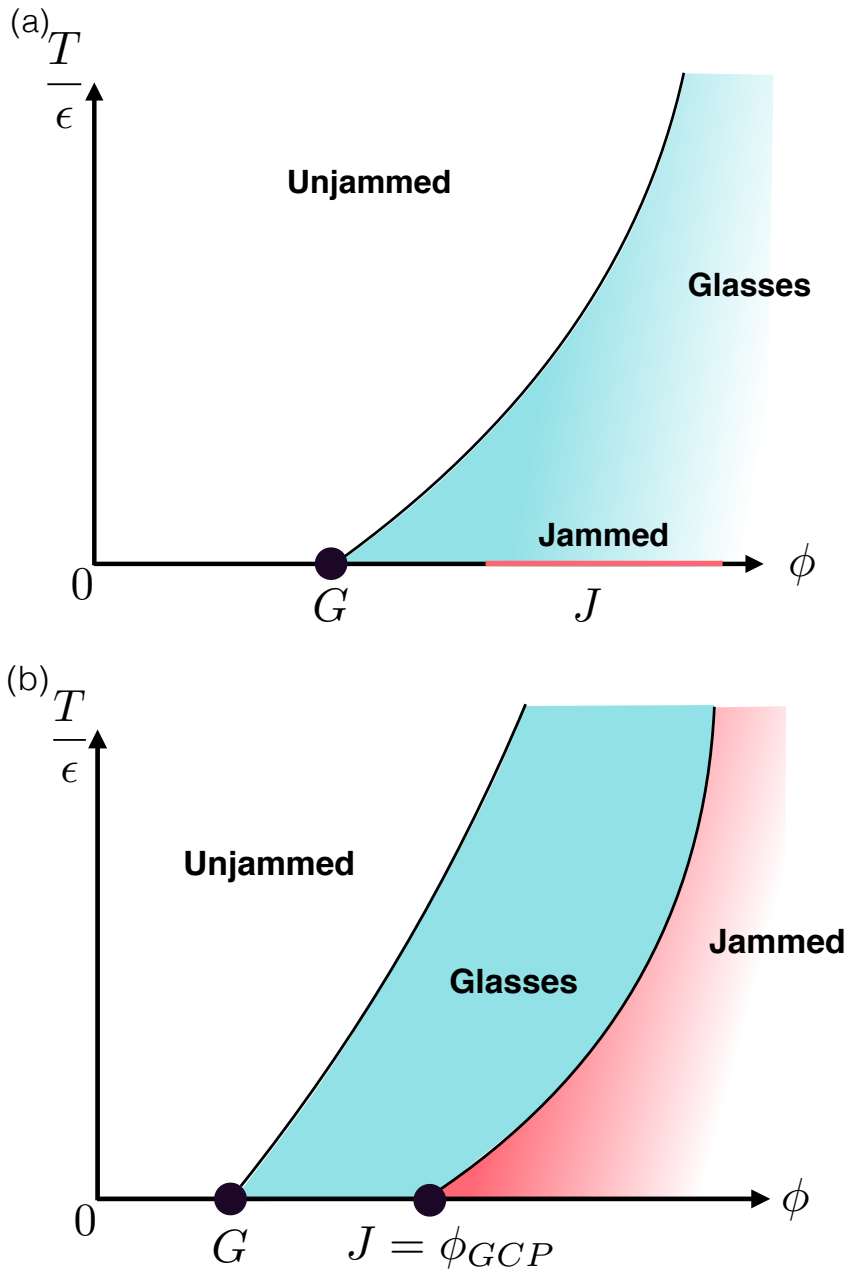

Figure 2.5: Two possible jamming-glass phase diagrams for particle systems assuming a glass transition. (a) If there is no unique value for ϕ_J then there is no jamming phase transition and instead there is a broad distribution of jammed packings at zero temperature. (b) If the jamming and the glass transition are separate then the points $\boldsymbol{G}$ and $\boldsymbol{J}$ represent two different transitions: the zero temperature glass transition at $\boldsymbol{G}$ and the lowest density jammed packing at $\boldsymbol{J}$ [55]. Both of these represent the ground state of a system at fixed ϕ, however slow dynamics in the glassy phase, and kinetic trapping in the jammed phase, may make packings characteristic of low-T impossible to reach.

ure 2.5(a). Point $\boldsymbol{J}$ then represents "glass close packing" (GCP), the lowest density where the pressure of the glass diverges and jamming occurs. There is controversy over how well defined $\boldsymbol{J}$ is, and whether a sharp transition in jamming behaviour persists at finite temperature[56, 57, 58]. We will follow the definition in Ref. [19] and consider jammed packings for hard particles to be packings that cannot be compressed further without causing particle overlaps, thus they have infinite pressure.

In hard systems there are models that suggest the pressure diverges at the same point as the relaxation time, hence the points $\boldsymbol{G}$ and $\boldsymbol{J}$ would be equal as in Figure 2.5(b). In this picture the ground state of a glass is a jammed packing, although slow dynamics may prevent this from being reached in real systems. This also does not preclude a finite temperature jamming transition at higher packing fractions.

It is accepted that glassy behaviour leads to a large range of jammed packing densities[19], whether this is due to ageing effects of the preceding glass, or due to an underlying thermodynamic effect is unknown. The dynamically inactive state previously found in particle systems occupies a different portion of the energy landscape from equilibrium, characteristic of a lower temperature system[16]. The relaxation of the high frequency vibrational motion in the system results in a higher value of the compressibility as particles are able to explore their local volume more easily. Configurations with higher compressibilities naturally jam at higher packing fractions.

The jamming density, ϕ_J is not well-defined for any system so we will consider distributions of ϕ_J produced by taking configurations for both dynamic phases and using a jamming protocol to find the "nearest" jammed packings in configuration space. The decomposition of configuration space as the system approaches jamming means that the active and inactive phases could correspond to different regions of the jammed space. We can associate the final jammed density of a configuration with the rate of compression, denser packings are the result of slower compression. Particles' ability to move and rearrange during compression affects the rate of compression, more local rearrangements effectively reduces the rate. If the active and inactive phases, once jammed, result in different distributions of ϕ_J then the structural difference between the two phases survives the jamming protocol and

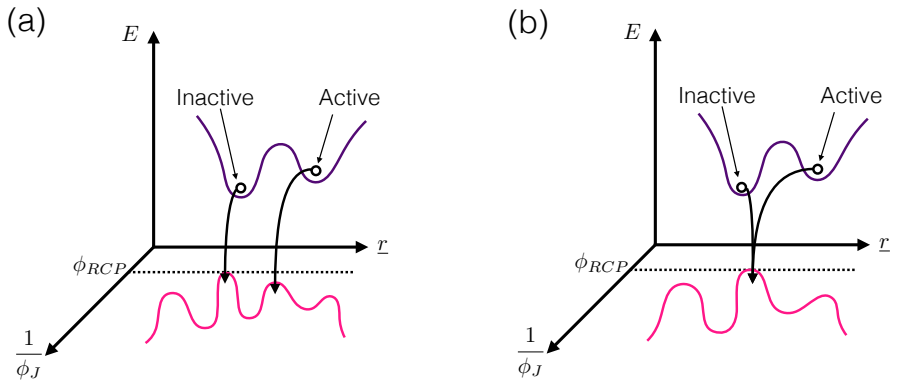

Figure 2.6: A possible schematic relation between finite-temperature states and zero-temperature jammed density ϕ_J. The exact results obtained will result upon the protocol used to move from the finite-temperature configurations to the jammed states. ϕ_{RCP} represents the hypothetical "random close packed" density, the maximum density a disordered packing can obtain. (a) The resultant distributions of ϕ_J may correspond to different regions of the jammed configuration space. (b) Or the two initial sets of configurations may correspond to the same region of the jammed configuration space and the same distribution of ϕ_J.

the jamming behaviour of the system is sensitive to dynamic behaviour. We can attribute this difference to the ease of local rearrangements and the nature of the system's stiffest vibrational modes. If the distribution of ϕ_J is the same in both phases then the dynamic behaviour of the system is not related to jamming and the change in the distribution of modes disappears under the jamming protocol. Figure 2.6 shows the possible scenario schematically, the two landscapes are shown with respect to a generalised set of coordinates in configuration space $\underline{r}$. Figure 2.6(a) shows the first situation described above, the active and inactive phases correspond to different minima on the energy landscape and when jammed they result in different jammed distributions. Figure 2.6(b) shows the degenerate situation described above, the active and inactive phases correspond to the same minimum on the energy landscape and when jammed they result in the same jammed distributions.

There is a long-range structural signature of jammed packings, the sup-

pression of infinite range density fluctuations, measured as a suppression of the structure factor $S(q)$ as $q \to 0$. This has been observed in may systems with quasi-long-range interactions and has been described as a sign of "maximally random jammed" configurations[59]. This phenomena is known as hyperuniformity and has been suggested as a physical mechanism to satisfy strong constraints. Hyperuniformity allows a system to have a crystalline long-range density profile and a fluid structure with translational symmetry. Systems that are subject to strong constraints or are highly optimised with respect to a fitness function tend to hyperuniformity: charged systems with strong long-range interactions[60], jammed packings of hard particles[59] and colloid[61] and the distribution of photosensitive cells in birds' eyes[62].

Chapter 3

Simulation methodology

We use numerical simulations to solve the relevant equations of motion and sample trajectories of several different systems under different conditions. There are two algorithms operating on two separate timescales: Monte Carlo techniques are used to propagate the system through time and generate trajectories, while transition path sampling is used to perform sampling across trajectories as entire objects.

We will study a one-dimensional model of hard particles diffusing in a periodic system. The particles have a finite length l_0 and the density of the system is defined as $\phi = Nl_0/L$ where L is the length of the system. We also study a three-dimensional binary system of harmonic spheres undergoing Brownian motion. We will study both systems in the constant-volume and constant-pressure ensembles, the models are discussed further in sections 4.1 and 5.1, here we discuss the specific method of simulating the equations of motion.

3.1 Monte Carlo dynamics

3.1.1 Metropolis algorithm

Particle motion was simulated using local move Monte Carlo dynamics and the Metropolis algorithm[63]. A particle, p, is chosen at random and is displaced by a random distance, δr. In d dimensions δr is obtained by drawing a random displacement for each dimension from the interval $\delta x_d \in$

$[-\Lambda, \Lambda]$, and proposing a particle move accordingly. The potential energy of the particle at its new position, $U_p(r + \delta r)$, is calculated and compared to the energy prior to being moved. The probability of the proposed move being accepted is subject to the conditions:

$$\boldsymbol{P}_{\text{accept}} = \begin{cases} \mathrm{e}^{-\beta(U_p(r+\delta r)-U_p(r))}, & \text{if } U(r+\delta r) > U(r) \\ 1, & \text{otherwise} \end{cases} \tag{3.1}$$

A random number is drawn from the interval $\mu \in [0, 1)$ and if $x < P_{\text{accept}}$ the proposed move is accepted. If $x > P_{\text{accept}}$ then the proposed move is rejected and the particle is returned to its original position. In either case the number of attempted moves and the simulation time are incremented accordingly.

This algorithm samples thermodynamic equilibrium by accepting or rejecting configurations with a probability equivalent to their weight in an equilibrium ensemble. The Metropolis-Hastings algorithm describes a Markov process that obeys detailed balance as defined by[64]:

$$\boldsymbol{P}(a)\boldsymbol{P}(a \to b) = \boldsymbol{P}(b)\boldsymbol{P}(b \to a) \tag{3.2}$$

for any two states a and b where $\boldsymbol{P}(a \to b)$ is the transition probability for the system to move from state a to b. At thermodynamic equilibrium the probability of being in a state a is dependent on the potential energy of the state, $U(a)$, and the inverse temperature. Hence to obey detailed balance the transition probabilities must obey:

$$\frac{\boldsymbol{P}(b \to a)}{\boldsymbol{P}(a \to b)} = \frac{\mathrm{e}^{-\beta U(a)}}{\mathrm{e}^{-\beta U(b)}} = e^{-\beta(U(a)-U(b))} \tag{3.3}$$

The acceptance probabilities in eq. (3.1) satisfy this criteria.

In the one dimensional systems the particles cannot overlap and a particle's neighbours remain constant so the conditions can be simplified to:

$$\boldsymbol{P}_{\text{accept}} = \begin{cases} 0, & \text{if } r_{p+1} - r_p + \delta r < l_0 \\ 0, & \text{if } r_p - r_{p-1} + \delta r < l_0 \\ 1, & \text{otherwise} \end{cases} \tag{3.4}$$

where $p\pm1$ indicates the right and left handed neighbours of particle p respectively. The probability that a particle move will be accepted is proportional to the free space around a particle, up to the limit Λ.

We are simulating the dynamics of diffusive systems and we need to set a physical timescale. In the dilute limit particles will undergo a free random walk through the Metropolis algorithm. We can relate the physical process to the random walk by comparing a physical diffusion time to the number of Monte Carlo moves that are attempted in the dilute limit. From a diffusive standpoint we expect the mean displacements to obey:

$$\begin{aligned} \langle \Delta r \rangle &= 0 \\ \left\langle \Delta r^2 \right\rangle &= 2dD_p t \end{aligned} \tag{3.5}$$

where d is the dimensionality of the system and D_p is the diffusion coefficient for particles.

The particle motion can be described by a random walk in d dimensions with random step sizes $\delta r \in [-\Lambda, \Lambda]$. The mean squared displacement for a single particle after N_s steps is:

$$\left\langle \Delta r^2 \right\rangle = \frac{dN_s\Lambda^2}{3} \tag{3.6}$$

We define a physical timescale called the Brownian time, τ_{B}, which is the average time for all N particles to move a diameter and define the particle diffusion coefficient as $D_p = \frac{l_0^2}{2\tau_{\mathrm{B}}}$ for the rods and $D_p = \frac{\sigma_A^2}{6\tau_{\mathrm{B}}}$ for the spheres. Generically we will use l_0 as the diameter of particles in the system and unless otherwise stated σ_A can be directly substituted. This means that the number of Metropolis algorithm moves in the simulation that correspond to a physical time of τ_{B} is:

$$N_s^* = \frac{3Nl_0^2}{\Lambda^2} \tag{3.7}$$

and the typical time for a single Metropolis step is:

$$\frac{t_{\mathrm{step}}}{\tau_{\mathrm{B}}} = \frac{\Lambda^2}{3l_0^2 N} \tag{3.8}$$

3.1.2 Continuous time Monte Carlo algorithm

In the constant density one dimensional system the only dynamics are local particle moves and the maximum number of possible moves is $2N$. Let $P(p^+)$ be the relative[1] probability of particle p successfully moving to the right and $P(p^-)$ be the relative probability of p moving left. Then:

$$\begin{aligned} \boldsymbol{P}(p^+) &= \min\left[(r_{p+1} - r_p - l_0), \Lambda\right] \\ \boldsymbol{P}(p^-) &= \min\left[(r_p - r_{p-1} - l_0), \Lambda\right] \end{aligned} \tag{3.9}$$

By symmetry $P(p^+) = P((p+1)^-)$ so we have:

$$\boldsymbol{P}_{\text{total}} = 2\sum_{i}^{N} \min\left[(r_i - r_{i-1} - l_0), \Lambda\right] \tag{3.10}$$

where $\boldsymbol{P}_{\text{total}}$ is the unnormalised sum of the probabilities of moving left and right over all particles. Using equation eq. (3.9) we can calculate the probability of every possible move and so instead of proposing and testing moves we can implement a rejection free algorithm.

Treating each possible move as a discrete event that corresponds to escaping the current state and entering a new state means that we calculate all possible transitions and the associated rate. The sum of all these probabilities is the total probability of escaping the current state and $\nu_{\text{esc}} = \alpha \boldsymbol{P}_{\text{total}}$ is the total escape rate for the current state where α is a constant that sets the relevant timescale. The value of α will be discussed below.

As this is a Markov process each event is independent of previous events and so the probability of remaining in a state after a time, t, follows an exponential form $\boldsymbol{P}_{\text{survival}}(t) = \mathrm{e}^{-\nu_{\text{esc}} t}$. The probability of not remaining in the state after a time t' is $1 - \boldsymbol{P}_{\text{survival}}(t')$, and equal to the probability that the system has escaped the original state during t'. Expressed in terms of the escape probability we can write $1 - \boldsymbol{P}_{\text{survival}}(t') = \int_0^{t'} \boldsymbol{P}_{\text{esc}}(t)\mathrm{d}t$. Transforming from $\boldsymbol{P}_{\text{survival}}(t)$ to $\boldsymbol{P}_{\text{esc}}(t)$ we have:

$$\boldsymbol{P}_{\text{esc}}(t) = \nu_{\text{esc}} \mathrm{e}^{-\nu_{\text{esc}} t} \tag{3.11}$$

and the average escape time is $\langle t_{\text{esc}} \rangle = \frac{1}{\nu_{\text{esc}}}$.

[1] Relative to the sum of probabilities $\boldsymbol{P}_{\text{total}} = \sum_i p_i^+ + p_i^-$.

All allowed configurations have equal energy so all moves are equally likely. By drawing a single random number from $\mu \in [0, \boldsymbol{P}_{\text{total}})$ we can select a particle, a direction and displacement with correct probability. This means that no time is wasted proposing and checking moves that will be rejected.

For each move the simulation time is incremented by a waiting time that represents the time for an event to occur. Hence we draw a random waiting time from the distribution $\boldsymbol{P}_{\text{esc}}$ and the simulation time is incremented by:

$$t_{\text{wait}} = \frac{-1}{\alpha \boldsymbol{P}_{\text{total}}} \ln\left(\mu'\right) \tag{3.12}$$

where μ' is a second random number drawn from the interval $(0, 1]$ and α is chosen to ensure $t_{\text{step}} = \langle t_{\text{wait}} \rangle$ in the dilute limit. In the dilute limit all particles can move the maximum distance so $\boldsymbol{P}_{\text{total}} = 2N\Lambda$. This means that the relationship between the available free volume to move into and the typical time for a particle to move into that volume is:

$$\frac{\Lambda^2}{3l_0^2 N} = \left\langle -\ln\left(\mu'\right) \right\rangle \frac{1}{2N\Lambda\alpha} \tag{3.13}$$

Hence,

$$\alpha = \frac{3l_0^2}{2\Lambda^3} \tag{3.14}$$

3.1.3 Monte Carlo volume dynamics

The constant pressure simulations include system wide barostat moves to change the volume of the system by scaling the positions of all particles uniformly. The changes in volume can be described by connecting the system to a hypothetical piston that moves and compresses or expands the system. The force exerted on this piston by the system is described as the instantaneous pressure, $\mathcal{P}$.

It is important that we simulate the dynamics of the volume coordinate consistently with the motion of the individual particles and that we understand the relationship between the structural and volume relaxation timescales. We need to relate the physical timescales for the particle coordinates and the volume, the relationship can be calculated by introducing a Langevin equation, describing the motion of the volume coordinate[65]:

$$\dot{V} = \frac{\delta P D_V}{k_B T} - \sqrt{2D_V}\eta_V(t) \tag{3.15}$$

where δP is the difference between the average applied pressure and the instantaneous pressure, the piston has been treated in the limit of having zero mass and D_V is the diffusion coefficient for the volume coordinate. η_V is the noise term, with zero mean and zero time correlation $\langle \eta_V(t)\eta_V(t')\rangle = \delta(t-t')$.

To a linearized approximation the isothermal compressibility, κ_T relates the volume and pressure:

$$\delta P \approx \frac{\partial P}{\partial V}\delta V = -\frac{1}{\overline{V}\kappa_T}\delta V \tag{3.16}$$

Where $\overline{V}$ is the average volume of the system. Using the linear approximation we can rewrite equation 3.15 as:

$$\delta\dot{V} = -\lambda\delta V + \sqrt{2D_V}\eta_V(t) \tag{3.17}$$

where $\lambda = \frac{D_V}{\overline{V}\kappa_T k_B T}$.

Solving equation (Equation 3.17) gives that the volume autocorrelation function can be written as:

$$\langle \delta V(t)\delta V(t+\tau)\rangle = V k_{\mathrm{B}} T \kappa_T \mathrm{e}^{-\lambda\tau} \tag{3.18}$$

for $\tau > 0$, so the volume relaxation time is $\tau_{VV} = \lambda^{-1}$.

From a hydrodynamic argument the time required for the system to equilibrate to a change in volume involves all particles and the information about the volume change must propagate across the system. Hence the relaxation time of the volume should be related to the collective diffusion constant D_C by:

$$\tau_{VV} = \frac{1}{D_C \overline{q}^2_{min}} \tag{3.19}$$

where $\overline{q}_{min} = \frac{2\pi}{\overline{L}}$ and $\overline{L}$ is the average length of the system.

Equating the two expressions for τ_{VV} and assuming that $D_p = D_C$ we can relate the particle and volume diffusion coefficients, where D_p is the individual particle diffusion coefficient.

$$\frac{D_V}{D_p} = \frac{\overline{V} k_{\mathrm{B}} T \kappa_T (2\pi)^2}{\overline{L}^2} \tag{3.20}$$

If we use this constraint then we can define the dynamics of the system with only four parameters N, T, P and one of the diffusion constants (D_p, D_V). All timescales can now be expressed in terms of τ_{B} at equilibrium, and volume changes can be incorporated into the Monte Carlo algorithm.

For every individual Monte Carlo step we can either propose a particle displacement or a volume change. We propose a volume change with probability $\boldsymbol{P}_{\mathrm{baro}}$, otherwise a particle displacement is attempted. We set $\boldsymbol{P}_{\mathrm{baro}} = (N+1)^{-1}$ so that, on average, each particle attempts a move for each proposed volume change. This means that a single volume move should correspond to a timescale, t_{baro}, equal to N particle moves, i.e. $Nt_{\mathrm{step}} = t_{\mathrm{baro}}$.

Combining with eq. (3.8) we have:

$$t_{\mathrm{baro}} = \frac{\Lambda^2 \tau_{\mathrm{B}}}{3l_0^2} \tag{3.21}$$

Relating this time to the duration of an average step in a one coordinate random walk we can calculate the corresponding mean squared attempted volume change:

$$2D_V t_{\mathrm{baro}} = \frac{\Lambda_V^2}{3} \tag{3.22}$$

where a proposed volume change is selected in the interval $[-\Lambda_V, \Lambda_V]$ with uniform probability. Combining eqs. (3.20) to (3.22) we can express the maximum volume change as:

$$\Lambda_V^2 = \frac{(2\pi)^2 \Lambda^2 \overline{V} k_{\mathrm{B}} T \kappa_T}{d\overline{L}^2} \tag{3.23}$$

where d is the dimensionality of the system and $\overline{V} = \overline{L}^d$.

If we use $\boldsymbol{P}_{\mathrm{baro}} = N^{-1}$ and choose volume changes in the interval defined above we can relate the physical volume relaxation time τ_{VV} with a simulation timescale:

$$\tau_{VV} = \lambda^{-1} = \frac{\overline{V} \kappa_T k_{\mathrm{B}} T}{D_V} \tag{3.24}$$

$$\tau_{VV} = \frac{\overline{L}^2 d \tau_{\mathrm{B}}}{2\pi^2 l_0^2} \tag{3.25}$$

the relaxation time for the volume scales as the length of the system size squared.

3.2 Trajectories

A trajectory is a single history of a system evolving through time, in practical terms it is a series of configurations stored in order with time Δt between them. From Equation 2.11 the activity is calculated from these configurations. In order to define a single value for a static structural measurement that can describe a trajectory we take an average over the configurations in a trajectory. For a static observable $A(x)$ we define $A([x(t)])$ for an entire trajectory as:

$$A[x(t)] = \frac{1}{M}\left(\frac{A(x(0))}{2} + \sum_{i=1}^{i=M-1} A(x(i\Delta t)) + \frac{A(x(M\Delta t))}{2}\right) \tag{3.26}$$

remembering that $t_{\text{obs}} = M\Delta t$. We use trapezium rule to calculate the average over the configurations. The temporal boundary effects shown in Figure 3.1 results in a subtle change in the value of observables and so we omit the start and end of trajectories to improve our measurements. Figure 3.1 shows the average potential energy profile across trajectories of particles. The temporal boundary effects can be seen at the start and end of the trajectory in Figure 3.1[38].

We use the notation $\langle\cdot\rangle$ for an ensemble average over many trajectories and define $\langle A\rangle = \frac{1}{N_{\text{traj}}}\sum^{N_{\text{traj}}} A([x(t)])$. This allows us to assign a single average quantity of a static observable to a trajectory and compare the value obtained to the activity and any correlations between them.

3.3 Transition path sampling

To generate new trajectories consistent with the bias s we use a form of iterative importance sampling in trajectory space. The algorithm takes a given trajectory, referred to as the *parent*, and copies a random number, μ from the interval $(0, M]$, of sections to a new trajectory, the *child*. Either μ sections are shifted from the end of the parent trajectory to the beginning of the child, or copied from the beginning to the end of the child trajectory with equal probability, the process is called a shifting move. The remaining $M-\mu$ sections are then generated using the relevant Monte Carlo algorithms described above. If the copied portion of the trajectory is placed at the end

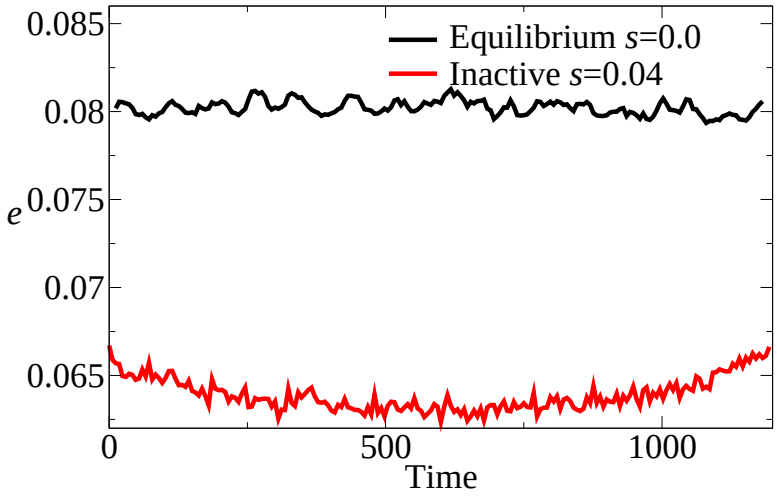

Figure 3.1: The average energy per particle throughout trajectories of $N = 100$ particles and $t_{\text{obs}} = 1200\tau_{\text{B}}$. There are temporal boundary effects at the start and end of the trajectories.

then the system is simulated backwards in time: hence it is necessary that the dynamics of the system are time reversible for these shifting moves to be performed. The algorithm is illustrated in figure 3.3.

Once a child trajectory is generated the activities of the two trajectories are compared and the child replaces the parent with probability:

$$\boldsymbol{P}_{\text{acc}} = \min\left[\mathrm{e}^{-s\Delta K}, 1\right] \tag{3.27}$$

where $\Delta K = K_{\text{child}} - K_{\text{parent}}$. This samples a set of trajectories in accordance with the definition of the s-ensemble in equation 2.14. For $s > 0$ any move that generates a less active trajectory is accepted and $s < 0$ similarly favours moves with more activity. The algorithm is then repeated with the relevant parent trajectory and a new child is generated.

The very first parent trajectory is generated using equilibrium dynamics, equivalent to no bias ($s = 0$), moving to a finite bias requires iterating many moves to "equilibrate" in trajectory space. After equilibration the algorithm samples trajectories from the ensemble defined in Equation 2.14.

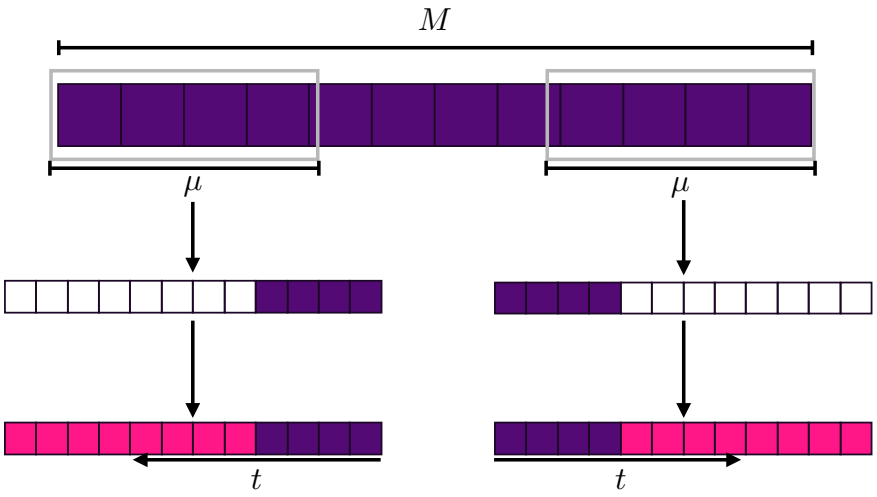

Figure 3.2: A schematic showing the TPS shifting algorithm. μ segments of the parent trajectory are copied from either the beginning of the parent to the end of the child (left) or from the end of the parent to the beginning of the child (right). The rest of the child trajectory is generated using Monte Carlo dynamics.

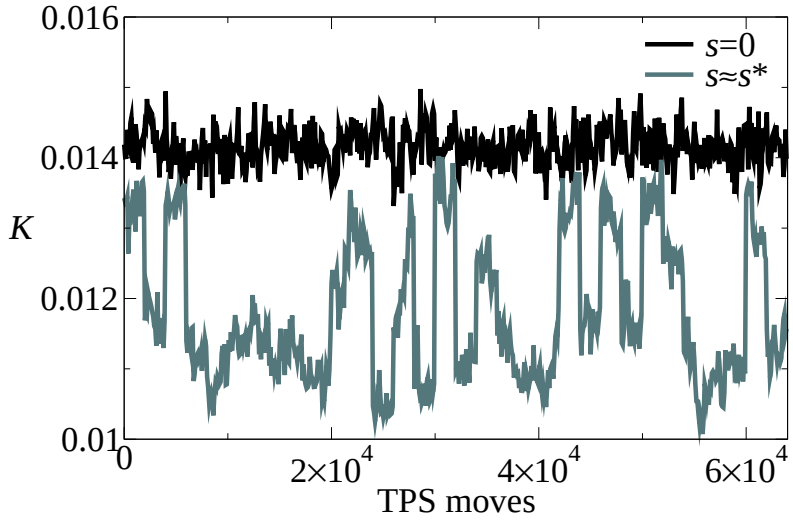

Figure 3.3: A plot of the sampled activity for a three-dimensional system of $N = 200$ spheres at constant volume as described below. When $s \simeq s^*$ the sampling moves between the active and inactive phases several times. This shows that the simulation has "equilibrated" in s and is sampling the distribution $\boldsymbol{P}_s(K)$.

The sampling becomes limited at extreme values of $|s|$ as the system becomes trapped in an extremely active or inactive trajectory. The algorithm cannot generate a more favourable trajectory from the parent and the probability of moving to a less favourable trajectory is too small. This is equivalent to kinetic trapping in trajectory space, the field s modifies the space and creates an activity landscape. There are locally favoured minima and the system can become trapped in them, taking a long time to relax to the global minima.

In the presence of a first-order transition the sampled activities will jump between the two coexisting phases as shown in Figure 3.3. It is important that sampling in the region of coexistence is performed long enough that the simulation moves between phases several times.

3.4 Weighted histogram analysis method

We will perform statistical sampling of observables at many different values of the biasing field. In order to combine all of our sampled distributions we will use the weighted histogram analysis method [66]. This method allows us to calculate the probability of a trajectory having a given activity under a given bias and calculate the average value of observables under a given bias.

If we perform R individual simulations with biases $\{s_j\} = s_0, s_1, \ldots, s_R$ and collect n_j samples per simulation such that $\sum_j^R n_j = N_{\text{samp}}$ then we can combine all of these sampled distributions. For an observable A measured at the same time as K, such that for every recorded K_i there is a corresponding A_i, the average value under a bias s_j is of the form:

$$\langle A \rangle_{s_j} = \sum_i^N \frac{A_i \mathrm{e}^{-s_j K_i - f_j}}{w(K_i)} \tag{3.28}$$

where f_j is a quantity applied to each sampled distribution that describes its relative weight compared to the unbiased, equilibrium distribution: the unbiased measurement is always denoted by f_0, s_0. For simplicity we define the quantity, $w(K)$, for each sample as the weighted sum over all biases:

$$w(K) = \sum_j^R n_j \mathrm{e}^{-s_j K - f_j} \tag{3.29}$$

The weights $f_j = \psi(s_j)$ are equal to the dynamic free energy (Equation 2.17) of the distribution at s_j and so they are related to the dynamic partition function, which can be estimated as:

$$Z(s) = \sum_i^N \left(\frac{\mathrm{e}^{-sK_i}}{w(K_i)} \right) \tag{3.30}$$

Note this is equal to the quantity $\left\langle \mathrm{e}^{-sK} \right\rangle_0$ and thus:

$$\mathrm{e}^{-f_j} = \left\langle \mathrm{e}^{-sK} \right\rangle_0 \tag{3.31}$$

To estimate values for f_j we begin with all weights set to unity and iteratively evaluate equations eqs. (3.29) to (3.31) until they converge, f_0 is always equal to 1 by definitions.

It is useful to note that n_j can be equal to 0 and we can calculate the relative weight and corresponding probability distribution for a bias value that we have not directly sampled.

We will use this to calculate $\langle k \rangle$ as well as the average pressure, energy and density of systems as a function of s.

3.5 Jamming protocol

We want to consider the jamming behaviour of the active and inactive phases of the three dimensional system. To do so we take configurations from the middle of trajectories and perform an athermal jamming protocol to find the closest jammed state. Previous work has suggested that glassy behaviour is responsible for a distribution of jammed packing fractions, rather than a single value for ϕ_J[19]. We will address the relationship between the initial dynamic phase the configuration is drawn from and the distribution of ϕ_J.

To probe the jamming behaviour of atomistic systems they must be driven into jammed sates. In experimental systems this can include compressing packings of hard discs on a vibrating bed[67], or increasing the particle size in a granular fluid until they jam[68]. In simulations it is possible to perform quenches, compressions and particle size inflation in any manner desired, this can be more of a hindrance than a help due to the sheer number of different procedures available. Different algorithms can produce different distributions of ϕ_J and even the same algorithm with different parameters can result in large variations[54].

For these reasons we have chosen to follow a well-defined protocol for investigating jamming behaviour and we will only consider distributions of ϕ_J relative to one another. For a given configuration we will find the nearest zero energy state using a conjugate gradient minimisation process[69]. Then we will perform cycles of particle inflation and repeated energy minimisation until a zero temperature jammed configuration is reached. Our jamming protocol reduces the initial configurations to zero temperature using a conjugate gradient method, as such we only aim to relate the initial properties of the active and inactive phases to the final values of ϕ_J reached. Our path through parameter is shown in Figure 3.4.

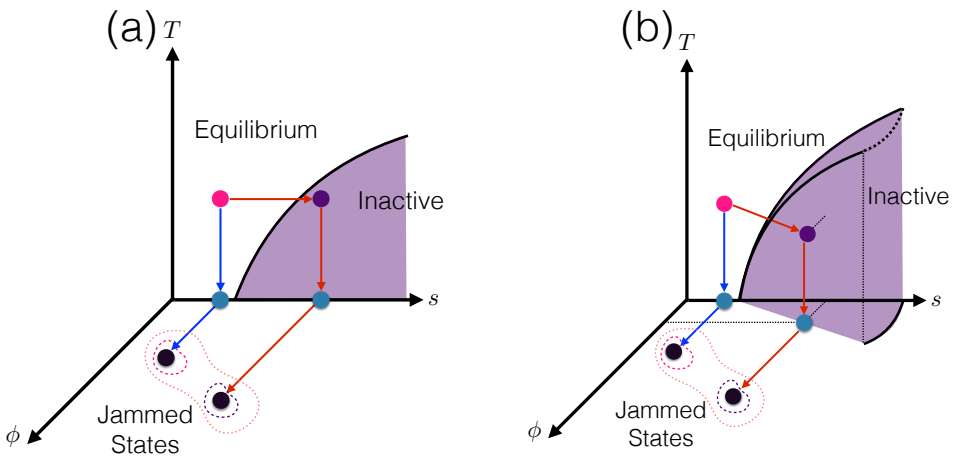

Figure 3.4: Paths through phase space during our jamming protocol. Equilibrium configurations are reduced to their zero energy state and then made denser until they reach a jammed state (blue arrows). Alternatively the equilibrium system is biased using the s-ensemble and enters a dynamically inactive phase. Configuration drawn form inactive trajectories are then reduced to zero temperature and jammed as before (red arrows). (a) The process when the initial configurations are drawn from the constant-volume ensemble. (b) The process in the constant-pressure ensemble, it is possible that ϕ changes between the active and inactive phases. In both ensembles we will study the resultant jammed distributions and investigate whether the dynamic phases correspond to the same jammed distribution (salmon pink dotted line) or two separate distributions.

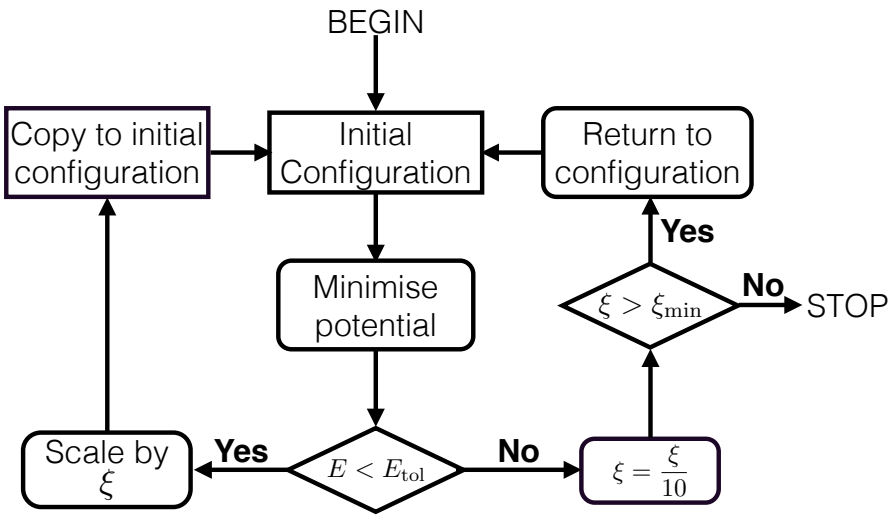

Figure 3.5: A schematic of the jamming protocol used, the particles are slowly inflated in size and the energy is minimised after each scaling step. If minimisation is not possible the rate of particle inflation is reduced.

Our jamming protocol is a cycle of potential energy minimisation moves followed by increasing the particle size until the energy cannot be minimised below a certain threshold. To minimise the energy we again use a conjugate gradient method to move the particles, if the energy can be reduced below the threshold ($E_{\text{tol}} < k_{\text{B}}T \times 10^{-10}$) then the particles are increased in size uniformly by a scaling factor, $1 + \xi$. If the energy cannot be reduced sufficiently the configuration is returned to its initial state before the most recent size scaling step and returned to their positions before the inflation. Then ξ is reduced and another inflation/minimisation cycle is attempted. This protocol is repeated until the energy cannot be minimised with $\xi = \xi_{\min}$, a preselected minimum inflation step. A schematic diagram of the jamming protocol is shown in Figure 3.5. We used the open source GNU scientific library implementation of the conjugate gradient minimisation method[70].

The final configurations produced by the protocol are effectively jammed

binary hard sphere configurations. We will compare the distributions of ϕ_J produced by this protocol and consider if they form one continuous distribution (the salmon pink dotted line in Figure 3.4) or two separate distributions (the dashed lines). If the distributions are separate we can conclude that the structure of the two phases are fundamentally different in terms of their relation to a jammed ground state.

Chapter 4

Dynamic phase transitions in a one-dimensional diffusive system

The study of dynamic facilitation models with trivial thermodynamic behaviour have been used to investigate and illustrate dynamic phase behaviour. We will consider a one-dimensional model of diffusing hard particles in the constant-volume ensemble (also described as the constant-density ensemble in this chapter) and the constant-pressure ensemble. In equilibrium systems we expect equivalence between constant-pressure and constant-volume ensembles because all equilibrium phases must have equal pressure. Phase coexistence in the constant volume ensemble corresponds to two constant-pressure systems, with equal pressure and different density, that the constant-pressure ensemble samples alternately. The use of a one-dimensional, diffusive model allows us to write an analytic expression for the dynamics of both the particle positions and the volume coordinate, this allows a comparison of the two relaxation timescales and their effect on the dynamic transition. Previous work on a non-equilibrium system showed ensemble in-equivalence when two dynamic mechanisms had widely separated timescales[20]. We will study the role of multiple timescales and ensemble equivalence with respect to dynamic phase transitions.

Systems with varying particle numbers, N, and trajectory durations, t_{obs},

will be biased to both higher and lower activities than equilibrium. Structural measurements will be used to characterise and compare the typical structures of equilibrium, active and inactive systems.

4.1 Description of the model

We have studied a system of hard particles undergoing Brownian motion in one dimension with periodic boundaries. Particle motion is described by the overdamped stochastic Langevin equation[71]:

$$\dot{r_i} = -\frac{D_p \nabla U}{k_B T} + \sqrt{2D_p}\vec{\eta_i}(t) \tag{4.1}$$

where r_i is the position of particle i, ∇U is the force acting on particle i and D_p is the diffusion coefficient for particle motion. $\vec{\eta_i}$ is a stochastic noise term with mean zero and no correlations in time.

$$\left\langle \vec{\eta_i}(t)\vec{\eta_i}(t') \right\rangle = \delta(t-t')\delta_{ij} \tag{4.2}$$

We are taking the limit where $U(r)$ is a a hard-core repulsive potential,

$$U(r_{ij}) = \begin{cases} \infty, & \text{if } r_{ij} \leq l_0 \\ 0, & \text{otherwise} \end{cases} \tag{4.3}$$

where l_0 is the length of a particle such that particles cannot interpenetrate or otherwise move past one another. For the derivatives in (4.1) to make sense, one should modify the potential by smoothing its discontinuities, and the hard-particle case obtained by taking a suitable limit. In practice, we will simulate the time evolution of (4.1) using the Monte Carlo scheme described in subsection 3.1.2, so no explicit regularisation is required.

The particle diffusion coefficient is defined according to the definition of τ_{B} in subsection 3.1.1:

$$D_p = \frac{l_0^2}{2\tau_{\mathrm{B}}} \tag{4.4}$$

remembering that $d = 1$ here.

We will simulate both constant density and constant-pressure systems at comparable equilibrium values, according to the equation of state:

$$\frac{P l_0}{k_{\mathrm{B}} T} = \frac{\phi}{(1-\phi)} \tag{4.5}$$

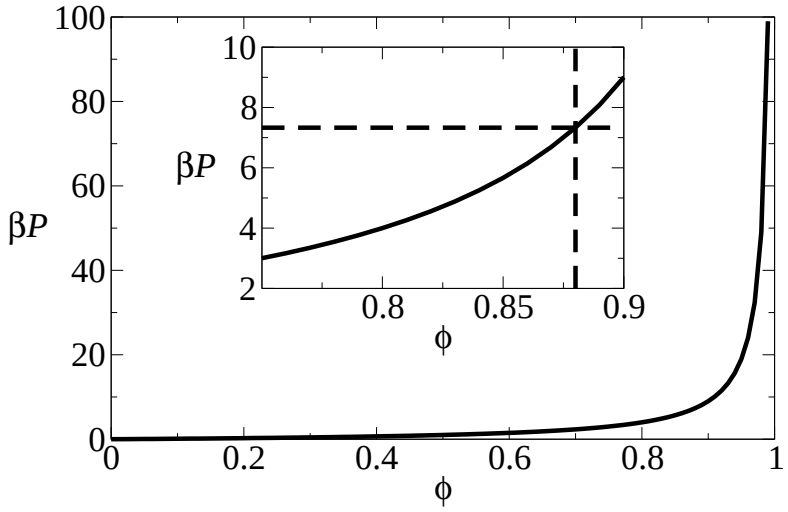

Figure 4.1: The equation of state for the one-dimensional hard particle system, the pressure diverges at $\phi = 1$. (Inset) The equilibrium state point chosen for simulations.

where $\phi = \frac{Nl_0}{L}$ is the packing fraction of the system and P the pressure of the system. The equation of state is identical to an ideal gas with excluded volume, this means that the system can be mapped onto an ideal gas by reducing particles to points as $l_0 \to 0$ and scaling the system size accordingly. Figure 4.1 shows the equation of state for the one-dimensional hard particle system.

To probe the structure of these systems it is convenient to make a change of co-ordinates: since the system is one-dimensional and the particles are hard, the ordering of the particle co-ordinates is fixed–there is no "overtaking". If we number particles so that their co-ordinates are in an increasing sequence then we can define new co-ordinates X_j which are also ordered in the same way. To perform the reduction the co-ordinates x_j become:

$$X_j = x_j - jl_0 \tag{4.6}$$

and the set of X_j diffuse freely around a ring of size $L' = L - Nl_0$. This reduction is useful as it removes the trivial length scale l_0 from real space

measurements of the density distribution $\rho(x)$ and the pair correlation function $g(x)$, and the trivial wavelength $q_0 = \frac{2\pi}{l_0}$ from measurements of the structure factor $S(q)$.

At equilibrium, the positions X_i are uncorrelated – they represent positions of ideal gas particles. For example, if we define a Fourier-transformed density $\delta\rho_q = \sum_j \mathrm{e}^{-iqX_j}$:

$$\rho_q = \sum_i^N \mathrm{e}^{-iqX_i} \tag{4.7}$$

and calculate the structure factor

$$S(q) = L\langle\rho_q\rho_{-q}\rangle \tag{4.8}$$

then we find $S(q) = \frac{1}{L'}\left\langle|\rho_q|^2\right\rangle = \frac{N}{L'}$ for all q.

Particles only interact through collisions and so the dynamic behaviour is characterised by the mean free space and collision time between particles. As such the length and time scales of the equilibrium system are functions of the global density. Figure 4.2 shows the average activity as a function of global density measured in the constant density system for several different step sizes, Λ. The activity of the system is a smooth function of ϕ and has the property $\frac{\partial^2}{\partial\phi^2}k_0(\phi) < 0$. Although in the limit of $\phi \to 1$ and if Λ is too large to accurately represent Brownian dynamics then the activity shows positive curvature.

At equilibrium the dynamic behaviour of the system is typical of $1d$ diffusive systems, the mean squared displacement was measured to characterise the dynamics of the system. We correct the MSD for the centre of mass motion, similar to subsection 2.2.1, such that:

$$\left\langle|\Delta x(t)|^2\right\rangle = \frac{1}{N}\sum_i^N |x_i(t) - x_i(0) - \overline{x}(t) + \overline{x}(0)|^2 \tag{4.9}$$

Figure 4.3 shows the MSD of particles for different system sizes and packing fractions. At short times $t < t_{\mathrm{coll}}$, where t_{coll} is the mean collision time, the motion is diffusive and $\left\langle|\Delta x(t)|^2\right\rangle \propto t$, for intermediate times particles are colliding and the dynamics are sub-diffusive, $\left\langle|\Delta x(t)|^2\right\rangle \propto t^{\frac{1}{2}}$[72]. Due to centre of mass corrections and the inability of particles to cross one another

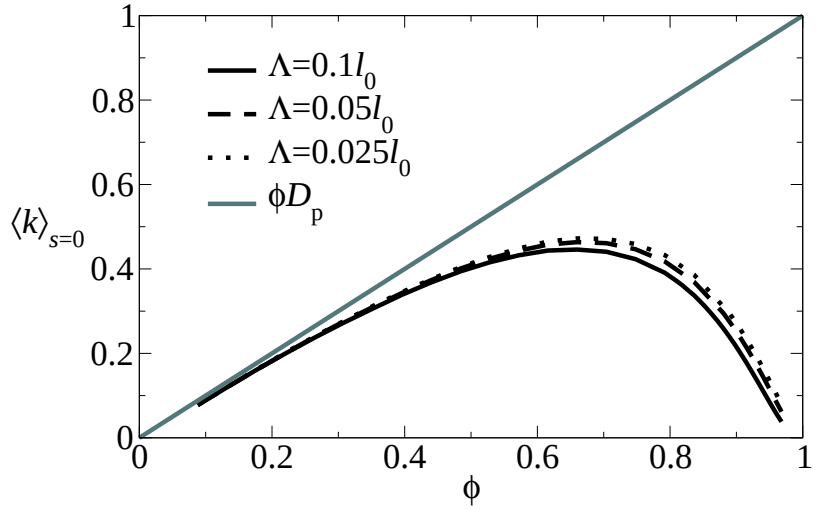

Figure 4.2: The average intensive activity of a constant density rod system at equilibrium, as a function of packing fraction. The change in maximum step size yields little change in the measured activity, thus the step size $\Lambda = 0.1l_0$ is adequate to realistically represent dynamics. As $\phi \to 1$ the activity must approach 0, hence there must be a point of inflection before $\phi = 1$.

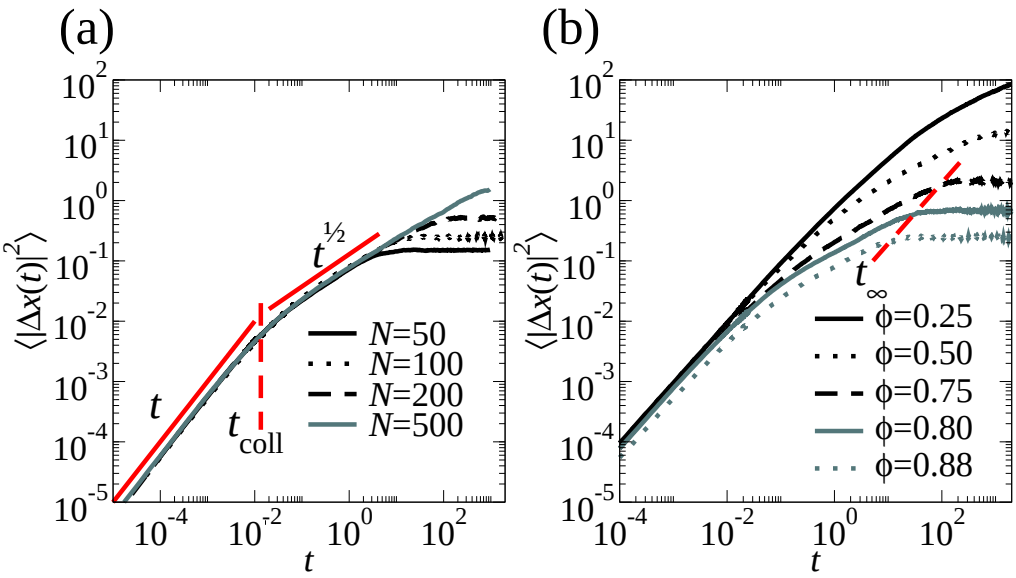

Figure 4.3: MSD of one dimensional systems at equilibrium. Solid red lines indicate scaling regimes, dashed red lines indicate typical timescales for particle collisions and saturation of the MSD. (a): Scaling of the MSD with system size at fixed packing fraction $\phi = 0.88$. Increasing system size increases the saturation limit and time. (b): Scaling of the MSD at fixed $N = 100$ for different packing fractions and the estimate of the saturation time t_∞.

there is a saturation value for the mean squared displacement, MSD_∞[73]. An individual particle cannot be more than $L - Nl_0$ away from the centre of mass taking into account the periodic boundary conditions:

$$\left\langle|\Delta x(t)|^2\right\rangle_\infty \propto L - Nl_0 \tag{4.10}$$

$$\left\langle|\Delta x(t)|^2\right\rangle_\infty \propto Nl_0\left(\frac{1-\phi}{\phi}\right) \tag{4.11}$$

The saturation of the MSD in a finite system as been observed before in single file diffusive systems[73]. If the centre of mass is ignored then a long-time regime for collective diffusion is observed where all particles move together[74].

Figure 4.3(a) shows the increase in MSD_∞ with N at fixed ϕ. The change from diffusive motion to sub-diffusive colective motion occurs at the the same

t_{coll} for all system sizes at fixed ϕ while the saturation time t_∞ changes with both ϕ and N. In Figure 4.3(b) the collision time changes with ϕ and the crossover occurs at different times. The long time limit t_∞ is shown in Figure 4.3(b) and the value of MSD_∞ increases with decreasing ϕ.

4.2 One-dimensional constant density system

In this section we present results for biased ensembles of the constant-density system. All results are for the case $\phi = 0.88$: as discussed above, we expect the same qualitative behaviour for almost all values of ϕ. We bias simulations to greater than equilibrium activity, $s < 0$, and less than equilibrium activity, $s > 0$. Some of the results included below, specifically regarding the dynamic phase transition and structural ordering in the constant-density ensemble, have been published in [75].

Figure 4.4 shows trajectories for the biased ensemble at several values of s, representing active, equilibrium and inactive trajectories. Note the length of the particles in space is reduced from their true value in order to aid comprehension of the images, as such the snapshots do not represent $\phi = 0.88$ but they do show position faithfully. At $s = 0$ the system is an equilibrium fluid of hard particles. For $s < 0$ the system has slightly higher than equilibrium activity and exhibits no obvious structural change from equilibrium (but see also Figure 4.8 below). In the inactive phase $s > s^*$ the system has fully phase separated for the whole trajectory, temporal boundary effects can be seen at the beginning and end of the trajectory where the separation deteriorates. Figures 4.4(c) demonstrates the persistence of density fluctuations in time. In the equilibrium fluid "bubbles" of local free volume are seen throughout the trajectory, distributed randomly in time and space. In the inactive trajectory, fluctuations in local density are only seen near the boundary between dense and sparse packing. Particles near the boundary can vary their position significantly and explore a local environment similar to the equilibrium fluid, the rest of the system is trapped in a dense packing.

Particles can only interact through collisions so to reduce activity it is required that motion is prevented geometrically, the particles must experience an increase in local density. At constant-volume the system must introduce

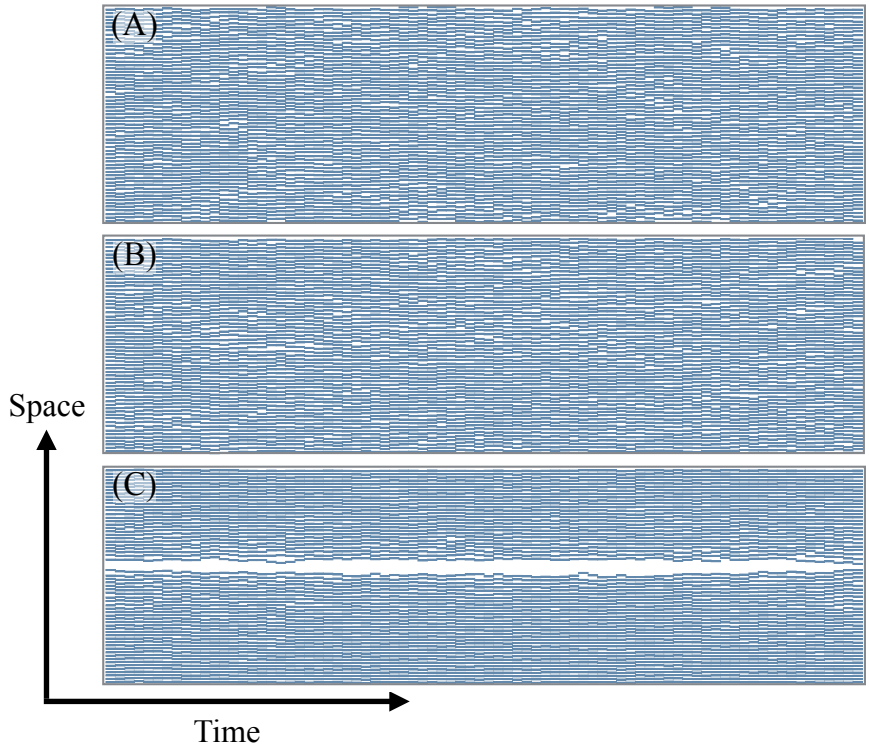

Figure 4.4: Trajectories of a constant density system at $N = 100$, $\phi = 0.88$ and $t_{\text{obs}} = 300\Delta t$. Blue boxes represent particles. Time runs horizontally, position vertically. Applied bias of (A) $s = -1$, (B) $s = 0$, (C) $s = 1$.

a large density fluctuation and phase separate into a dense cluster region of the system and a sparsely populated vapour. Phase separation leading to dynamic frustration has been reported before in exclusion processes[40]. Due to diffusive scaling a density fluctuation of length R would take a timescale $t \sim \frac{R^2}{D}$ to relax back to equilibrium, hence phase separating into a single cluster leads to the longest relaxation time.

The behaviour in the $s < 0$ regime is more subtle and it is not intuitive to consider how the system could maximise activity. From an equilibrium density of $\phi = 0.88$ Figure 4.2 indicates a reduction in density will increase the activity, but with a fixed system size this is not possible. To reduce the local density one might expect the particles to become periodically spaced, each with the maximum allowed separation from its neighbours. However from Figure 4.4(A) we can see this is not the case, any structural change is quite subtle.

4.2.1 Inactive regime

We first consider the phase transition that occurs in the presence of a bias $s > 0$. Phase transitions are signalled by singularities in the free energy ψ, which appear only in the limit when both the observation time t_{obs} and the system size N are very large. Figure 4.5 shows the average activity $k(s)$ for different system sizes and observation times. The systematic increase in activity with N at $s = 0$ is due to a finite size effect where larger systems exhibit larger spatial density fluctuations and hence higher activities. In particular, Figure 4.5(a) shows the effect of increasing t_{obs} at fixed system size $N = 100$, while Figure 4.5(b) shows dependence on system size N, all obtained for large $t_{\text{obs}} = 20\tau_{\text{B}}$. As in glass-forming systems, one observes a crossover from equilibrium to inactive dynamics at a finite value of $s^* > 0$ that depends on both N and t_{obs}. In the $s < 0$ regime the average activity of the system increases as expected but there is no sign of a dynamic first order transition to a more active phase.

We note that for $s \to \infty$, the system must arrive at the state with minimal propensity for activity, which should be the fully phase-separated state, where the particles in the cluster are all touching each other. It is

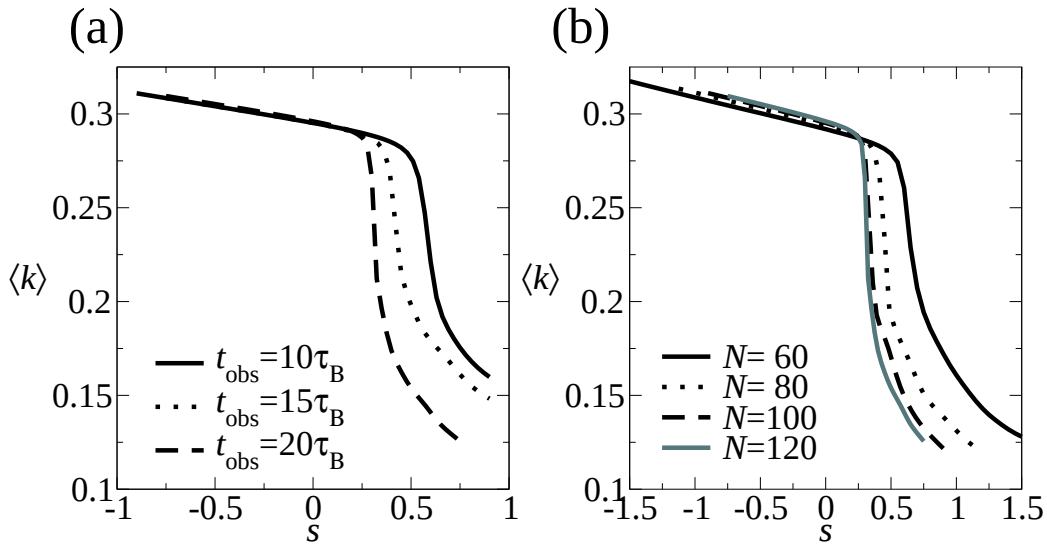

Figure 4.5: The average intensive activity for constant-volume rod systems at $\phi = 0.88$, as $t_{\rm obs}$ increases the critical bias reduces as expected for a first-order transition. (a) The saturation of activity in the long $t_{\rm obs}$ limit. (b) The effect of changing the number of rods in the system at constant $t_{\rm obs}$, there is small increase in k with N due to a finite-size effect discussed in the text.

therefore clear that phase separation must occur at some field s^*.

Figure 4.6 shows the scaling behaviour of the transition with system size at fixed $t_{\rm obs} = 20\tau_{\rm B}$. Scaling s by system size causes $k(s)$ to collapse onto a single curve and the critical value of the field s^* scales with N^{-1} at fixed $t_{\rm obs}$. The height of the peak in the dynamic susceptibility, χ^*, increases linearly with system size at fixed $t_{\rm obs}$ and the peak occurs at a constant value of sN.

To investigate the phase-separated state illustrated in Figure 4.4(c), we consider the one-body density. We define d_i as the separation between particle i and its right neighbour:

$$d_i = |x_{i+1} - x_i| \tag{4.12}$$

Since the system has periodic boundaries, it is necessary to fix the origin, which we accomplish by finding the largest 'gap' d_i in any configuration and

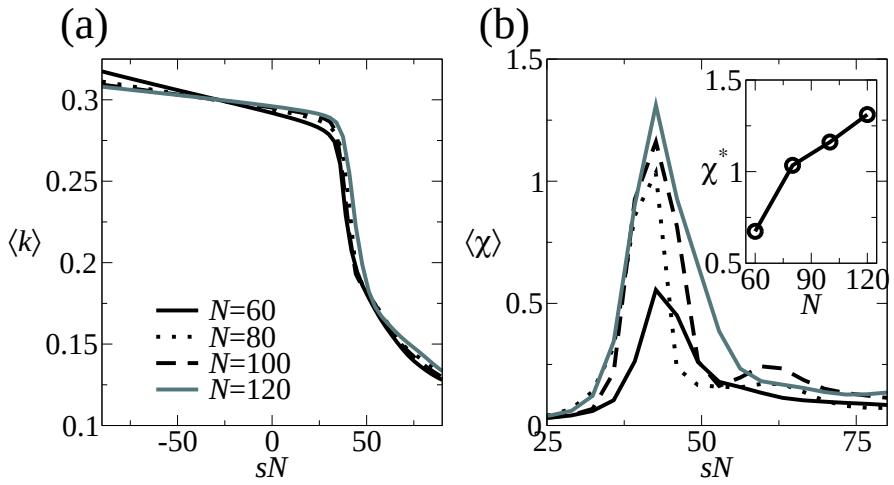

Figure 4.6: The scaling of the equilibrium/inactive phase transition with system size. (a) $\langle k(s)\rangle$ collapses onto a single curve when scaled by N. (b) The peak in the dynamic susceptibility occurs at a constant value of s^*N. B inset: The height of χ^* increases with increasing system size as the magnitude of fluctuations in the activity increases with N.

defining the location of $L/2$ to be a random point within that gap. The density of point-particles is then $\rho(X) = \sum_j \delta(X - X_j)$, and we average this quantity to obtain the one-body densities shown in Figure 4.7(a). At equilibrium, the density profile is uniform, as expected (up to weak boundary effects that arise because the origin was constrained to lie in the largest gap). As s is increased, the phase separation in Figure 4.4 appears as a non-uniform density profile, with most particles concentrated in a single large cluster.

The probability distribution of separations, $\boldsymbol{P}(d)$, was recorded for systems at $s = 0$ and $s > s^*$ and shown in Figure 4.7(b). The equilibrium distribution is an exponential decay typical of a one-dimensional equilibrium fluid, however the distribution of separations in the inactive phase is bimodal. Separations between particles within the cluster are distributed exponentially with a mean separation smaller than that of the equilibrium fluid. For each configuration the separation between the two particles either side of the void contributes a single delta peak to $P(d)$, at large d. Averaged over many configurations this becomes a broad distribution of large sepa-

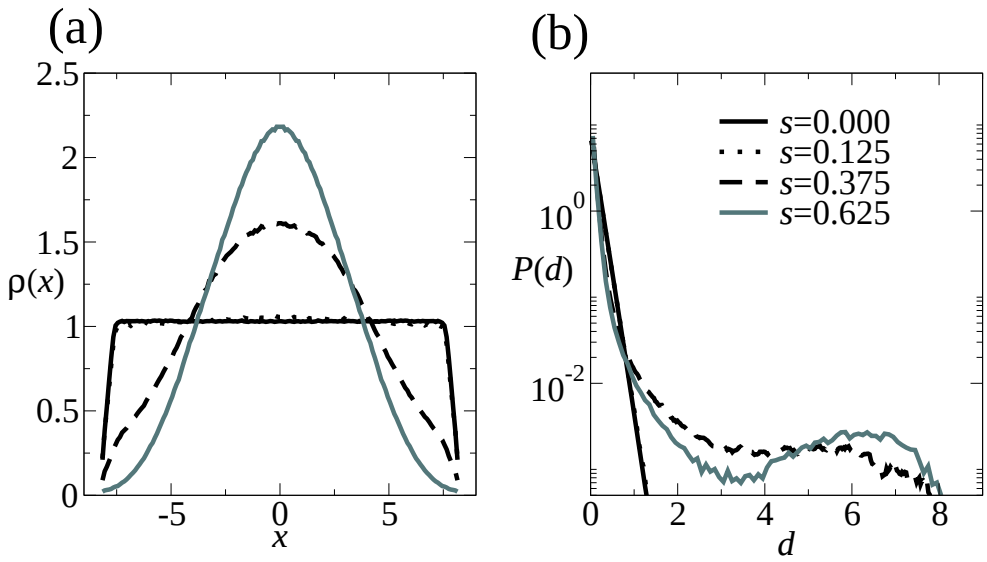

Figure 4.7: Structural measurements in the constant-density regime with point particles at $\frac{N}{L'} = 7.33$ with $N = 120$ for equilibrium and inactive systems. (a): Measurements of $\rho(x)$ across the transition. (b): distribution of separations for the equilibrium and inactive phases.

rations that are comparable to the system size and are indicative of phase separation.

To relax to equilibrium the phase separated state requires requires the two particles on the edges of the cluster to move away from the cluster, movements within the cluster do not contribute to structural relaxation. Hard geometrical constraints mean there is a finite number of moves that lead to relaxation, hence the escape rate remains finite regardless of system size. The creation of an inactive state through geometrical constraints has been seen in discretised exclusion processes and kinetically constrained models[40] as discussed in chapter 2.

In a lattice model, space is discretised so that all moves contribute to activity equally and a single vacant site has as much propensity for activity as a chain of vacancies. This is not true for a model in continuous space, the coarse graining of motion over a time window Δt means that small regions of free space have less propensity for motion up to a limiting size $\sim \sqrt{2D_p\Delta t}$. A high density cluster can allow a small yet finite amount of activity from interior particles without reducing the overall density and relaxing back to equilibrium. This means that the system can evolve through time, experiencing thermal fluctuations with the cluster, and still retain the density and order necessary to prevent long length scale relaxation. Thus, unlike discrete dynamic models, the inactive phase still exhibits a finite value of k, similar to the inactive phase of soft models.

To form the cluster from an equilibrium configuration it is required that two neighbouring particles experience a net force pushing them apart, thereby sweeping all other particles ahead of them. To stabilise the cluster and prevent melting the two boundary particles must experience a net force that pushes into the cluster. These forces must arise from the stochastic noises $\eta_i(t)$, the field s is creating a finite mean force on the boundary particles. Considering the forces within the cluster we can use force balance to write:

$$\frac{\partial}{\partial t}\langle x_i\rangle = -D_p\nabla P(x_i) + \sqrt{2D_p}\langle\eta_i\rangle \tag{4.13}$$

where $P(x_i)$ is the pressure at x_i. To maintain the cluster as a stable state the two terms on the right hand side of this equation must balance and $\langle\eta_i\rangle$

must be finite to counteract the pressure from inside the cluster. This means that there is a pressure difference inside and outside the cluster. The bias required to change the noise is fixed for all system sizes, in one-dimension only two particles need to be influenced to form a cluster, hence in the long time limit $s^* \sim (1/N)$.

Coexistence between two phases with different pressures has also been shown in active matter systems[76], systems where particles have an internal driving force upon them (see [77] for a review of active matter systems). In "swimming" systems particles have a propulsion force acting in one direction relative to their orientation, as the particles rotate the average force becomes zero. However particles can aggregate and form stable clusters, the outward force caused by the internal pressure of the cluster is mechanically balanced by the swimming force of particles in the cluster pointing inwards. Clustering arises when particle rotation is relatively slow compared to translational motion and spontaneous collisions of particles moving in opposite directions nucleate clusters. This phenomena is known as motility induced phase separation and is described in[78], further discussion and comparison to Brownian dynamics can be found in[79, 80].

In our system the boundary between the two regions is also maintained by a finite mean of stochastic forces, however the forces arise from the applied bias s. The non-zero average of stochastic forces leads to phase-separation through the same mechanism as active matter systems, only the mean forces acting on the boundary particles need to be finite. As the pressure is different in the dense and sparse phases it is not possible for a constant-pressure system to sample both equally, as it would in an equilibrium phase-separated system.

4.2.2 Active regime

We now consider the active ($s < 0$) regime. The pair correlation function $g(r)$ is defined as:

$$g(r) = \frac{1}{N(N-1)} \left\langle \sum_{i}^{N} \sum_{j>i}^{N} \delta(r - r_{ij}) \right\rangle \tag{4.14}$$

where r_{ij} is the separation between particles i and j.

If a particle's propensity to move is proportional to its local free volume then in the active, $s < 0$, regime one would expect a depression in the short range pair correlation function $g(r)$. Figure 4.8(a) shows the pair correlation function for the $s < 0$ regime. The creation of small depletion regions around particles ensures all particles have local free volume and are able to move.

Figure 4.8(b) shows the structure factor of the system when biased to $s < 0$. At equilibrium the system behaves like an ordinary fluid with $S(q) =$ const. for all q[46]. The structure factor of configurations drawn from the $s < 0$ regime show markedly different behaviour from the equilibrium fluid as $q \to 0$, small wave vector fluctuations are suppressed. This suppression of long range density fluctuations is a sign of hyperuniformity[81], which has been found in jammed systems[82, 83] and highly optimised structures[84, 62].

Hyperuniform states are distinguished by anomalously small local density fluctuations on long length scales, eventually vanishing at infinite range, hence $S(q) \to 0$ as $q \to 0$. There is a limit to the numerical evaluation of $S(q)$ in finite systems with a minimum wave vector $q_{\min} = \frac{2\pi}{L'}$.

The suppression of long range density fluctuations is a subtle effect and in figures 4.4(a) and (b) there is no discernible difference between the hyperuniform configuration and the equilibrium configuration.

The suppression of density fluctuations at $q_{\min}$ increases with increasing negative s. As system size increases $q_{\min}$ reduces and $S(q_{\min})$ becomes smaller at fixed s. Figure 4.8(b) shows that all values of $S(q)$ collapse onto one curve at fixed s.

This suggests that for any $s < 0$ then:

$$\lim_{N\to\infty} S(q_{\min}, s) = 0 \tag{4.15}$$

4.2.3 Linear response

For an insight into the response of the system to s we consider the linear response of of the system. A linear response expression can explain the behaviour of the system under positive and negative bias, and the transition to phase separated and hyperuniform configurations respectively. In the biased ensemble the probability of a configuration $p_{\mathcal{C}}(s)$ is dependent on the dynamic propensity of the configuration $\langle \delta k(r,t) \rangle_{\mathcal{C}}$. The propensity is the

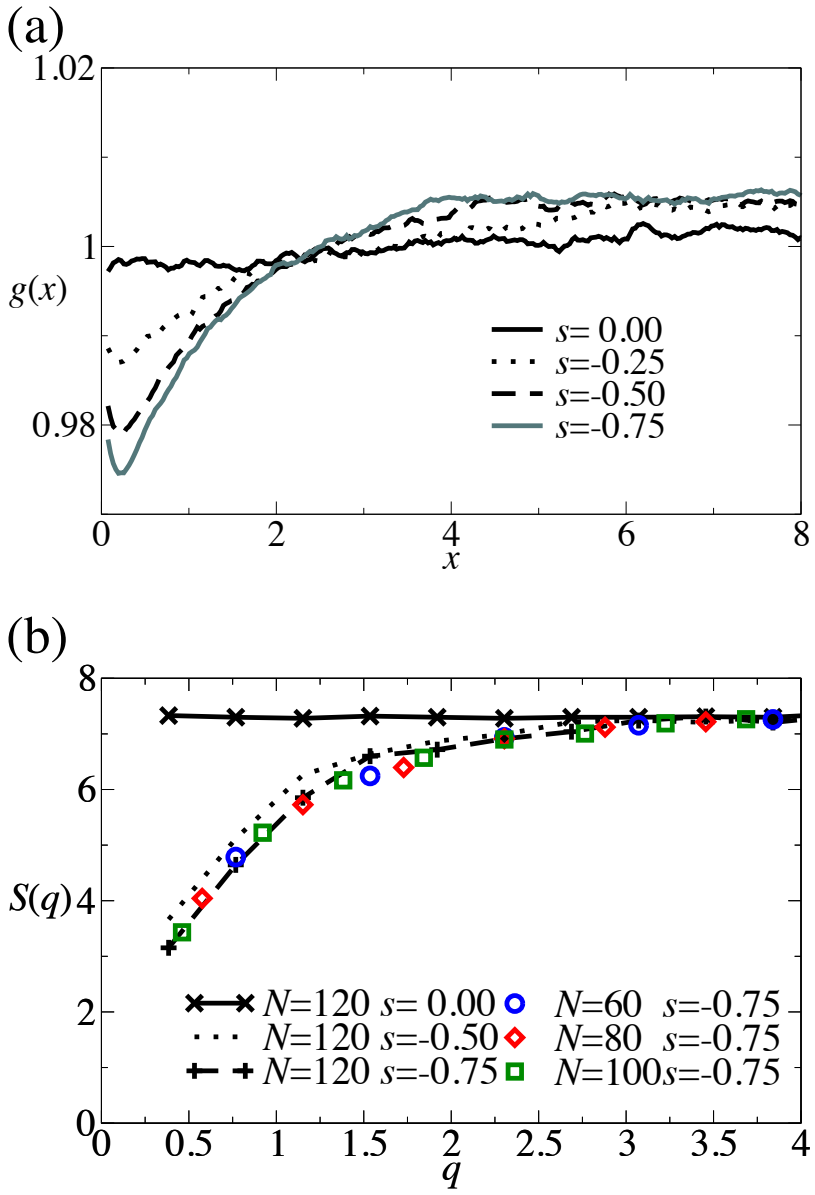

Figure 4.8: (a): The pair correlation function, $g(r)$, for point particles in the constant density regime with $N = 100$ $\phi = 0.88$ in the active phase. The depression in short range $g(r)$ shows an increase in local free volume around the particles as activity increases. (b): Small q structure factor measurements for constant density rod systems at $\phi = 0.88$. Biasing to $s < 0$ causes the suppression $S(q) \sim q$ consistent with the onset of hyperuniformity. At fixed s all system sizes collapse onto a single curve.

average activity of trajectories that start in configuration $\mathcal{C}$ compared to typical equilibrium activity.

The probability of a configuration $\mathcal{C}$ is:

$$p_{\mathcal{C}}(s) = p_{\mathcal{C}}(0)\left[1 - 2s\int dr dt\,\langle \delta k(r,t)\rangle_{\mathcal{C}} + \mathcal{O}(s^2)\right] \tag{4.16}$$

Our definition of activity means that s couples most strongly to diffusive motion and timescales that play a role in structural relaxation[16]. This agrees with the fact that longer relaxation times are associated with long range density fluctuations in diffusive systems and it is on these scales that we see the greatest change.

If the configuration $\mathcal{C}$ has a density fluctuation on a long length scale $q \approx R^{-1}$, expanding δk to quadratic order in $\delta\rho$ and using diffusive scaling gives[75]:

$$\langle \delta k(r,t)\rangle_{\mathcal{C}} \sim \left[|A_{\mathcal{C}}|^2 - S_0(q)\right] \mathrm{e}^{\frac{-D_p t}{R^2}} \tag{4.17}$$

where $A_{\mathcal{C}} = \frac{\rho_q(0)}{L^{d/2}}$ is the amplitude of the density fluctuation and $S_0(q) = \frac{N}{L^\prime}$ is the structure factor of the unbiased system.

A phase-separated system has a large density fluctuation on the scale $R \sim L$ of amplitude $A_{\mathcal{C}} \sim L^{d/2}$, hence equation (4.17) becomes:

$$\langle \delta k(r,t)\rangle_{\mathcal{C}} \sim (L)\,\mathrm{e}^{\frac{-D_p t}{L^2}} \tag{4.18}$$

and the response to s is of the form:

$$\frac{d}{ds} p_{\mathcal{C}}(0) \propto \frac{L^3}{D_p} \tag{4.19}$$

Hence configurations with large scale, long lived density fluctuations have strongly enhanced (diverging as $N \to \infty$) probabilities in ensembles biased with $s > 0$.

To achieve higher than normal activity it is necessary to suppress density fluctuations on long length scales. Suppression of density fluctuations such that $\frac{\rho_q}{L^{d/2}} \ll S(q)$ means that equation (4.17) becomes:

$$\langle \delta k(r,t)\rangle_{\mathcal{C}} \sim -S_0(q)\mathrm{e}^{\frac{-D_0 t}{R^2}} \tag{4.20}$$

Hence a system with suppressed fluctuations responds to s as:

$$\frac{d}{ds}p_{\mathcal{C}}(0) \propto -S_0(q)\frac{R^2}{D_p} \tag{4.21}$$

this diverges for large R so $p_{\mathcal{C}}$ for configurations with suppressed long range density fluctuations is strongly increased for $s < 0$.

In the constant-volume ensemble of the one-dimensional system there is a first-order dynamic phase transition between equilibrium and inactive phases. The inactive phase is characterised by phase separation and the transition scales as $s^* \sim N^{-1}$, we have presented an argument for this scaling based on creating a finite mean for the stochastic forces on two particles. The finite forces create a kink in the mechanical pressure profile of the system and prevent the phase-separated cluster from relaxing. When biased to higher activities ($s < 0$) the system adopts hyperuniform character. All dynamic regimes are characterised by long-range structural properties, in diffusive systems these arrangements have the slowest relaxation times.

In a constant-volume system of hard particles the arrangement of particles is the only degree of freedom in the system. We will study a constant-pressure system which has another degree of freedom, the system volume, and thus the density, can fluctuate.

4.3 One-dimensional constant-pressure system

We now consider the constant-pressure version of the model, in which the system size evolves in time according to equation (3.15). At equilibrium, one expects properties of single phases to be independent of ensemble. For example, since the pressure is constant throughout an equilibrium system, one may think of the constant-pressure simulation as representing a subsystem of a very large constant-volume system. One might expect the same equivalence to hold in biased ensembles at $s \neq 0$, but we will see that the applied bias s leads to a breakdown of ensemble-independence. A similar effect was discussed in [20].

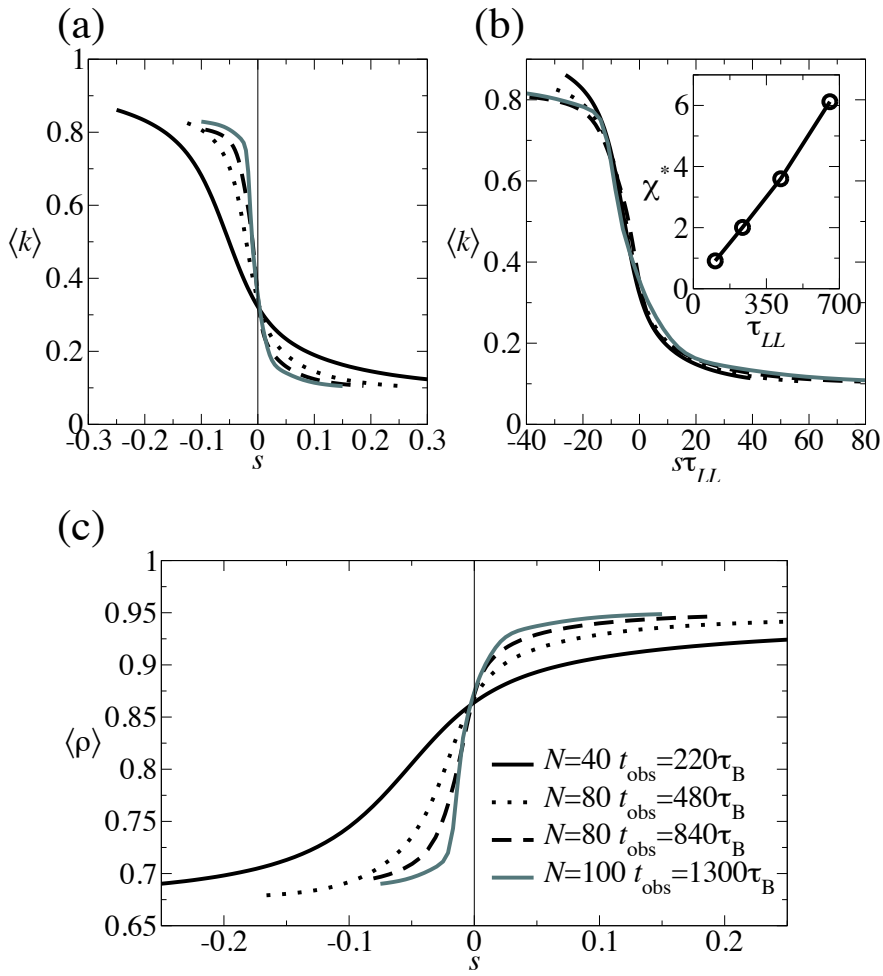

Figure 4.9: Dynamic behaviour of the constant-pressure trajectories of duration $t_{\rm obs} \sim 2\tau_{LL}$ at $P = 7.33$. (a): the intensive activity and dynamic susceptibility of the system as a function of s, $s^* = 0$ for all system sizes and the width of the crossover is proportional to $(\tau_{LL})^{-1}$. (b): The data for all system sizes collapses when scaled by τ_{LL}, (inset) the peak in the dynamic susceptibility scales with τ_{LL}. (c): There is an equivalent transition in $\rho(s)$.

4.3.1 Overview of results

We take the pressure $P = 7.33l_0^{-1}$ so that the mean volume fraction at equilibrium is $\langle\phi\rangle = 0.88$, consistent with section 4.2. The effect of the biasing field s is shown in Figure 4.9. Comparing with Figure 4.5, a similar transition is apparent, but instead of a crossover at $s^* > 0$ that depends on Nt_{obs}, one instead observes a crossover very close to the equilibrium point $s = 0$. The transition in $\langle k\rangle$ becomes sharper with increasing Nt_{obs}, the average activity of the active and inactive phase saturate at a constant value with respect to N. Note that the values of t_{obs} used here are significantly larger than those used in the constant-volume system: they are comparable with the volume relaxation time $\tau_{LL} \sim \overline{N}^2$ (recall subsection 3.1.3). When scaled by the volume relaxation time, the data collapses for all system sizes as shown in Figure 4.9(b). This suggests that the chief dynamic timescale in the constant-pressure system is associated with relaxation of the total volume. For comparison the constant-volume system showed collapse of $k(s)$ when scaled by system size sN, due to a difference in the mechanism of structural relaxation. Figure 4.9(c) shows the average density of the system as a function of s, there is a sharp change in the density that scales with N like the transition in k.

Figure 4.10 shows representative trajectories from biased ensembles in the constant-pressure system. Comparing with Figure 4.4, no phase separation occurs. We also note that the system size varies with s, consistent with Figure 4.9(c).

Figure 4.11 shows the correlation between activity and global density for all dynamic regimes. The average total density of a trajectory is highly correlated with the activity, consistent with the similarity in Figures 4.9(a) and (c). In hard systems the density is the only parameter that controls the behaviour of the system, in constant-volume systems density fluctuations control the dynamic behaviour [21, 75]. In the constant-pressure system the global density of the system changes across the transition and local density fluctuations are weaker than in the constant-volume system (see below).

Given this strong correlation, we can connect the phase transition that takes place at $s = 0$ in this system with the diverging hydrodynamic time

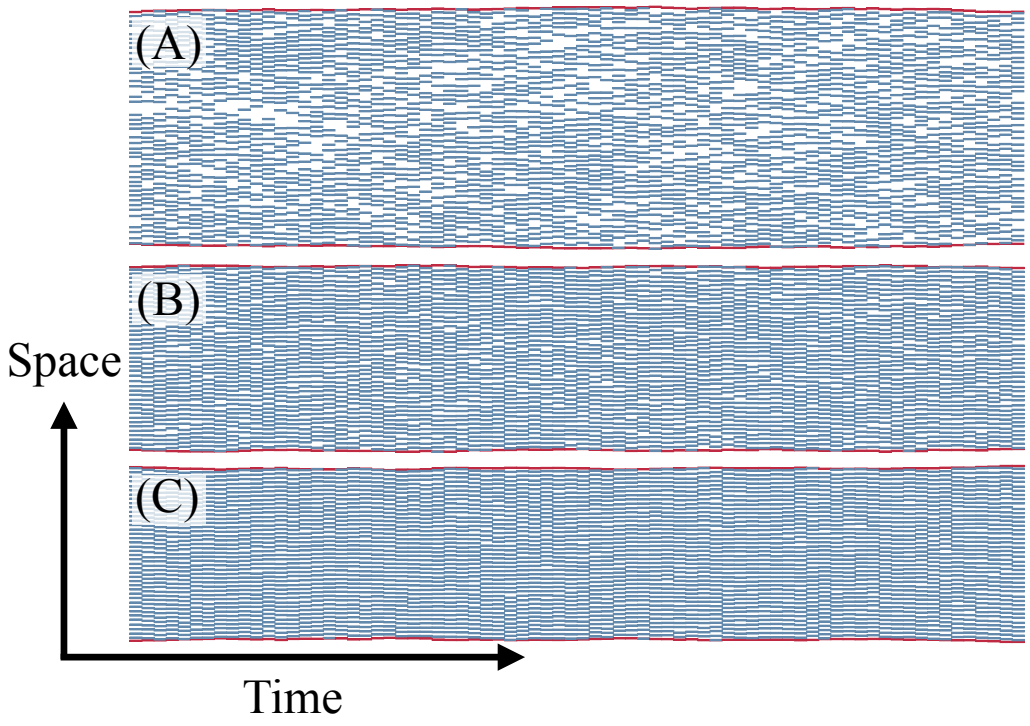

Figure 4.10: Trajectories of constant-pressure systems at $P = 7.33l_0^{-1}$ with $N = 40$, $t_{\text{obs}} = 220\tau_{\text{B}}$ at different biases. Red boxes represent the boundaries of the system. (A): $s = -0.250$, the active systems increase in length and thus reduce global density. (B) $s = 0$, the equilibrium system has a fluctuating volume but maintains $\langle\phi\rangle = 0.88$. (C): $s = 0.375$, the inactive system is compressed relative to equilibrium and thus has suppressed activity.

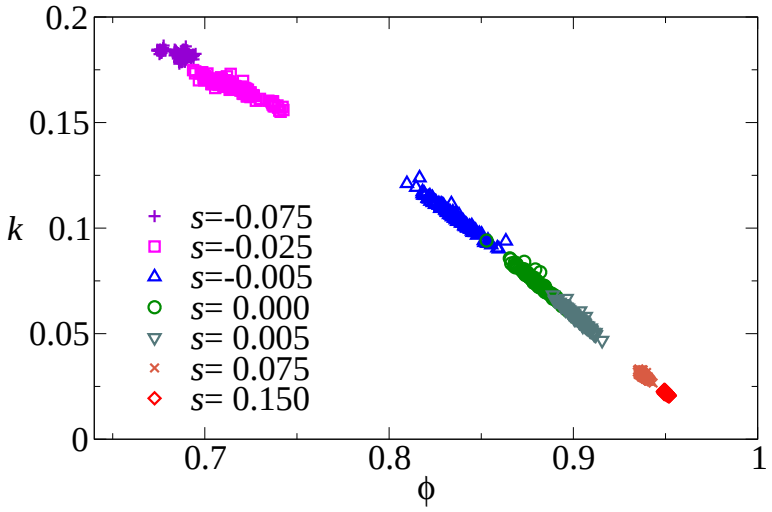

Figure 4.11: The activity against the average density of trajectories of duration $1300\tau_{\mathrm{B}}$ with $N = 100$ particles from biased ensembles. There is a strong correlation between the activity and the density of the trajectories.

scale τ_{LL}. We define the (normalised) autocorrelation function of the system size

$$C_{LL}(t) = \frac{\langle \delta L(t')\delta L(t'+t)\rangle_{\mathrm{eq}}}{\langle \delta L(t')^2\rangle_{\mathrm{eq}}} \tag{4.22}$$

which is evaluated at equilibrium (so there is no dependence on t'), with $\delta L = L - \overline{L}$. This correlation function decays on a time scale close to τ_{LL}. Similarly the correlation function of the activity is

$$C_{kk}(t) = \frac{\langle \delta k(t')\delta k(t'+t)\rangle_{\mathrm{eq}}}{\langle \delta k(t')^2\rangle_{\mathrm{eq}}} \tag{4.23}$$

where $k(t) = \sum_i |r_i(t+\Delta t) - r_i(t) - \Delta\overline{x}(t)|^2$ is the quantity that appears in the definition of the activity K, recall equation(2.11). To show the long-time behaviour of $C_{kk}(t)$ more clearly we smooth the function by convolving it with a Gaussian window, with variance $\sigma^2 = \tau_{\mathrm{B}}^2/4$, so that $C_{kk}(t) = \Gamma \sum_{t'} C_{kk}(t')\mathrm{e}^{-2(t-t')^2/\tau_B^2}$, where Γ is a normalisation constant.

The correlation functions $C_{kk}(t)$ and $C_{LL}(t)$ behave very similarly, consistent with the idea that the the activity fluctuations are strongly correlated to

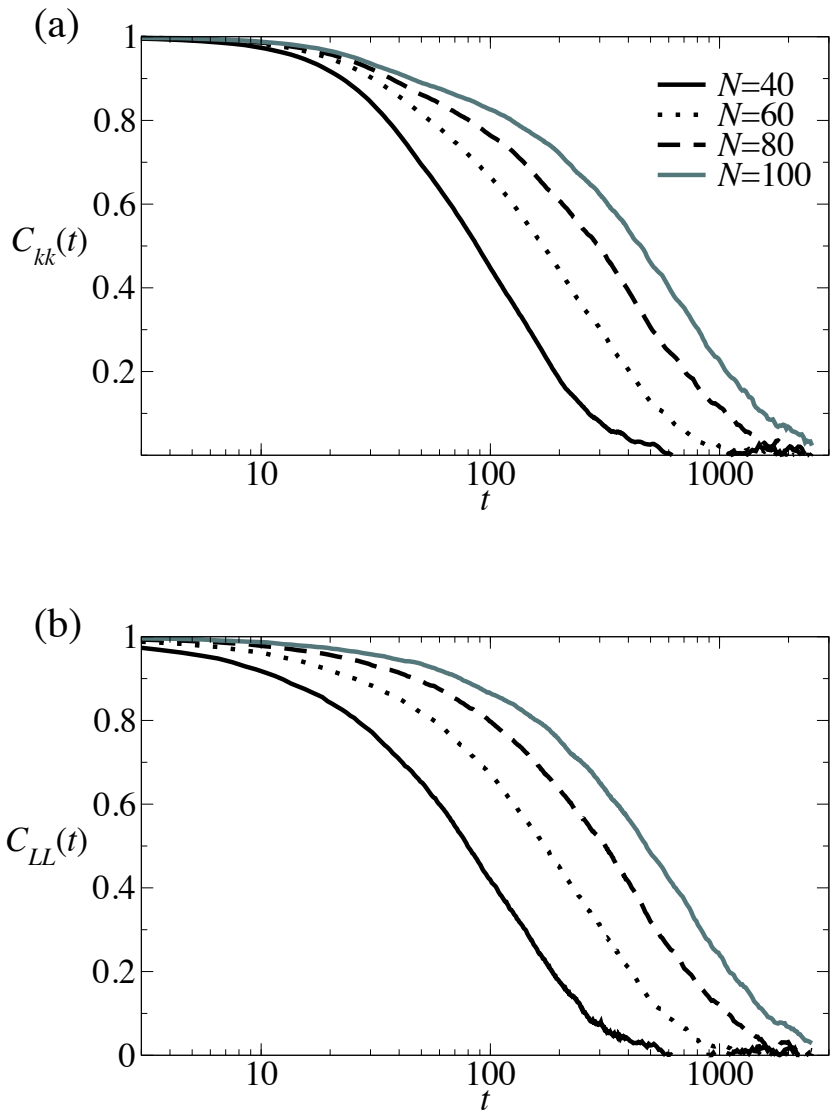

Figure 4.12: The activity and volume correlation functions for equilibrium constant pressure systems with different system sizes. The correlation time, τ_{kk}, is strongly correlated to τ_{LL}. To display the long-time behavior most clearly, $C_{kk}(t)$ has been smoothed with a Gaussian window (see main text).

those of the global density (and hence to the system size). Since the volume relaxation time τ_{LL} diverges as $\overline{L}^2$, we therefore expect a similar divergence in the relaxation time of the activity.

This divergent time scale is important because the susceptibility χ is related to the autocorrelation function of the activity as

$$\chi(s=0, t_{\rm obs}\to\infty) \simeq \frac{2}{\overline{L}}\int_0^\infty \langle \delta k(0)\delta k(t)\rangle_{\rm eq} \tag{4.24}$$

so that $\chi \sim \tau_{kk} \sim \overline{L}^2$ diverges at $s=0$, which we interpret as a dynamical phase transition. (The equal time value of the correlator in this equation scales as $\overline{L}$ since δk is extensive in the system size: this $\overline{L}$-dependence cancels with the prefactor so that the right hand side scales with τ_{LL}, with a prefactor of order unity.) Since $\chi = -dk(s)/ds$, this amounts to a perturbative argument for the existence of the phase transition: in [75], a related perturbative argument based on fluctuations at finite wavevector was used to explain the existence of phase transitions in systems at fixed volume.

In Figure 4.13(a), we show the structure factor of the constant-pressure system for $s<0$. For a given bias s, the fluctuations in the total system size small in relative terms so we evaluate the structure factor at wavevectors $q = 2n\pi/L'$ as usual, and calculate $S(q)$ by an ensemble average at fixed n. This provides an estimate of $S(\overline{q})$ with $\overline{q} = 2\pi n/\overline{L'}$. The results of Figure 4.13(a) are consistent with hyperuniformity of the active ($s<0$) phase, although the effect is weaker than that shown in Figure 4.8, for the constant-density system. We also show the distribution of particle separations in Figure 4.13(b), for comparison with Figure 4.7(b). The distribution fits well to an exponential form, independent of s. Given the correlations that are apparent from Figure 4.13(a), this result is somewhat surprising. It might be that there are long-range correlations between separations that lead to hyperuniformity, or that $S(q)$ falls to a finite value at $q=0$.

In the one-dimensional constant-pressure ensemble there is a first-order dynamic phase transition between equilibrium and inactive phases, equivalent to the transition in the constant-volume ensemble. However the critical bias is $s^*=0$ for all system sizes, unlike the system-size dependence of the constant-volume ensemble. The inactive phase has a higher global density than equilibrium and the dynamically active regime has lower density. The

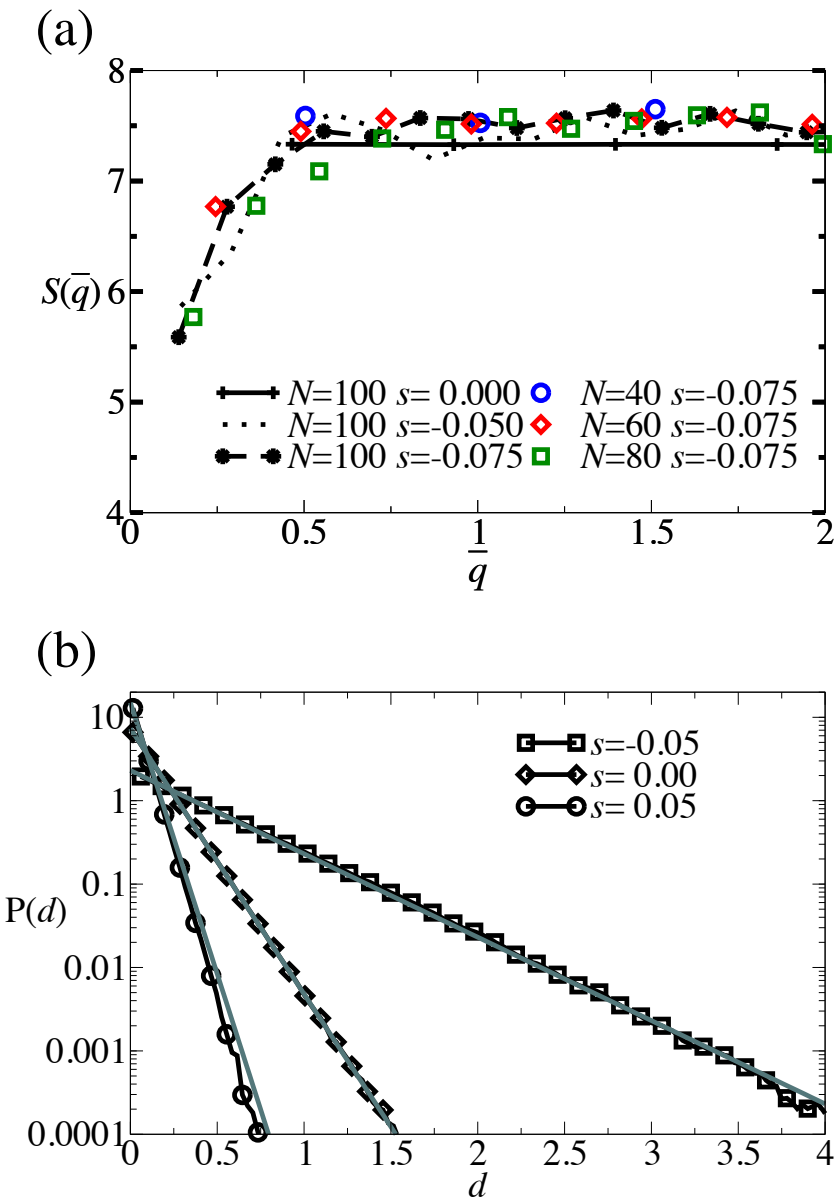

Figure 4.13: (a): Structure factor measurements in the constant-pressure regime when biased to higher than equilibrium activities. There is a suppression of long range density fluctuations as in the constant-density active phase. (b): The distribution of separations for a system of $N = 100$ particles. Symbols represent measured distributions, solid lines are exponential distributions with a mean separation calculated from the mean volume. In all regimes the separations are distributed exponentially and are similar to equilibrium, albeit with a different mean separation.

change in density is maintained through a finite average of a stochastic noise, similar to the constant-volume ensemble. However the forces on individual particles are not biased, instead the noise acting on the system volume is biased through the barostat. As the bias does not act on particles, the change in structure is much weaker in the constant-pressure ensemble compared to the constant-volume ensemble, compare figures 4.8 and 4.13.

4.3.2 Breakdown of ensemble equivalence

The strong correlation between the activity and the density of the system means that in the constant-pressure system the barostat is the dominant mechanism with respect to the system dynamics, hence $s^* \sim N^{-2}$. For the constant density system there is no such mechanism and the structure controls the dynamics, the transition between active and inactive regimes scales as $s^* \sim N^{-1}$. This creates a difference between the two ensembles that is not present in equilibrium systems, the introduction of a new timescale changes the scaling of the transition.

For $s > 0$ the constant-volume system undergoes phase separation and introduces interfaces to create a region of high density. There is a difference in mechanical pressure between the high density cluster and the vapour, the biasing field s creates a net force on the boundary particles that balances the pressure from within the cluster. Normally we would expect the constant-pressure system to remove the interfaces and to sample both the high density and low density regions alternately. However because there is a change in pressure between the two regions then a constant-pressure system cannot sample both regions equally. Instead the system remains in the dense phase for $s > 0$, never sampling the low density vapour, the barostat acts to maintain the high density phase and hence suppress activity. The applied field s causes the stochastic force acting on the barostat η_L to have a finite mean, similar to the effect of s in the constant-volume ensemble.

In the active phase, $s < 0$, the constant-volume system undergoes subtle structural changes to a hyperuniform state. The constant-pressure ensemble achieves higher activity in a different manner, again the barostat is influenced and favours expansion moves over compression. By reducing the density of

the system the average activity is increased without requiring any deviation form equilibrium structure (see Figure 4.2). The increase in activity caused by modification of structure couples more weakly to s than the increase produced by decreasing volume. This is expected as changing the structure requires a series of local particle rearrangements, the required bias must act on each particle and hence is at least $\mathcal{O}(1)$, and the relaxation time is relatively fast. However reducing the density requires only one stochastic force to be biased and the relaxation time τ_{LL} is much longer than the structural relaxation time as shown above.

4.3.3 Fluctuating hydrodynamics

Finally we note that this system can be described using fluctuating hydrodynamics on large length scales[75]. On large length scales the density of a system can be considered as a continuous distribution by coarse graining over particles. In diffusive systems the time-evolution of the density can be expressed in terms of fluctuating hydrodynamics[85]. By considering the density as a locally conserved field the dynamics of the system on long length scales can be written as a Langevin equation like Equation 2.19 with $D[\rho(x,t)]$ a local, instantaneous measure of diffusivity and $\sigma[\rho(x,t)]$ a measure of mobility. The expressions for diffusivity and mobility are model dependent and can include non-equilibrium forces. In this manner fluctuating hydrodynamics can describe the evolution of the density profile for biased and driven diffusive systems.

Eyink showed[86] that for systems in the hydrodynamic limit the density can be described with a dynamic fluctuation-dissipation hypothesis. A variational approach can be used to predict the most probable trajectories of the system either at equilibrium or subject to a constraint. Furthermore a "dynamic potential" can be proposed for non-equilibrium states, which acts analogously to the equilibrium free energy. Fluctuating hydrodynamics have been used to describe the discrete SSEP and calculate the response of the activity to s analytically[21]. The hydrodynamic expression that describes the activity of a diffusive system is valid in all dimensions, provided the system is large enough.

The work in this chapter demonstrates the importance of understanding the roles of different timescales with respect to dynamic behaviour. The existence of a new timescale in the constant-pressure ensemble leads to qualitatively different phase behaviour, $s^* = 0$ for all system sizes and the dynamic transition scales with the volume relaxation time rather than system size. In an equilibrium system the constant-pressure analogue to phase separation is phase switching, where the density of the system alternates between the two coexisting phases. However the inactive system only samples the dense cluster phase, the sparse phase of the phase-separated system is never seen. The biasing of the stochastic forces η_i and η_L maintains the structural constraints that define the dynamic phases: phase separation and hyperuniformity in the constant-volume ensemble: and the change in ϕ in the constant-pressure ensemble.

Chapter 5

Dynamic phase transitions in a three-dimensional system of nearly hard particles

We investigate dynamic phase transitions in a glass-forming binary mixture of spherical particles with contact-only repulsive interactions in the constant volume and constant pressure ensembles. Dynamic phase transitions have so far only been studied in particle systems with power law ranged interactions, we will extend the dynamic transition framework to a new system. The mixture of harmonic particles is known to exhibit glassy behaviour[7] and the low temperature limit is an intuitive approach to considering the hard sphere limit of particle behaviour. The behaviour of the harmonic system has been studied with respect to packing fraction and the relaxation time appears to diverge at a lower packing fraction than the pressure, suggesting that the glass transition occurs before jamming[7]. By comparing the constant-volume and constant-pressure ensembles we will investigate dynamic ensemble equivalence in three-dimensional systems, and whether allowing the density to fluctuate will lead to the inactive phase spontaneously increasing in density to ϕ_G.

Previous studies of the binary Kob-Andersen (KA) glassforming mixture[14], using the s-ensemble formalism described above, have shown a first order dynamic phase transition separating equilibrium trajectories and "inactive"

glassy trajectories. Work by Hedges et al.[13] in the constant-volume ensemble examined the first-order behaviour of the transition and characterised the scaling behaviour with respect to the observation time t_{obs}. They found coexistence between active and inactive trajectories occurred at a finite value of $s^* \propto t_{\text{obs}}^{-1}$ and the transition between K_{active} and K_{inactive} was consistent with a first-order dynamic transition in a system with space-time volume Nt_{obs}. The inactive phase was characterised by lower potential energy and a lack of structural change (as measured by pair correlation functions), relative to the active phase.

Kinetically constrained models (see section 2.3) with hard constraints have a dynamic transition at $s = 0$, coexistence occurs at equilibrium. Work by Elmatad et al.[32] studied the East model with softened dynamic constraints and found that the transition between active and inactive phases moved to $s > 0$. They showed that the first-order transition line terminated in two finite-temperature critical points and extended the framework of kinetically constrained models to thermal soft systems. It is discussed that the low temperature critical point may be hard to observe in particle systems as supercooling the system to such low temperatures is difficult.

At sufficiently high temperatures the dynamic constraints become effectively weak enough that the correlations are diminished and a dynamic transition does not occur. The equilibrium dynamics of the system correspond to the active phase, with the size and duration of inactive fluctuations depending upon the free energy difference and surface tension between phases (as described in subsection 2.3.1). As $s \to s^*$, the typical size and duration of inactive space-time bubbles in trajectory space increase until at s^* the system undergoes a first-order dynamic transition between active and inactive phases.

The work of Hedges et al. used the same definition of the activity as Equation 2.11, which is sensitive to motion on length scales that contribute to structural relaxation. The same transition is observed with other dynamic order parameters, Speck & Chandler[17] showed the same phase behaviour in the KA mixture using an order parameter that measured the density of "active" particles over time. The inactive phase is characterised by a reduction in the density of active particles and a reduction in energy, in

contrast to Hedges et al., Speck & Chandler measured a change in local structure across the transition. Work on the KA mixture and the softened East model showed finite-size scaling of the transition with respect to N and t_{obs} that was consistent with a first-order transition.

Widmer-Cooper et al.[34] showed that dynamic heterogeneities are reproducible for a given configuration, they are centred around certain local structures. The structure of a configuration can predict the spatial variations in particle dynamics, although it cannot predict the dynamics themselves. That the spatial distribution of active regions is structurally defined allows one to consider the spatial density of localised excitations as a structural property. The concept of dynamic behaviour being dominated by localised excitations was discussed by Garrahan & Chandler[49]. Garrahan & Chandler considered dynamic heterogeneity as evidence of localised dynamic excitations that facilitated structural relaxation and found that they could describe the behaviour of supercooled glass-formers approaching T_g in trajectory space. They were able to describe the super-Arrhenius increase in structural relaxation time of glass-formers, and the accompanying increase in specific heat capacity, without an underlying thermodynamic transition.

Speck & Chandler[17] attributed structural relaxation to active particles in the KA mixture, these particles act as localised excitations and facilitate local dynamics. The presence of these excitations allow cooperative particle motion and large scale relaxation events that move the system from one inherent structure energy basin to another. In this picture structural relaxation is not dominated by thermal crossing of energy barriers but through rare collective motion, transitions between structural energy minima become super-Arrhenius with respect to temperature in fragile glass-forming systems. The relative dearth of excitations in the inactive phase means that particles remain in the same inherent structure and vibrate about fixed positions, in this manner Speck compares the inactive phase to jammed states.

Returning to the work of Sir Charles Frank and the relationship between local structure and the dynamic behaviour of glassy systems Speck et al.[18] found the same transition between active and inactive trajectories could be driven by a dynamic chemical potential coupled to a specific local structural ordering. Using the number of particles within $11A$ clusters as a dynamic

order parameter they drove the system from the equilibrium state to an inactive state with a higher number of $11A$ clusters. The extent to which this finding depends upon the specifics of the KA system is unknown as the order parameter requires a prior choice of a local cluster. However the relationship between dynamics and short-range structure gives an intuitive physical insight into the transition. The concept of a relatively stable amorphous order in the inactive phase will be discussed further below.

All of the work discussed above focusses on the KA mixture, a supercooled soft particle system with attractive interactions that decay as a power law. The reduction in potential energy in the inactive phase means a more stable structure over the interaction length scale, with or without longer range ordering. We focus on a nearly-hard system of repulsive particles, the range of local interactions between particles is reduced and particles can only interact through contact. Previous work on repulsive sphere mixtures have suggested that glassy behaviour can lead to a finite range of packing fraction where jamming occurs[19]. The packing fraction of the binary system is defined as:

$$\phi = \frac{N\pi}{12V}\left(\sigma_A^3 + \sigma_B^3\right) \tag{5.1}$$

where V is the volume of the system, σ_i is the diameter of species i and there is an equal number of A and B particles.

We will study the system in both the constant-pressure and the constant-density ensembles, and investigate the properties of ensemble equivalence with respect to a dynamic transition. By allowing the volume of the system to change we will investigate whether the change in energy between the phases is accompanied by a change in density. We will work at sufficiently low temperatures that increasing the density is a sufficient control parameter to drive the system from equilibrium fluid behaviour to configuration with diverging τ_α at ϕ_G. By choosing a value for the equilibrium density, ϕ_0, that is close to the onset of glassy behaviour, and allowing the density of the system to change, we will investigate if inactive states of the constant pressure system change so that $\langle\phi\rangle_{\text{inactive}} > \phi_0$ and if $\langle\phi\rangle_{\text{inactive}} = \phi_G$.

To investigate possible links between jamming and glassy behaviour we will also take equilibrium and inactive configurations and subject them to

a jamming protocol. We will compare the packing fractions of the jammed states to see if inactive configurations achieve higher final packing fractions compared to equilibrium, and if there is a inherent link between glassy and jammed configurations.

5.1 Description of the model

We study a binary mixture of N harmonic particles undergoing Brownian motion in a three dimensional system with periodic boundary conditions at temperature $k_{\mathrm{B}}T = 1$. The particle mix is an equal number of A and B particles with size ratio $\sigma_B = 1.4\sigma_A$. The particle motion is described by the Langevin equation:

$$\dot{\vec{r_i}} = -\frac{D_p \nabla U}{k_B T} + \sqrt{2D_p}\vec{\eta_i}(t) \tag{5.2}$$

as in Equation 4.1. The noise obeys:

$$\left\langle \eta_i^{\alpha}(t)\eta_i^{\beta}(t') \right\rangle = \delta(t-t')\delta_{ij}\delta_{\alpha\beta} \tag{5.3}$$

where α and β are cartesian components of the vector $\vec{\eta}$.

The interaction potential between particles is:

$$U(r_{ij}) = \begin{cases} \epsilon\left(1 - \frac{r_{ij}}{\sigma_{ij}}\right)^2, & \text{if } r_{ij} \leq \sigma_{ij} \\ 0, & \text{otherwise} \end{cases} \tag{5.4}$$

where $\sigma_{ij} = (\sigma_i + \sigma_j)/2$. Figure 5.1 shows $U(r_{ij})$ for the system.

We work at low temperatures, $k_{\mathrm{B}}T = 10^{-5}\epsilon$, similar to the work of [19]. We will use transition path sampling and the s-ensemble to investigate possible inactive states at $s > 0$. We measure the activity and average energy of trajectories, as well as the average volume in the constant pressure ensemble. The virial pressure is used to calculate the instantaneous pressure of the systems, defined as[87]:

$$P(\mathcal{C}) = \frac{N k_{\mathrm{B}} T}{V} - \frac{1}{3V}\sum_{i=0}^{N}\sum_{j=i+1}^{N} r_{ij}\frac{\partial}{\partial r_{ij}}U(r_{ij}) \tag{5.5}$$

We will work at a constant volume such that $\phi = 0.57$ and a constant pressure $P = 11.50$ so that $\langle\phi\rangle_0 = 0.57$ (see Figure 5.2).

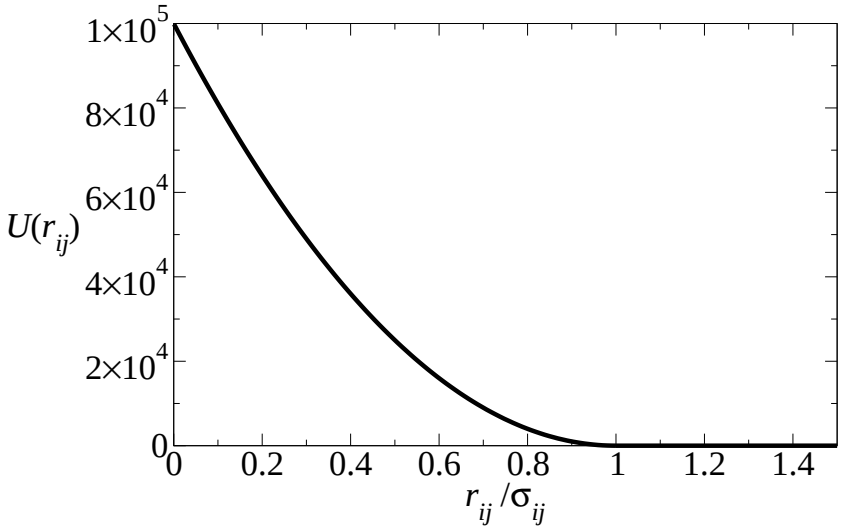

Figure 5.1: A plot of the harmonic potential with $\epsilon = 10^5$, the potential is purely repulsive for overlapping particles.

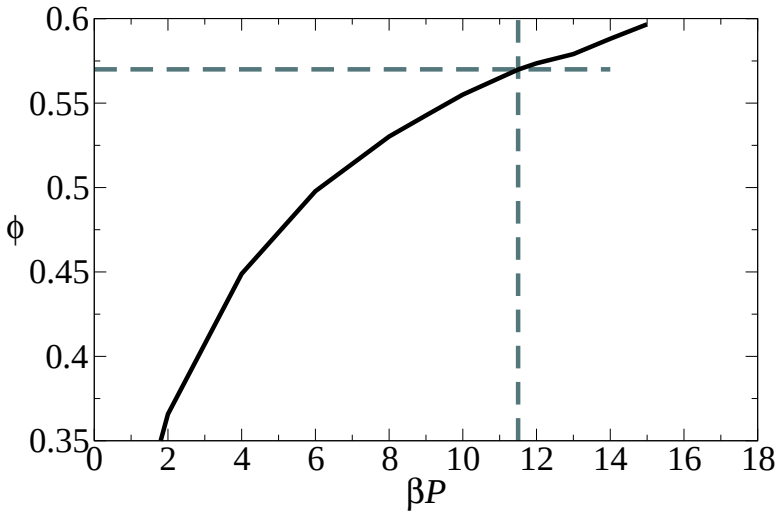

Figure 5.2: A plot of the equation of state for three-dimensional harmonic sphere system at $k_{\mathrm{B}}T = 10^{-5}$. We simulate constant volume systems at $\phi = 0.57$ and constant pressure systems at $P = 11.5$.

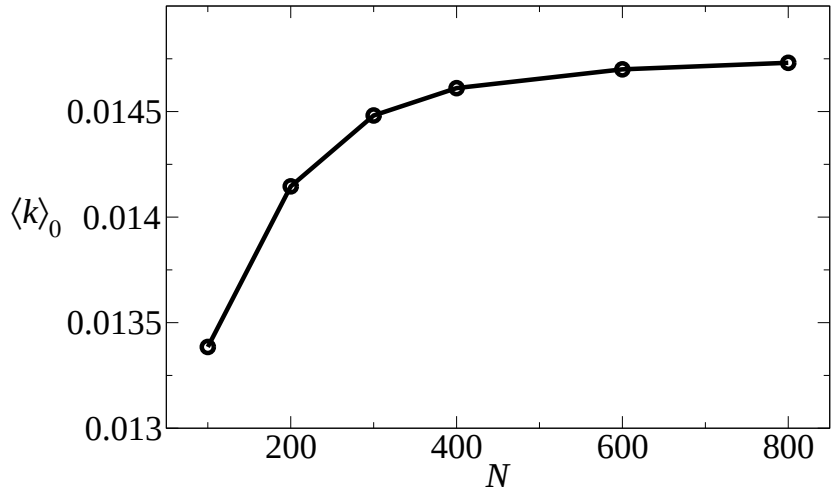

Figure 5.3: The intensive activity of the three-dimensional constant volume system at $\phi = 0.57$ and $t_{\text{obs}} = 1200\tau_{\text{B}}$. The intensive activity has a finite size dependence on N that saturates as $N \to \infty$.

In our system there is a small increase in the intensive activity at equilibrium ($\langle k \rangle_0$) with N, and the effect weakens as N increases, see Figure 5.3 and recall the definition of k in Equation 2.13. Although ϕ is fixed in all of these systems there is an increase in absolute system size, hence longer wavelength vibrational modes can be sustained, causing a higher activity. As this finite-size correction to k is due to a dynamic length scale present at equilibrium, we expect it to exist under all values of s. As $N \to \infty$ the intensive activity of trajectories with space-time volume Nt_{obs} will self average and the variance in k over an ensemble of trajectories will reduce.

5.2 Three-dimensional constant-volume ensemble

First we address the dynamic transition in the binary harmonic sphere system at constant-volume. We used biased transition path sampling of the system to generate trajectories with fixed t_{obs} and measure the distribution of K under several values of the bias s. There is a first order transition in k

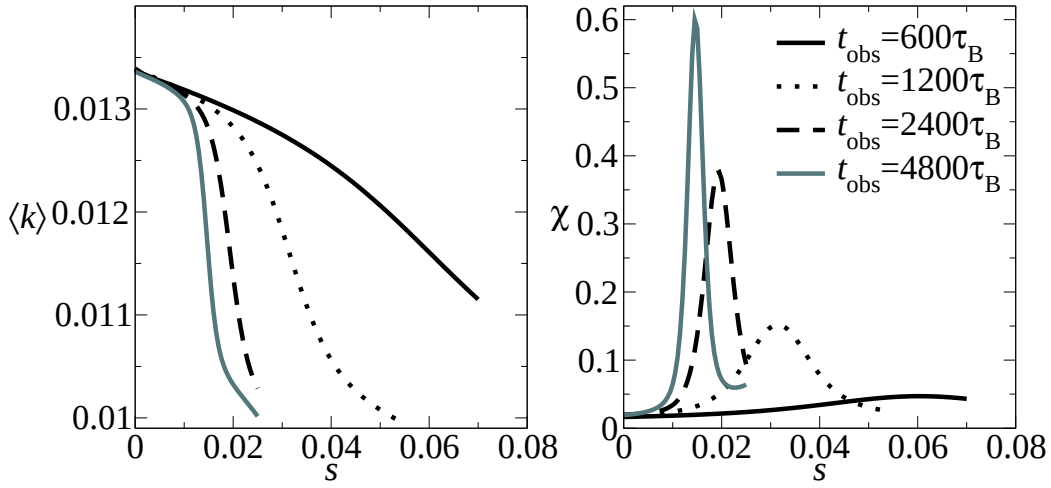

Figure 5.4: The dynamic phase behaviour of a constant volume three-dimensional systems with $N = 100$, $\phi = 0.57$. (a) The first-order transition in the activity shows a finite value for $s^* \propto \frac{1}{t_{\text{obs}}}$. (b) The peak in the susceptibility χ^* increases with t_{obs}.

between equilibrium and inactive trajectories at a finite value of $s^* > 0$. Figure 5.4 shows the average intensive activity of trajectories under different values of s at a constant system size $N = 100$ for a series of observation times. The value of s^* decreases with increasing t_{obs}, and χ^* increases as expected for a first-order transition. The equilibrium activity, $\langle k \rangle_0$ is constant with respect to observation time at fixed N.

Figure 5.5 shows the distribution $\boldsymbol{P}_s(k)$ for constant volume systems, with $N = 100$ and $t_{\text{obs}} = 1200\Delta t$, at equilibrium and near s^*. The sampled distribution at $s = 0.03 \simeq s^*$ is bimodal, consistent with a first order transition. Using WHAM (see section 3.4) we can reconstruct the distribution of the activity at a given value of s. From Figure 5.4 we can extract $\chi^* \equiv \chi(s = 0.033)$ and reconstruct the bimodal histogram $\boldsymbol{P}_{s^*}(k)$. The distribution $\boldsymbol{P}_{s^*}(k)$ has equal weight in the two peaks, k_{active} and k_{inactive}.

In accordance with a first-order phase transition the distribution of the order parameter becomes bimodal around s^*. Measurements of $\boldsymbol{P}_s(k)$ show

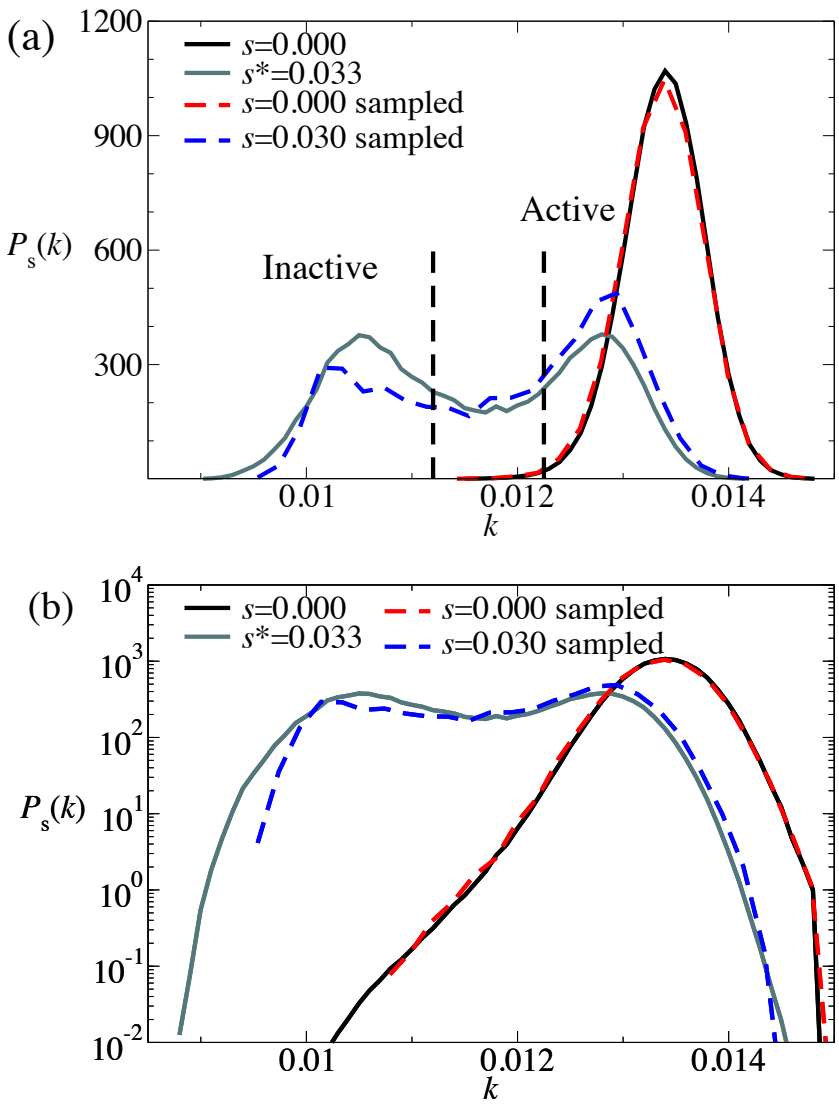

Figure 5.5: The distribution of activity for the three-dimensional system in the constant volume regime with $N = 100$ and $t_{\text{obs}} = 1200\Delta t$. Sampled distributions (shown with dashed lines) are measured directly from simulations at fixed s, other distributions are reconstructed using WHAM (solid lines). (a) The distribution on a linear scale showing the sampled bimodal distribution near s^*, and the reconstructed $\boldsymbol{P}_{s^*}(k)$. The bimodal distribution can be split into three sections, inactive, active and mixed trajectories. (b) The same distributions plotted on a logarithmic scale show the reconstructed histograms, the reconstructed equilibrium distribution shows the non-Gaussian feature of a nearby phase transition.

coexistence of two dynamic phases at s^*, the region between the active and inactive peaks represents the overlap of the two distinct distributions. The ratio between the maximum height of the peaks and the height of the trough between them is a measure of how well the two phases are separated, and how sharp the transition between the two is. As $t_{\text{obs}} \to \infty$ at s^* and fixed N the intensive activity of a trajectory self-averages over short-time fluctuations, reducing the variance in the order parameter. By reducing the variance of the individual active and inactive distributions the overlap shrinks and the two distributions become more distinct. Longer observation times mean that the dynamical free energy barrier between the phases increases, and the probability of a system switching from one phase to another decreases[46].

To examine how the transition scales with system size and observation time we show the same transition in systems with different values of Nt_{obs} in Figure 5.6. For all systems $s^* \propto t_{\text{obs}}^{-1}$ and $\chi^* \propto t_{\text{obs}}$ at fixed N, this agrees with the observation time scaling found in the Kob-Andersen mixture. χ^* increases with N at fixed t_{obs} however doubling t_{obs} produces a larger change in χ^* than doubling N. This also suggests that long lived fluctuations in the activity have a larger effect on the variance of k than the possibility of large scale collective motion. To satisfy the long-time limit, the observation time must be long enough that any structural fluctuations have time to relax.

We measure the average time integrated energy of trajectories from across the dynamic regime and see a decrease in potential energy for the inactive trajectories. Figure 5.7 shows that there is a change in potential energy between the equilibrium and inactive trajectories, as interactions are contact only this means that there is a reduction in the average number of overlaps per particle. The change in energy is concomitant with the change in activity, the value of s where the change occurs and the relative sharpness of the change is similar to that of the activity.

Previous studies of the KA glass former found the inactive phase had a lower potential energy relative to the equilibrium system[13, 17]. The lower potential of the inactive phase reflects the increase in structural stability of the inactive phase relative to the equilibrium system.

We performed finite-size scaling of the transition with respect to N and t_{obs}. The effect of system size on coexistence is shown in Figure 5.8(a), there

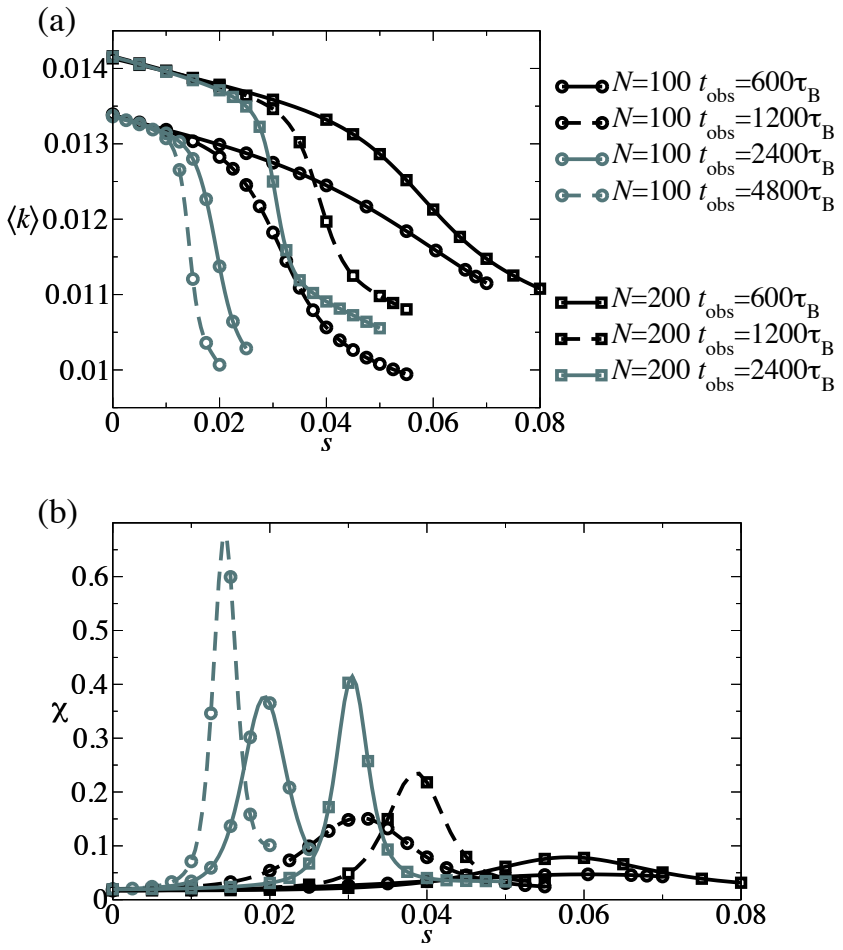

Figure 5.6: The scaling of the dynamic phase transition in the three-dimensional constant volume system. (a) There is a slight increase in the equilibrium activity with N, consistent with Figure 4.2. The transition occurs for all system sizes and Δk is constant, but the position of s^* is more sensitive to changes in $t_{\rm obs}$ than in N. (b) The value of χ^* increases with $t_{\rm obs}$ as expected, at fixed $t_{\rm obs}$ χ^* increases with N. However the scaling is stronger with respect to $t_{\rm obs}$.

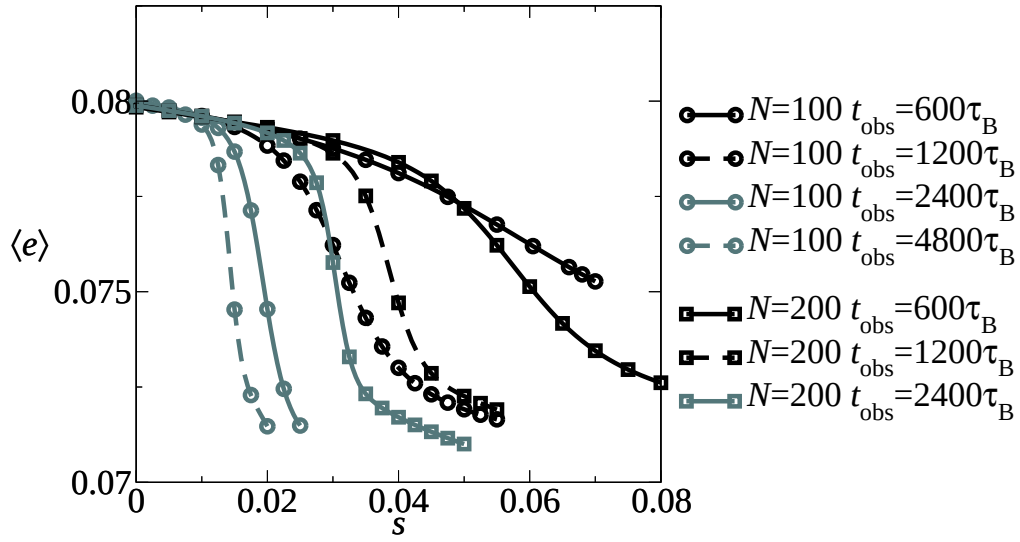

Figure 5.7: The average time integrated energy per particle, e, for $N = 100$ and $N = 200$ and different t_{obs}, the energy of the inactive phase is lower than that of the equilibrium system. The intensive energy of the two phases is constant with respect to N.

is a small shift in k due to the increase in system size. Not only is the value of the activity in each phase different between the two systems, the difference in activity between the two phases Δk changes with respect to N. In the $N = 200$ system Δk reduces by 7% compared to the $N = 100$ system. Doubling the system size increases the peak to trough ratio from 2.35 to 5.04, the change is linear with N, however for large N the scaling should go as $N^{2/3}$ (see section 2.3.1). This may be due to the relatively small system size and for large N the correct scaling may emerge. Figure 5.8(b) shows the scaling of $\boldsymbol{P}_{s*}(k)$ with observation time, the intensive activity of the two phases remain constant with respect to t_{obs}. The separation Δk increases with respect to t_{obs} by 20%. The peak to trough ratio increases with t_{obs}, doubling the observation time increases the ratio from 2.35 to 5.28, a linear scaling with t_{obs}. We conduct more detailed finite-size scaling and consider the non-linear scaling of Δk in section 5.3.

The three-dimensional constant-volume system of harmonic spheres exhibits a dynamic phase transition similar to the KA mixture discussed above. The inactive phase has a lower energy than the equilibrium phase and the transition is at a finite bias s^* that reduces with increasing t_{obs}. The separation between the active and inactive phase is not fixed with respect to N or t_{obs}, Δk reduces with increasing system size and increases with increasing observation time. The scaling of the change in the average energy per particle is consistent with the scaling of the activity. The total change in energy ΔE is larger for longer observation times at fixed N, and the sharpness of the change increases with both N and t_{obs}.

The increase in Δk with increasing observation time is consistent with finite-size scaling for relatively small systems, as the peak to trough ratio increases then the separation between the two peaks increases. The position of the active and inactive peaks are fixed, and Δk is constant in the limit $Nt_{\text{obs}} \to \infty$. However in finite systems there is an overlap of the active and inactive distributions, and the position of the two peaks becomes closer together. As the peak to trough ratio increases more of the total distribution contributes to the active or inactive distributions and thus each peak moves closer to the value of the activity at $t_{\text{obs}} \to \infty$ and Δk increases. Thus we expect Δk to increase with the peak to trough ratio and to saturate in the

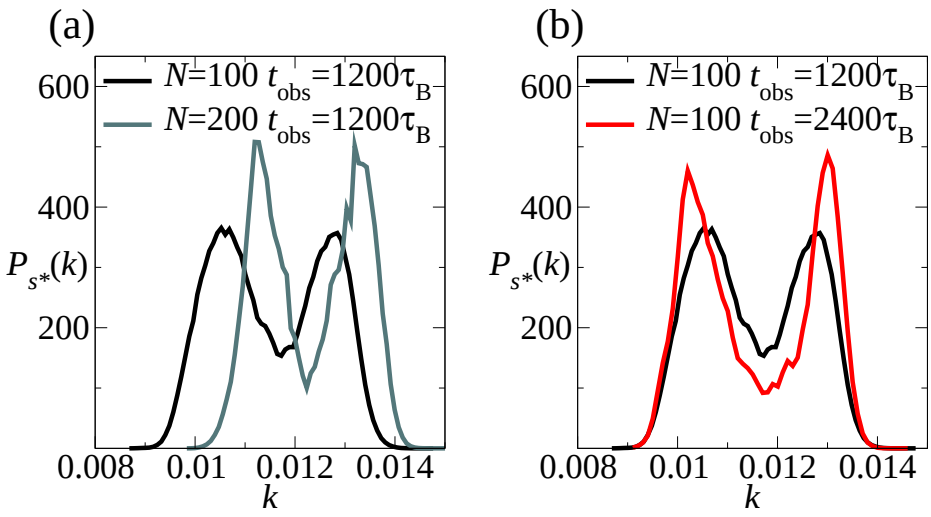

Figure 5.8: Finite-size scaling of the bimodal probability distribution $\boldsymbol{P}_{s*}(k)$ in the constant-volume three-dimensional system. The separation between peaks Δk changes with N and t_{obs}. (a) As N increases there is a constant increase in k due to the increase in the largest available vibrational mode (as discussed above). The peak to trough ratio of the bimodal distribution is greater for the larger system and Δk reduces by 7%. (b) As t_{obs} increases the peak to trough ratio of the distribution increases and Δk increases by 20%.

thermodynamic limit.

However we also find that the separation between peaks reduces with increasing system size at fixed t_{obs}, even as the peak to trough ratio increases. There is an increase in the equilibrium activity for larger systems which is attributed to larger modes of vibrational motion becoming sustainable in the system. In the context of cooperative motion this means that relaxation events can involve more particles and also that relaxation events of a fixed size are more likely to occur in the system. In section 6.1.1 we show that for larger systems the inactive phase melts back to equilibrium faster, this suggests that the inactive phase becomes less stable as system size increases and we propose an explanation below. A reduction in stability would lead to a decrease in Δk as system size increased. We conduct a more detailed finite-size scaling analysis in section 5.3.

5.3 Three-dimensional constant-pressure system

We have seen in the one-dimensional system that the equivalence between constant-volume and constant-pressure ensembles is changed in the dynamically inactive phase. At equilibrium, phase separation in a constant-volume ensemble corresponds to spontaneous switching in the constant-pressure ensemble, and avoids the formation of interfaces. As seen in chapter 4 this is not always true in non-equilibrium systems, the presence of driving forces in the constant-volume system can cause a difference in pressure between the two coexisting phases. Thus the constant-pressure system cannot sample the two phases equally and still maintain a constant pressure.

However the three-dimensional constant-volume system does not phase separate, so there are no interfaces to remove, hence one expects stronger ensemble equivalence. The freedom of the density to fluctuate means that the system can increase local density, which is known to increase glassy behaviour in harmonic systems[19]. The constant-volume dynamic transition case is driven by a subtle change in the underlying structure to a more inherently stable state that can sustain thermal vibrations – a glassy state. The role that the density will play in the transition to a glassy state is unknown, all previous work has focussed on the constant-volume ensemble. The same transition could occur equally in both ensembles and maintain ensemble equivalence trivially; or the system could be driven to a higher density and break ensemble equivalence by only sampling a dense phase in the same manner as the one-dimensional system.

The barostat in the three-dimensional system follows the common practice of attempting a change in system volume one average every N attempted particle moves[88]. Thus the timescale of the barostat is not attributed to a diffusion mechanism within the system, but instead scales linearly with τ_{B}. The value of the maximum volume change, Λ_V^2, is chosen to be $(5 \times 10^{-4})V$ so that at equilibrium the volume fluctuates smoothly and the average acceptance ratio is sufficient to maintain $\mathcal{P} = P$ (see subsection 3.1.3).

We choose a pressure ($P = 11.5$) that corresponds to an $\langle\phi\rangle = 0.57$ so the unbiased ensembles of trajectories will be equivalent. we will bias the system using s as described above and look for a first-order transition to a

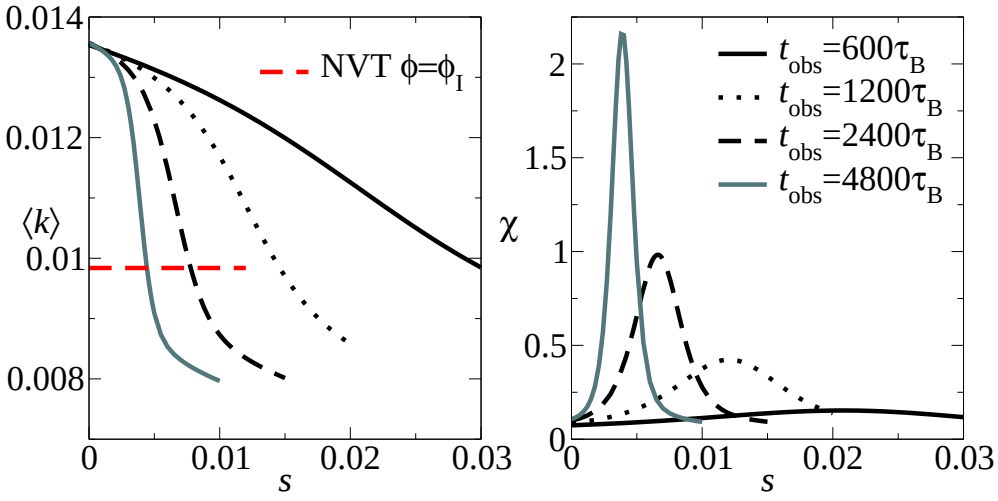

Figure 5.9: The dynamic phase behaviour of the constant pressure system is very similar to the constant volume system (Figure 5.4) but the range in s is greatly reduced. There is a first order transition in the activity at a finite s^* that reduces with increasing t_{obs}. The red line is the equilibrium activity of a constant density system at an equal density (ϕ_{I})to the inactive phase (see below). The peak in susceptibility increases linearly with t_{obs} as expected from a first-order transition.

dynamically inactive phase. We will investigate the finite-size behaviour of the transition and characterise the inactive state, paying particular attention to the density.

The equilibrium value of $\langle k \rangle$ is equal in both ensembles as expected and the first-order dynamic phase transition occurs at a finite value of $s > 0$. Figure 5.9 shows the transition for $N = 100$ spheres and $t_{\text{obs}} = 600\tau_{\text{B}}$. The dashed red line in the figure is the average equilibrium intensive activity for a constant volume system at a density equal to the inactive phase of the constant pressure system. The constant pressure system still has a lower value for the activity, thus the inactive phase is characterised by more than just an increase in the average density of trajectories.

Figure 5.10 shows the transition for $N = 100$, $= t_{\text{obs}} = 2400\tau_{\text{B}}$ in both

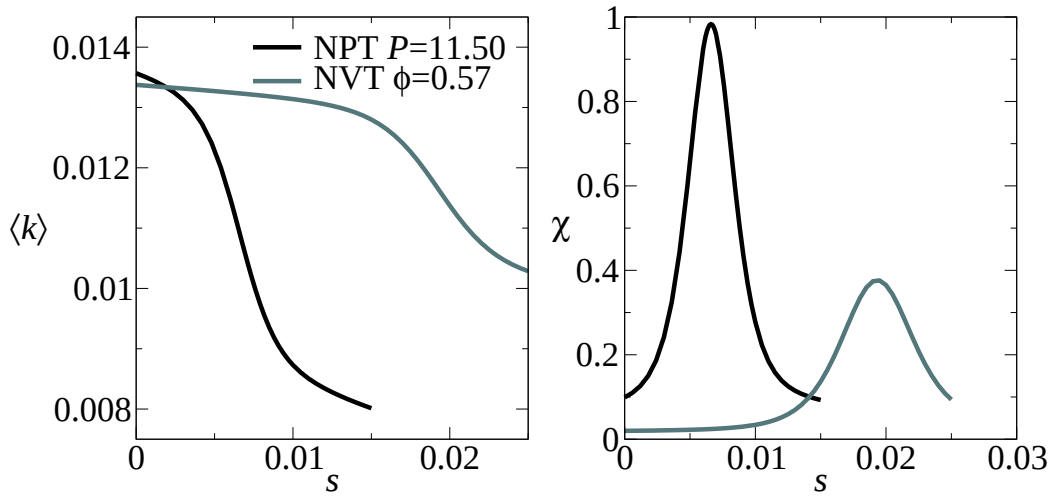

Figure 5.10: The dynamic phase transition in the constant pressure and constant volume ensembles for $N = 100$ and $t_{\text{obs}} = 2400\tau_{\text{B}}$ reproduced to allow direct comparison. The constant pressure system exhibits a lower activity in the inactive phase and the critical bias is reduced relative to the constant volume system, hence the constant pressure inactive phase is more stable.

the constant pressure and constant volume ensembles for ease of comparison. The critical bias is reduced in the constant-pressure ensemble relative to the constant-volume ensemble, $s_P^* < s_V^*$, for all values of N and t_{obs} studied. Furthermore the activity in the inactive phase, k_{inactive}, is smaller in the constant-pressure ensemble. Allowing the density of the system to change means that the system can access a relatively more inactive regime closer to equilibrium.

The sampled probability distribution from equilibrium is Gaussian near its peak, and close to s^* the distribution becomes bimodal, see Figure 5.11, consistent with a first-order transition in the activity. Using all of the sampled distributions and estimating the distributions using WHAM allows us to reconstruct the distributions $\boldsymbol{P}_{s^*}(k)$ and the equilibrium probability of inactive states at equilibrium. The non-Gaussian behaviour of the reconstructed

equilibrium distribution shows inactive trajectories can exist at equilibrium albeit very rarely.

The system size scaling of the intensive activity is consistent with a first-order transition, Figure 5.12 shows the transition for all values of Nt_{obs} sampled. The value of s^* decreases and χ^* increases with increasing t_{obs}. The value of $k(0)$ increases slightly with N, this is the same finite-size effect seen in Figure 5.3.

The scaling of s^* and χ^* with t_{obs} at fixed N is consistent with a dynamic first-order transition in an observable that is extensive in time. The scaling with system size is different however, the position of s^* does not change, although the transition becomes sharper and χ^* increases. The fact that s^* is effectively independent of N suggests that the transition requires a bias proportional to N, hence all particle motion requires an applied bias. The scaling of s^* and χ^* is qualitatively the same in both three-dimensional ensembles. This is in contrast to the one-dimensional constant-pressure system which required only a single stochastic force to be biased and hence $s^* = 0$ independent of system size.

We expect the differences in the dynamic transition between the two ensembles to be due to the system's ability to change the global density. Figure 5.13 shows the change in the average density of the system across the dynamic transition, there is a change in the system density that scales with observation time like k. The inactive phase is consistently more dense than the equilibrium system, the change in density remains constant with system size, as expected for an intensive observable. The volume relaxation time (λ^{-1} see section 3.1.3) is proportional to N^{-1} and so the effect of the barostat, and the change in density, depends only upon t_{obs}. This agrees with the independence of s^* and N, the change in density only depends upon the length of t_{obs} relative to the barostat time. The change in density is small and ϕ_{inactive} is far from any suggested ϕ_J or ϕ_{GCP} for the system, predicted at $\phi \simeq 0.64$, however the increase in density is consistent with an increase in glassy dynamics[19]. Even as $Nt_{\text{obs}} \to \infty$ there is no evidence that the system will adopt jammed states in the ensemble of biased trajectories.

Comparing the change in density between the equilibrium and inactive phases $\Delta\phi$ we see a change in the finite-size scaling. The dependence of $\Delta\phi$

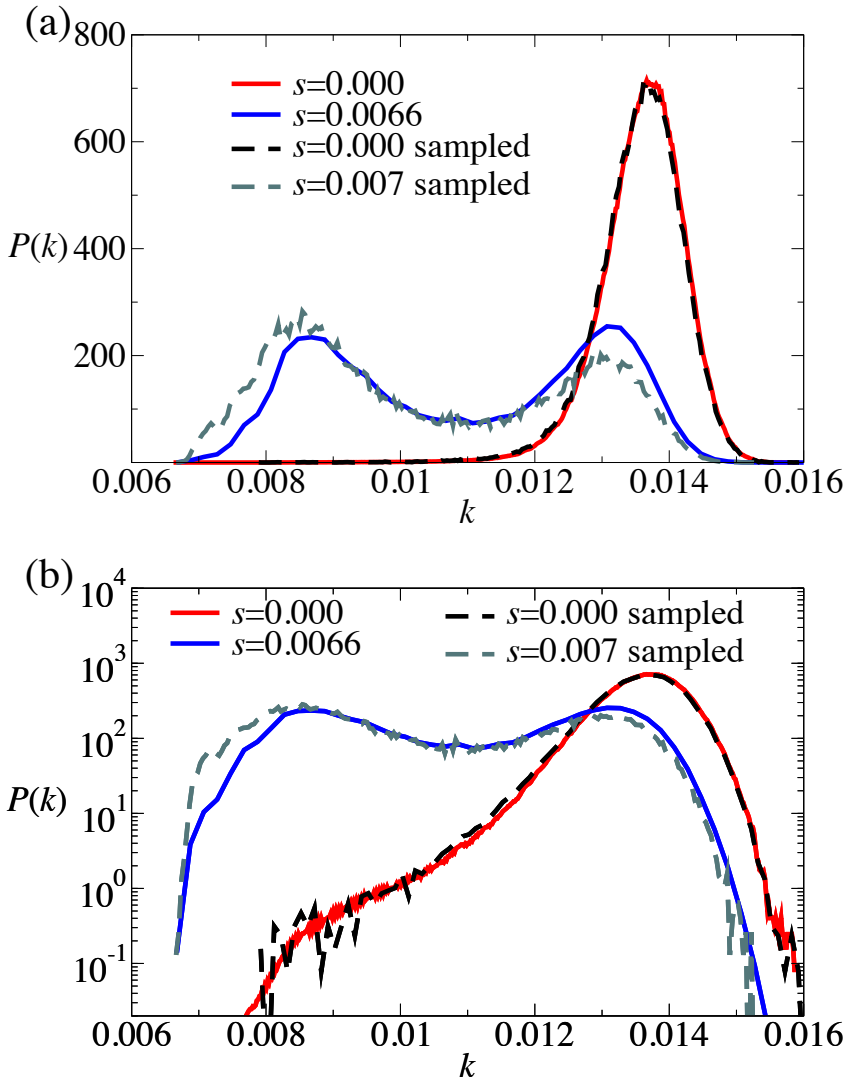

Figure 5.11: The probability distributions $\boldsymbol{P}_s(k)$ for the three-dimensional constant pressure system with $N = 100$, $t_{\text{obs}} = 2400\tau_{\text{B}}$. (a) Sampled distributions are collected at equilibrium and close to s^*, the distributions at equilibrium and coexistence ($s^* = 0.0066$) were estimated using WHAM. (b) The reconstructed equilibrium distribution shows a strong non-Gaussian tail towards the inactive phase, indicative of a first-order phase transition.

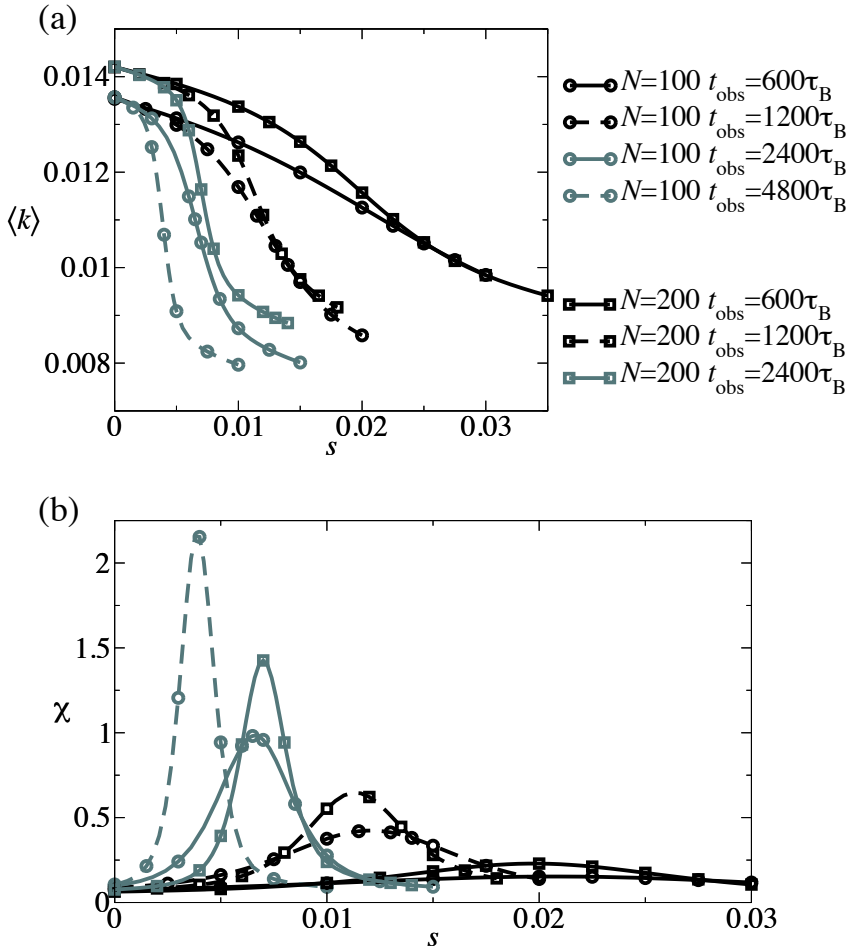

Figure 5.12: Finite-size scaling of the dynamic transition in the three-dimensional constant-pressure system. (a) The value of s^* is inversely proportional to $t_{\rm obs}$ at fixed N, but remains constant with changing N at fixed $t_{\rm obs}$. There is a slight discrepancy in $k(0)$ for different system sizes. (b) Again the value of s^* is independent of N, but the value of χ^* increases with N at fixed $t_{\rm obs}$ due to the relative duration of $t_{\rm obs}$ compared to τ_{VV}.

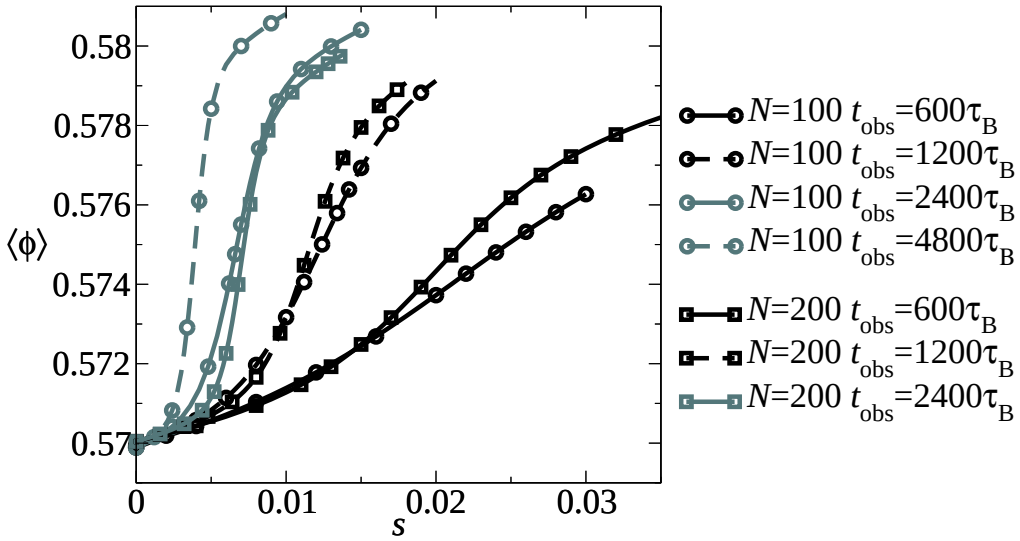

Figure 5.13: The average packing fraction of constant pressure systems at different $Nt_{\rm obs}$. All systems exhibit an increase in packing fraction in the inactive phase, and the increase scales strongly with observation time at fixed N. Note that the smaller system size shows a much larger increase in ϕ with increasing $t_{\rm obs}$.

on t_{obs} at fixed N is much stronger for the smaller system. The maximum volume change for a single Monte Carlo volume move is a fixed fraction of the current system volume and the rate of volume moves is fixed as N^{-1} (see section 3.1.3), this means that the barostat of the larger system is twice as fast as the smaller system. Compare the two system sizes for $t_{\text{obs}} = 600\tau_{\text{B}}$ and $t_{\text{obs}} = 2400\tau_{\text{B}}$, for the longer observation time the smaller system is consistently at a higher density, while for the shorter observation time the larger system is denser. The faster barostat means that high density configurations are less stable and are more prone to relaxation in larger systems.

To investigate the effect of the change in density we compare the activity of the inactive, constant pressure system with an equilibrium constant volume system at equivalent ϕ. We choose the $P = 11.50$, $N = 100$, $t_{\text{obs}} = 2400\tau_{\text{B}}$ constant pressure system for comparison and measured the density of the inactive phase as $\phi_{\text{I}} = 0.5804$. We simulated a constant volume system at $\phi = \phi_{\text{I}}$ with equal N and t_{obs}, this is shown in Figure 5.9(a) and the activity of the equilibrium system is higher than the inactive constant pressure system. This shows that the inactive phase is not just caused by an increase in density, the inactive phase is not equivalent to an equally dense equilibrium state. There is a further cause for the reduction in activity due to changes in structure. If dynamic activity is linked to glassiness then the dynamic bias is more effective at producing glassy states than the change in density alone.

There is a strong correlation between the activity of a trajectory and the average time-integrated density of a trajectory. Figure 5.14 shows the correlation between k for a trajectory and the packing fraction of the middle configuration ϕ, the points are drawn from the equilibrium distribution, an active distribution sampled from $s \simeq s^*$ and an inactive distribution sampled at $s > s^*$. The distribution near co-existence is over a broad range of activity and density and there is a strong correlation between the two observables across the entire range. The width of the density distribution is fixed for all values of k, the correlation between activity and density is very strong, compare to the relatively weak correlation between k and energy in [13].

The finite-size scaling of $\boldsymbol{P}_{s*}(k)$ is shown in Figure 5.15, the bimodal

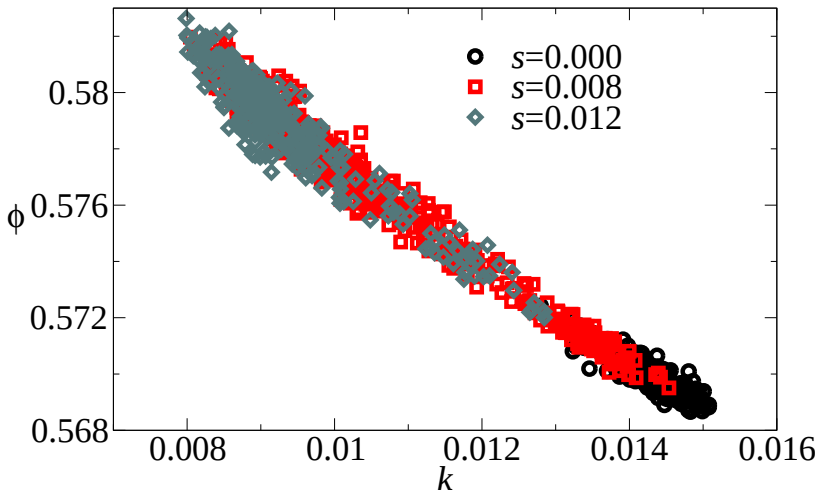

Figure 5.14: Activities and time integrated densities from trajectories sampled, $s = 0.008$ which is close to $s^* = 0.0073$ and $s = 0.012$. There is a strong correlation between the two observables at all values of s. The width of the distribution of ϕ does not change with s.

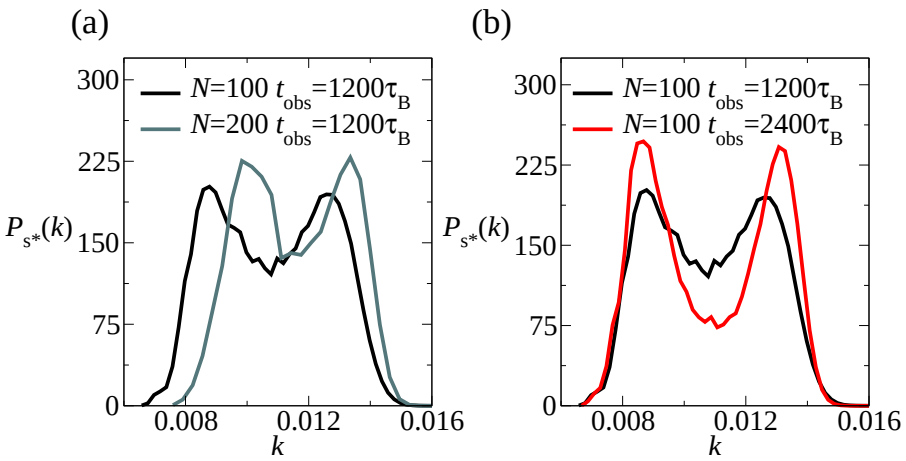

Figure 5.15: The bimodal probability distributions of the three-dimensional constant-pressure system. (a) As system size is increased there is a small increase in k as discussed in the main text. Doubling the system size causes the separation Δk to become smaller by 16%. (b) As the observation time is increased at fixed $t_{\rm obs}$ the peak to trough ratio of the histogram increases and Δk increases by 20%.

histogram is shown for different system sizes and observation times. We use the difference between the two peaks Δk to quantify the scaling behaviour of the transition. As system size is increased the separation becomes smaller (by 13%) and the separation becomes larger (by 15%) as $t_{\rm obs}$ is increased, this is the same qualitative behaviour as the constant-volume ensemble.

Finite-size scaling of the transition is shown in Figure 5.16, we measure the critical bias, s^*, and the peak in the susceptibility. The value of s^* scales inversely with $t_{\rm obs}$ and remains constant with changing N, if we extrapolate to the limit $t_{\rm obs} \to \infty$ then we can see $s^* > 0$. The dotted lines in Figure 5.16(b) show the linear scaling of χ^* with $t_{\rm obs}$ at fixed values of N, the three system sizes shown have a different gradient for the scaling. The thin lines in Figure 5.16(b) show system size dependence at fixed $t_{\rm obs}$, there is a sub-linear dependence of χ^* with system size, suggesting that the extent in space and the extent in time are not equivalent. The slower behaviour of χ^* with respect to system size is linked to the narrowing of $\boldsymbol{P}_{s*}(k)$ with respect

to N.

By allowing the density of the system to fluctuate the constant-pressure ensemble shows a change in the dynamic transition, s^* reduces and there is a change in the density concurrent with the activity. The inactive phase of the system increases in density to $\phi \sim 0.58$, although it is not the sole cause of lower activity, an equilibrium system with $\phi = 0.58$ has a larger activity.

We have performed finite-size scaling of the dynamic transition in figures 5.8, 5.15 and 5.16. The value of the critical bias scales as $s^* \sim t_{\text{obs}}^{-1}$, the susceptibility χ^* increases linearly with observation time and the separation between the two phases increases with t_{obs}. The peak susceptibility scales sub-linearly with system size, this can be explained by the reduction in Δk at fixed t_{obs}. Recall subsection 2.3.1, as system size increases the separation in the bimodal distribution should remain constant and hence $\text{Var}[k(s*)] =$ cosnt. and $\chi^* = N\text{Var}[k(s*)]$ is proportional to N. However we have that Δk reduces with increasing system size and hence the variance in k reduces also, thus χ^* scales sub-linearly with N.

Comparing figures 5.8(a) and 5.15(a) we can see that when system size is increased at fixed t_{obs}, the peak to trough ratio of the constant-volume ensemble increases more than in the constant-pressure ensemble and Δk reduces by a larger percentage. This might be explained by the inconsistency of the barostat timescale with respect to changing N. The barostat acts faster for larger systems, this has the effect of destabilising high density configurations and increasing the average activity of the inactive phase, hence Δk reduces. As the two peaks move closer to one another there is an increase in the overlap of the two distributions, and although the width of the two peaks narrows and the ratio increases, the overall effect is weakened. The destabilising effect of the faster barostat couples with the increase in the probability of observing a nucleation event, thus the reduction in Δk is larger than in the constant-volume ensemble, a reduction of 16% compared to 7%.

The scaling of the transitions with observation time at fixed system size is consistent in both ensembles. At a fixed system size of $N = 100$ particles and doubling the observation time results in an increase in Δk of 20% in both the constant-pressure and constant-volume ensemble. As discussed above the increase in Δk is caused by the active and inactive peaks of $\boldsymbol{P}_{s*}(k)$ becoming

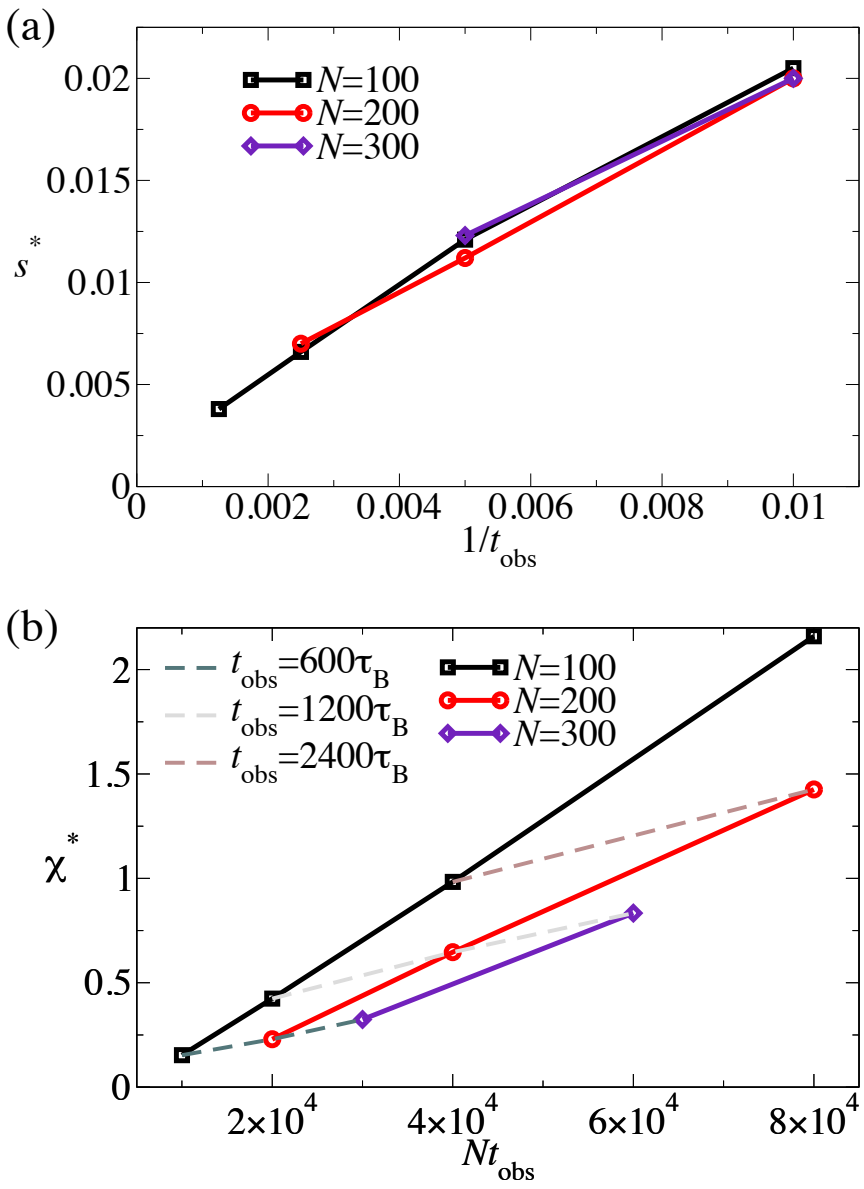

Figure 5.16: The scaling of the critical bias and the susceptibility for the three-dimensional system in the constant-pressure regime. (a) The value of s^* remains constant at fixed $t_{\rm obs}$ with changing N and reduces with increasing $t_{\rm obs}$. (b) The peak in the susceptibility scaling with respect to space-time volume, the dotted lines show linear scaling with respect to $t_{\rm obs}$ indicative of a first-order phase transition. The thin lines show a slower linear dependence of χ^* at fixed $t_{\rm obs}$ and varying N.

clearer and approaching the large Nt_{obs} limit as the peak to trough ratio increases.

There is a first-order dynamic phase transition in the activity of harmonic sphere systems, allowing the system density to fluctuate reduces the critical bias s^*. There is a spontaneous increase in the density of the constant-pressure ensemble in the inactive phase. To investigate the effect that the increase in density has on the inactive phase itself we will characterise the dynamic phases of the two ensembles. To achieve this we will study the properties of configurations taken from active and inactive trajectories.

Chapter 6

Characterising the inactive phase of the three-dimensional system

We have showed a dynamic phase transition in a system of nearly-hard harmonic spheres, similar to the transition seen in the KA mixture. The constant-pressure ensemble exhibits an increase in density between the active and inactive phases, as well as a reduction in the critical bias: the effect this has on the properties of the inactive phase is unknown. We will characterise the inactive phase with respect to glassy properties, namely amorphous structure and slow relaxation times. We calculate the average of static properties across a trajectory as described in 3.2. By comparing these properties in equilibrium and inactive trajectories we aim to characterise the transition and the effect of the dynamic constraint.

6.1 Stability of the inactive phase

Detailed studies of the inactive phase of the KA mixture were performed by Jack et al.[22] and Fullerton & Jack[16], they found that the inactive phase corresponded to a quantitatively different local energy landscape than equilibrium. The average potential energy of the inactive state was lower than equilibrium. To investigate the origins of this reduction they measured two

separate contributions to the potential energy: the inherent structure (IS) energy[23], which measures the energy of the "nearest" energy minimum: and the vibrational energy, which measures the contribution of thermal fluctuations around the IS. The average inherent structure energy of inactive states was much lower than that of equilibrium states at equal temperature, and lower even than equilibrium states at cooler temperatures. However the average vibrational energy of the inactive and equilibrium states are almost identical at equal temperature. Thus the inactive phase behaves like a thermally equilibrated state, fluctuating in a deep energy basin.

The work mentioned above measured the vibrational density of states[50] for the IS configurations, allowing comparison of the propensity for motion on different length scales. The inactive phase had fewer "soft" small-eigenvalue modes, associated with large scale structural relaxation, suggesting that the inactive state was more rigid than equilibrium and less prone to structural relaxation. Correspondingly the inactive phase exhibited a decrease in "soft" modes with large eigenvalues, these modes correlate to fast vibrational motion about an underlying structure. The inactive phase of the KA glass former corresponds to a system whose vibrational degrees of freedom are thermally equilibrated, but whose structural degrees of freedom are typical of a much lower temperature, lying deep in energy basins.

This was reflected in the melting of inactive configurations and equilibrium low-temperature configurations of the KA mixture. The energy of the low-temperature configurations melted to the higher temperature equilibrium value in two stages, a rapid increase in energy associated with the fast vibrational modes equilibrating rapidly, then a slower change in the soft structural modes. The inactive state melted to equilibrium energy in a single slow process, consistent with structural relaxation from a configuration typical of a lower temperature. The lack of a fast equilibration process agrees with the equilibrium behaviour of the hard vibrational modes, only the soft vibrational modes need to change in the melting process.

6.1.1 The inactive phase of the constant-volume ensemble

In glass forming systems there is little structural change between the supercooled fluid and the glass. The pair correlation function $g(r)$ is almost identical across the glass transition in experiments and static simulations[2]. Measurements of $g(r)$ for equilibrium and inactive trajectories of a Kob-Andersen glassformer were unable to discern between the two dynamic regimes[13]. More complicated collective structural measurements of the same system have shown that there is a change in the distribution of local particle cluster configurations[18]. The specific local cluster configurations are dependent upon the model, in the absence of attractive potentials we do not analyse local cluster configurations. We measure $g(r)$ for the constant volume system, see Figure 6.1, and find no change in the structure beyond a small suppression in the value at contact $g^*_{xy} = g_{xy}(\sigma_x + \sigma_y)$, where x and y denote particle species. As s increases there is a reduction in $g(r)$ at contact (shown in the inset of Figure 6.1), this is expected from the decrease in potential energy. The harmonic potential is contact only and so to reduce the potential energy there must be fewer particle overlaps. The lack of structural change shows that the system is not crystallising in the inactive regime, it also supports the inactive regime being the glassy state of the system.

We take trajectories from a sampled distribution at $s \simeq s^*$ and split the distribution into three intervals of k, creating active, inactive and a mixed population(see Figure 5.5(a)). The three intervals are shown in Figure 5.5 and are of equal width in the sampled range of k. We can distinguish between the two dynamic phases by activity alone and any change in static properties will be reflected in the two populations without further selection. Hence equilibrium configurations and the active population from $s \simeq s^*$ should have similar static properties and the inactive population should be markedly different.

To investigate the relative stability of the inactive phase to the equilibrium phase we take configurations form the inactive regime and simulate motion using equilibrium dynamics. This causes the configurations to "melt" back to equilibrium behaviour. The time required to return to equilibrium is a sign of how stable the inactive phase is, we measure the intermediate

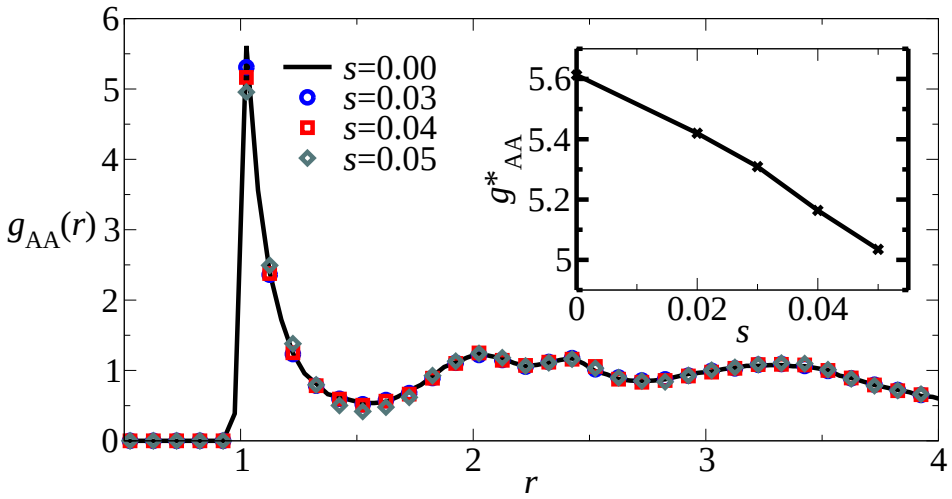

Figure 6.1: The pair correlation function for small particles in the constant-volume three-dimensional system with $N = 200$ and $t_{\rm obs} = 1200\tau_{\rm B}$. Measurements are taken across the dynamic transition and $s^* = 0.039$. There is little change except for the value at contact. (Inset) The value of $g_{AA}(r)$ at contact reduces linearly with s and is continuous across the transition.

scattering function to probe structural relaxation[89]:

$$f_s(q,t) = \frac{1}{Nt_{\text{obs}}} \sum_{j=1}^{N} \left\langle \mathrm{e}^{\imath \vec{q}\cdot[\vec{r}_j(t_0+t)-\vec{r}_j(t_0)]} \right\rangle \tag{6.1}$$

This is a measure of overlap between an initial configuration $x(t_0)$ and a later configuration $x(t_0+t)$. We choose $q = \frac{2\pi}{\sigma_{AA}}$ to be the wave vector that corresponds to the first peak in the structure factor for type A particles. As such $f_s(q,\tau_\alpha) = \mathrm{e}^{-1}$ is a measure of the structural relaxation time τ_α.

We will measure the intermediate scattering function using different initial configurations for $\vec{r}(t_0)$, the function decays as a single exponential for high temperature simple fluids at equilibrium, but glassy behaviour leads to a slower, two-step relaxation[2]. We measure $f_s(q,t)$ beginning from equilibrium configurations as well as configurations drawn from the active and inactive populations close to s^*. Figure 6.2(a) shows structural relaxation from the three initial distributions, the equilibrium function decays exponentially as expected for a fluid. The structural relaxation measured from active initial configurations at $s \simeq s^*$ is qualitatively identical to the equilibrium, the scattering function decays on a similar timescale. Using initial configurations drawn from inactive trajectories the structural relaxation becomes a slower, two-step process, indicating glassy behaviour and a different mechanism for structural relaxation.

Figure 6.2(b) shows the average potential energy per particle of the three regimes over time. The active configurations have a very similar potential energy to the equilibrium configurations, and rapidly become indistinguishable. The inactive configurations have a much lower initial potential energy and melt back to equilibrium energies over a timescale roughly ten times larger than τ_α. The energy melts back to equilibrium in a single step process, in agreement with the melting of the KA mixture in [22].

Comparing the melting of inactive configurations from two different system sizes in figures 6.2 and 6.3, we show that τ_α is faster for larger systems. If melting from the inactive phase is caused by a localised relaxation nucleating the active phase and facilitating relaxation throughout the system, then the larger system is more likely to contain a nucleation event in a given period of time. This means that the inactive phase of larger systems will have

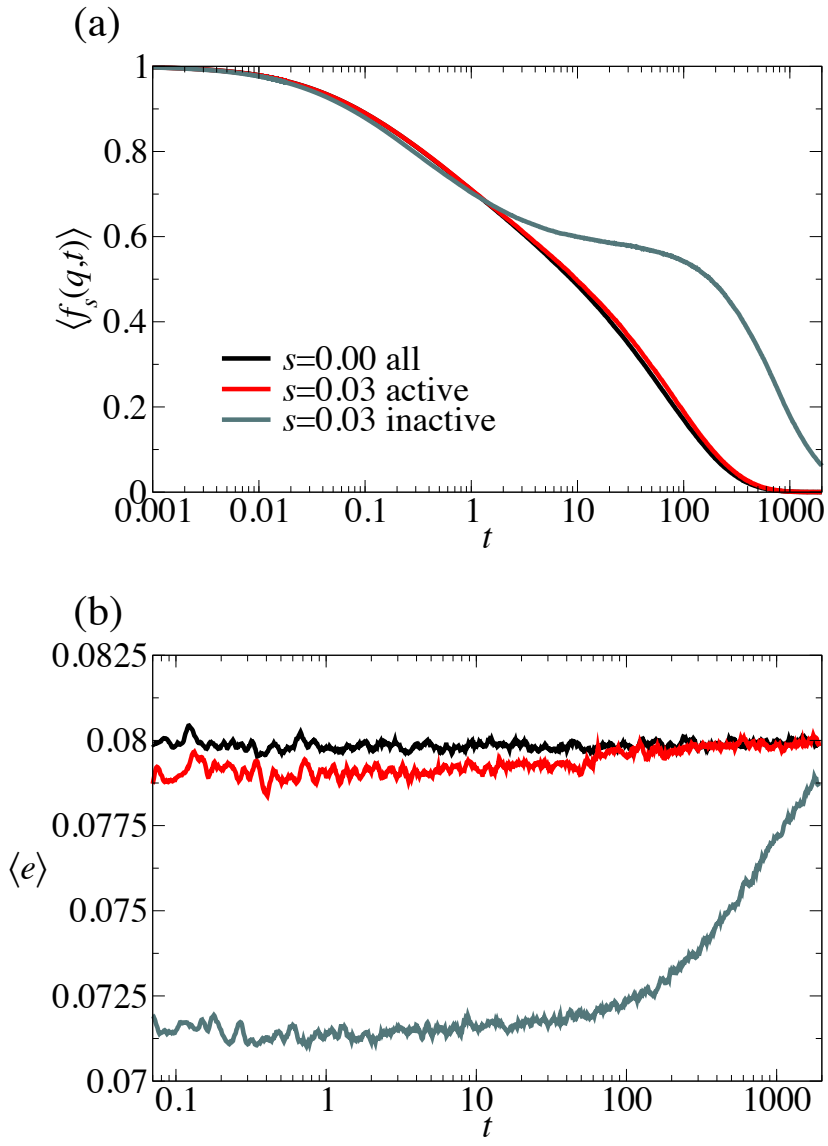

Figure 6.2: Melting of inactive and equilibrium configurations of the three-dimensional system at constant volume with $N = 100$ and an original observation time of $1200\tau_{\mathrm{B}}$. (a) The structural relaxation time, τ_α, for inactive trajectories sampled at $s \simeq 0.03$ shows a marked increase relative to equilibrium, while active trajectories sampled at a similar bias are very similar to equilibrium. (b) The average potential energy per particle of the system is lower in the inactive phase and as the system relaxes back to equilibrium behaviour the energy increases back to the equilibrium value.

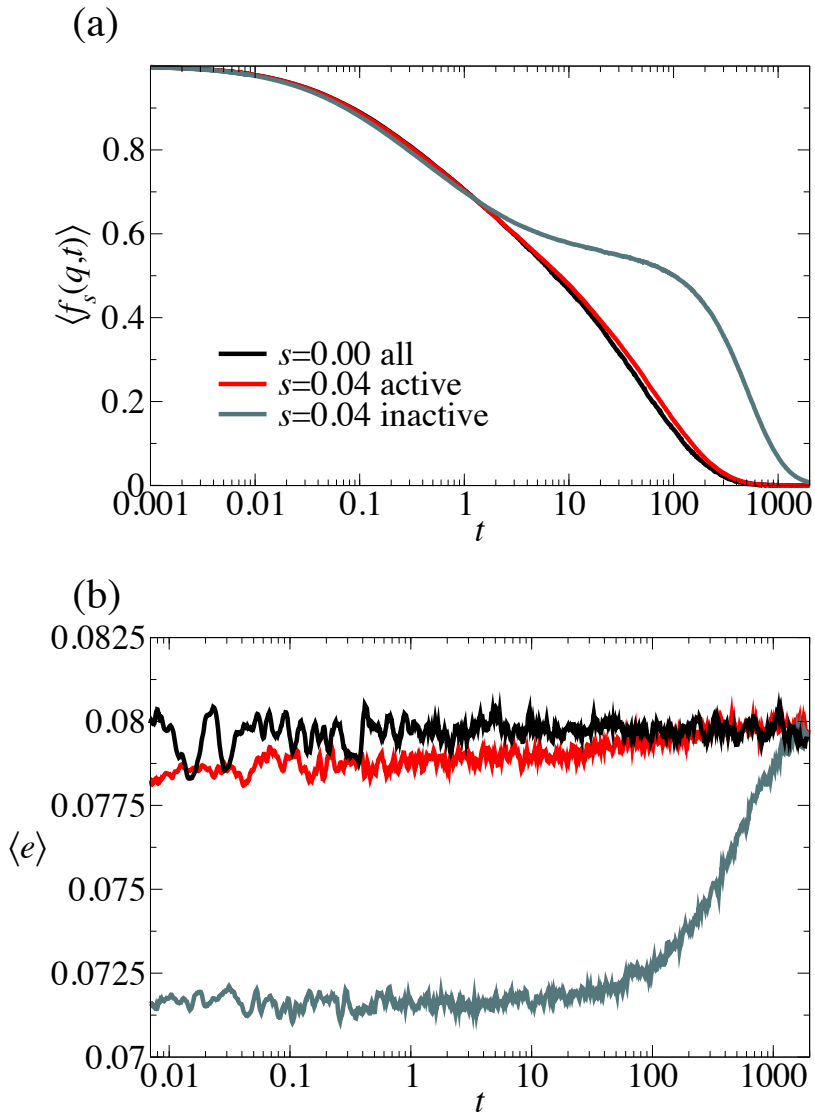

Figure 6.3: Melting of inactive and equilibrium configurations of the three-dimensional system at constant volume with $N = 200$ and an original observation time of $1200\tau_{\mathrm{B}}$. (a) The structural relaxation time for inactive trajectories sampled at $s \simeq s^*$ is faster compared to the $N = 100$ system. (b) The average potential energy per particle of the system in all dynamic phases is consistent with increasing system size.

faster relaxation times, and thus the inactive phase of larger systems is less stable compared to smaller systems. The reduction in stability explains the decrease in Δk with increasing system size at fixed t_{obs}, as discussed above in section 5.2, figure 5.8(a). The average energy per particle remains constant in all dynamic phases with respect to changing system size, we conclude that the inactive phase is structurally consistent with changing system size, and relaxes through localised nucleation events.

6.1.2 The inactive phase of the constant-pressure ensemble

In the constant volume ensemble we saw little change in $g_{AA}(r)$ between equilibrium and the inactive phase, in the constant pressure regime the density of the system can change and this may induce a change in structure. We measure $g_{AA}(r)$ in the constant pressure regime, see Figure 6.4 and see no discernible change in structure nor signs of crystallisation.

The lack of any discernible change in the pair correlation function agrees with observations of the glass transition, although there must be a subtle change in structure to denser configurations. There was no discernible change in pair correlation functions of the KA mixture between the active and inactive phases, although measurements of the vibrational density of states showed there was a subtle difference in the IS. We find a subtle difference in the underlying structure of the two phases that we discuss below in section 6.2. We can only conclude that pair correlation functions are too coarse to distinguish between the two phases, and indeed other work suggests more complex structural measurements can separate the two phases – e.g. measurements of the activity in systems with pinned particles[90].

We take configurations from trajectories sampled at equilibrium and from $s \simeq s^*$, splitting the bimodal population into active and inactive configurations. Using these configurations as initial conditions we simulate the system with equilibrium dynamics and measure how initial conditions taken from different dynamic phases a bias melt back to equilibrium behaviour. Figure 6.5 shows the average intermediate scattering function and the average density over time for the the three different initial populations.

The intermediate scattering function shows similar behaviour to the con-

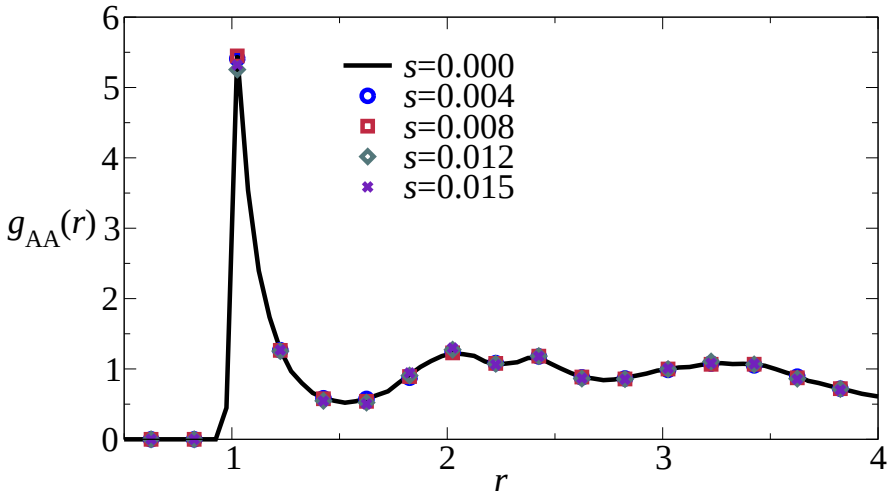

Figure 6.4: The pair correlation function measured at equilibrium, coexistence and in the inactive phase for the smaller particles in a three-dimensional constant pressure system with $N = 200$, $t_{\text{obs}} = 1200\tau_{\text{B}}$. There is a no consistent change in the contact peak unlike the constant volume system. There is no discernible change in the structure that might lead to slow dynamics, and crystallisation has not occurred.

stant volume three-dimensional system, structural relaxation from an inactive initial configuration becomes a two step process. In contrast the active population, from the same value of s, has a similar relaxation time to the equilibrium system. The slower, two-step relaxation is indicative of the inactive phase being more stable compared to typical equilibrium states.

The active population from coexistence rapidly returns to equilibrium behaviour, the density of the system returns to the mean equilibrium value for the system. The density of the inactive population is much higher than the active population and takes much longer to relax back to the equilibrium value. The density relaxes on the timescale of the α-relaxation time for both the active and inactive population, suggesting that the structure cannot relax completely without the volume also relaxing, the two mechanisms complement one another.

Our characterisation of the three-dimensional inactive phase have shown a lack of obvious structural change, in stark contrast to the one-dimensional system. There is no interface that the system must maintain and instead the dynamics are dominated by cooperative relaxation and local kinetic trapping. Configurations taken from the inactive phase show one-step melting back to equilibrium, indicative of a long-range structural relaxation between the phases without a rapid thermalisation of particle vibrations. This suggest the inactive phase has an inherent structure typical of a lower temperature system, while maintaining the short-range particle fluctuations of the equilibrium system. The different inherent structure in the inactive phase has been shown to have a relaxed vibrational modes and hence a greater compressibility. We will study the jamming properties of the two dynamic phases as a means of investigating how the structural properties of the different phases affect the distribution of jammed packings.

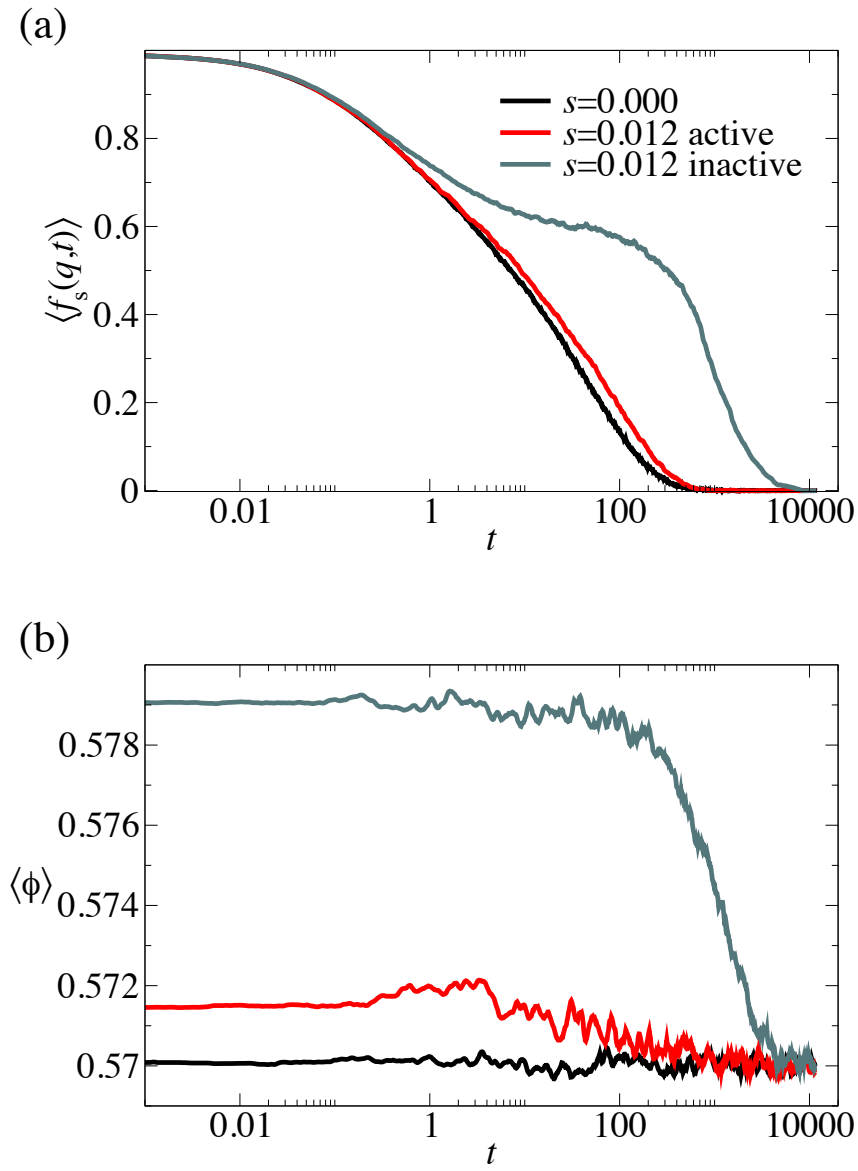

Figure 6.5: Melting of configurations taken from active and inactive trajectories at $s \simeq s^*$ with $N = 200$, $t_{\rm obs} = 1200\tau_{\rm B}$. (a) The structural relaxation time for inactive configurations is much longer than for equilibrium configurations. The active population of the biased system behaves like the equilibrium system. (b) The packing fraction of the systems as they melt, the inactive configurations begin at a much higher density and relax back to the equilibrium value over a similar timescale as the structural relaxation. It is possible that the volume must first relax to a lower density to facilitate structural relaxation.

6.2 Jamming

The increase of the constant-pressure system's density across the dynamic transition is not entirely responsible for the decrease in activity (see Figure 5.9). However the strong correlation between the structural and volume relaxation times, shown in Figure 6.5, suggests that the increase in density causes or allows a more stable particle structure, which in turn hinders volume relaxation. Compression studies have shown that the jamming densities ϕ_J of particle systems are dependent upon the density before compression ϕ_i. Berthier & Witten concluded that slow, non-equilibrium glassy dynamics could be responsible for a finite range of ϕ_J due to the metastability of glassy states[19]. We will compress configurations, drawn from both constant-volume and constant-pressure trajectories, and compare the distributions of ϕ_J.

In order to measure the vibrational density of states, previous work[22, 16] used a conjugate gradient method to minimise the energy and find the IS of configurations. We use the jamming protocol described in section 3.5 as a means to investigate changes in underlying structure and the separate contributions to energy rather than the vibrational density of states.

It is known that the inactive phase represents configurations from an energy basin typical of a lower temperature compared to the equilibrium system. The different inherent structures may correspond to separate distributions of ϕ_J, recall the discussion of vibrational modes and compressibility in section 2.6. However if ϕ_J is indeed unique then both dynamic phases would jam at the same packing fraction. A difference in ϕ_J would lend support to proposed universal jamming–glass phase diagrams, as discussed in section 2.6 and reference[5]. A correlation between the dynamic propensity of configurations and their jamming density would provide a link between the dynamic nature of the glass transition and the static jamming transition.

We take configurations from the middle of equilibrium trajectories, as well as from active and inactive trajectories with $s \simeq s^*$: these configurations are jammed according to the protocol in section 3.5. Recall Figure 3.4 showing the paths that our jamming protocol takes through configuration space, configurations are taken from a finite temperature system and re-

duced to the inherent structure. Then the particles are inflated isotropically while conjugate gradient minimisation maintains a zero energy configuration. We aim to measure and compare the distribution of ϕ_J for the active and inactive phases.

Recall the discussion of the distribution of modes above, the inactive phase of particle systems is typical of lower temperatures and the stiffest modes of the system are relaxed. Coupled with the reduction in particle overlaps that the reductionin energy suggests, there is an increase in the local free volume of particles and particles can explore their local volume more easily. If this is true the system would be more compressible and there should be a difference in the jamming behaviour of the active and inactive phase.

6.2.1 Jamming in the constant-volume ensemble

All configurations have the same ϕ_i in the constant-volume ensemble so any variation in the distribution of ϕ_J is due to structure, and the relative glassiness of configurations.

Figure 6.6 shows the distributions of ϕ_J that are obtained when three sets of configurations are subjected to the jamming protocol described in section 3.5. By using the same selection criteria to decide active and inactive trajectories that we use near s^*at equilibrium we see that the equilibrium distribution is indeed identical for all activities. The active population of the $s \simeq s^*$ distribution achieves denser values for ϕ_J than equilibrium and have slightly reduced activities, but there is a strong amount of overlap. They resemble a constrained sampling of the same distribution, consistent with them being in the same dynamic phase as equilibrium. The inactive configurations jam at considerably higher densities, with an increase of about 1%. Comparing to the pressure-density relations measured for harmonic spheres in Ref. [91], the difference between $\phi = 0.65$ and $\phi = 0.66$ causes a large change in the virial pressure and is close to diverging virial pressure.

There is a correlation between the activity and ϕ_J, configurations drawn from more inactive trajectories yield higher jammed packing fractions. Thus the inactive states are not only lower in energy but they are characteristic of

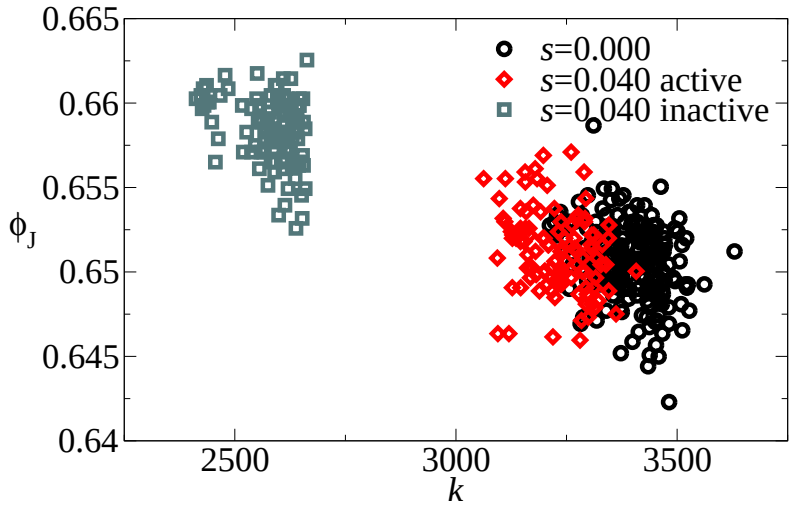

Figure 6.6: The distributions of ϕ_J for different phases of the three-dimensional constant-volume system with $N = 200$, the configurations were taken from the middle of trajectories with $t_{\rm obs} = 1200\tau_{\rm B}$. There is an equal number of active and inactive configurations. The inactive configurations jam at a higher packing fraction than the active and equilibrium configurations. There is a clear correlation between the activity of the trajectory the configuration is drawn from and the value of ϕ_J that is achieved.

a state that can jam more easily. This is in agreement with the concept of a relaxation of the stiffest vibrational modes in the system and an increase in local particle movement.

The jammed state is mechanically stable and corresponds to zero temperature with no vibrations possible, hence it is the natural state for zero activity. However the inactive phase still exists at the same packing fraction as the active phase, an increase in density is not required for glassy behaviour, to either ϕ_{GCP} or ϕ_{RCP}. The change in the distribution of ϕ_J is further evidence that ϕ_J is not a unique value for the system.

6.2.2 Jamming in the constant-pressure ensemble

In the constant-pressure ensemble ϕ_i can vary and we have shown that an increase in density occurs across the transition, as well as a more subtle change in structure. We do not make predictions for the finite temperature behaviour of jammed configurations and do not drive the system in the $T-\phi$ plane. The dependence of ϕ_J on ϕ_i is unknown: any correlation between the two distributions would lead to the different finite-temperature dynamic phases having different distribution of ϕ_J (the dashed lines in Figure 3.4). However if ϕ_J is not related to ϕ_i and is instead solely dependent on the model then the two phases would correspond to the same distribution of ϕ_J (the dotted pink line in Figure 3.4).

Figure 6.7 shows the jamming behaviour of the dynamic phases in the constant-pressure ensemble. Figure 6.7(a) shows the final jammed packing fraction of configurations drawn form trajectories with different activities. The range of activities is larger in the constant-pressure ensemble as seen above, and there remains a large overlap between equilibrium configurations and the active population of $s \simeq s^*$. The inactive population jams at higher densities that the other populations, and with a slightly higher average density than the constant-volume inactive configurations. The correlation between activity and ϕ_J appears a little stronger in the constant-pressure ensemble than constant-volume.

Figure 6.7(b) shows the initial and jammed packing fraction of each configuration. The width of the initial packing fraction for the inactive config-

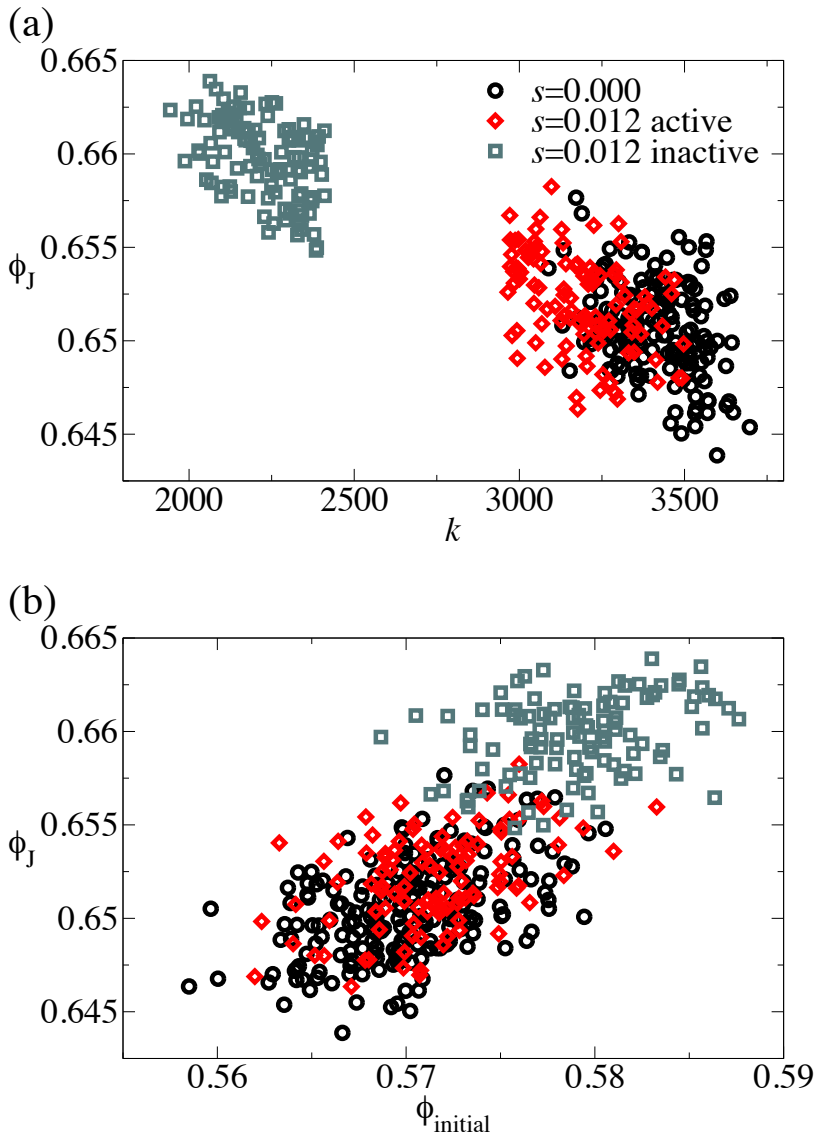

Figure 6.7: The distributions of ϕ_J for different phases of the three-dimensional constant-pressure system with $N = 200$, the configurations were taken from the middle of trajectories with $t_{obs} = 1200\tau_B$. (a) Again the inactive configurations jam at a higher packing fraction than the active and equilibrium configurations. (b) The initial and final packing fractions for all configurations, there is a positive correlation between ϕ_i and ϕ_J.

urations reinforces that although there is an increase in the average density, it is not necessary to increase in density to become dynamically inactive. There is a positive correlation between ϕ_i and ϕ_J, but the range in initial densities is much larger than the range in jammed packings.

The distribution of ϕ_J is very similar in both ensembles, the average jammed packing differs by $\sim 0.25\%$ between the constant pressure and constant volume configurations. Again this is evidence that ϕ_J is not unique. If we consider the previous work on the distribution of vibrational modes in Ref. [16] then the inactive phase exhibits a relative suppression of the modes with smallest and largest eigenfrequencies. The suppression of the stiffest modes with highest frequencies leads to a suppression of the fastest rattling motion and was interpreted as a softening of the most steeply curving direction on the energy landscape. This slackening of the stiff modes means that particles can explore their local volume without causing as many overlaps. In a jamming context we interpret this as particles having more available space to increase in size and rearrange positions on short scales in order to facilitate higher jammed packings.

If we consider a single particle inflation cycle which causes two particles which previously did not interpenetrate to do so, then the protocol will move the particles apart. However this may cause an overlap with a third particle which then has to be moved, this can repeat until n particles have to be displaced before a zero energy configuration can be reached. These large scale particle interaction chains are resolved through cooperative structural relaxation[92]. The jammed state is reached when the number of particles involved in a single "chain" of displacements is equal to N, and a zero energy state cannot be found.

Our analysis of jamming behaviour shows that there is a change in the structure of the system between equilibrium and the inactive phase in both ensembles. We associate the higher packing fractions of the jammed inactive state with the suppression of "stiff" structural modes leading to a lack of structural relaxation. Preventing structural relaxation limits the region of phase space that the system explores, the inactive phase is structurally metastable and survives for long times with low dynamic activity. The jammed state is the most extreme form of kinetic trapping in phase

space, a configuration that cannot structurally relax and has zero activity. Our findings suggest that the inactive state is part of the same continuum of metastable configurations with low activities as the jammed state, although the jammed state cannot be accessed using equilibrium dynamics. The highest density of the glassy particle system we observed was $\phi_{\mathrm{I}} = 0.5804$, far from the final jammed densities of $\phi_J \approx 0.66$.

Finally we note that in kinetically constrained models with a time varying density profile (such as the SSEP), the inactive state is jammed and the activity falls to zero. In the one-dimensional systems studied in chapter 4 the dynamic transition in both ensembles corresponded to forming a high density state close to jamming which sustained small activity. In the three-dimensional systems the inactive state was far from jammed, although in the constant-pressure ensemble the density did increase by $\sim 1\%$. This small change in density across the transition suggests that the density of the inactive phase is lower than the proposed $\phi_G < 0.664$[7]. The soft constraints and the complexity of three-dimensional configuration space prevent large changes in density, and from our results high densities are not required to create a dynamically inactive phase. The transition can be interpreted by subtle, small-scale structural changes that are metastable and reduce the dynamic propensity for long timescales.

Chapter 7

Conclusion

We have shown dynamic phase transitions in constant-density and constant-pressure ensembles of repulsive systems. The two ensembles are not equivalent with respect to dynamic transitions, although the ensembles are defined in terms of static constraints, i.e the average value of the static volume and pressure. There is a fundamental difference in the behaviour of the two systems, the one-dimensional model is governed by diffusive dynamics and undergoes phase separation into an inactive state, the three-dimensional glass-former falls out of equilibrium and develops long relaxation times with little structural change. Both are controlled by behaviour on the longest timescales in the system: in diffusive systems $\tau_\rho \sim l^2$ so large scale fluctuations dominate: in the glassy systems the suppression of low frequency modes acts on the slowest timescales of the system.

Diffusive systems can be described on hydrodynamic length-scales by the theory of fluctuating hydrodynamics, systems are described by the distribution of the density and their behaviour is controlled by fluctuations in the local density. Fluctuating hydrodynamics predicts phase separation and hyperuniformity as the means to change dynamic activity[75], for $s \to \infty$ the system will jam, either locally or globally, as $k \to 0$. We have shown the transition to a phase-separated inactive phase and the existence of a hyperuniform active phase in the constant-density one-dimensional system. The transition to the inactive phase is first-order with respect to the dynamic activity K and occurs at a finite critical bias s^*, which we have shown scales

with the system size as $1/N$. The emergence of hyperuniformity as a result of biasing to greater activity is equal for all N at fixed s, for finite systems there is a limit to $q_{\min} = 2\pi/L'$.

In the one-dimensional constant-pressure system the change in density is much more influential than changes in structure. The inactive phase is much more dense than equilibrium and the system approaches the jammed state rather than phase-separating. The transition to the inactive phase occurs at $s^* = 0$ for all system sizes, provided the observation time is long enough. When biased to higher activities than equilibrium the constant-pressure system reduces the density, there is a small suppression of short-wavelength $S(\bar{q})$ but the onset of hyperuniformity is weaker than the constant-volume system for equal N.

That the behaviour of the system is dominated by the density was expected, from hydrodynamic arguments diffusive systems on long length scales are controlled by the density distribution. The minimisation of power to maintain dynamic constraints means that the s-ensemble couples most strongly to processes that occur on the longest time scales[16], in all cases the observed dynamic phenomena occur on the longest time scales. In diffusive systems the characteristic relaxation time for a fluctuation of size l is $\tau \sim l^2$, hence fluctuations on the longest length scales correspond to the processes with the slowest relaxation. Hyperuniform ordering is, by definition, a long length scale phenomena and is seen in both ensembles. The dense particle cluster seen in the inactive phase of both ensembles is the largest density fluctuation that can occur in the system.

Fluctuating hydrodynamics provides a theoretical framework that can describe the dynamic phase behaviour of the one-dimensional model, discussed further in [75]. Analytic descriptions of the simple symmetric exclusion process predict the transition to the inactive phase occurs at $s^* \sim N^2$ in the constant volume ensemble. We observe weaker scaling with system size due to the continuous nature of the particle position.

Forming the inactive phase requires a biasing of the noise forces in the Langevin equations 4.1 and 3.17. Phase separation requires two neighbouring particles to be driven apart from one another until they force all other particles in a cluster between them. This requires a biasing of two particles,

regardless of total system size, hence the critical bias scales as $\sim N^{-1}$. In the constant-pressure system jamming requires the volume of the system to contract and increase the global density, this requires biasing one noise term, η_L. This is true for all system sizes, only the timescale that the volume relaxation changes, thus $s^* = 0$ for all N. As $N \to \infty$ the two ensembles are equivalent with $s^* = 0$.

The constant-pressure one-dimensional system is not equivalent to the phase-separated constant-volume system, only the dense phase is seen in the constant-pressure ensemble. There is work done on the particles at the two boundaries of the dense phase separated state, this work acts to cause a kink in the pressure profile. The constant-pressure ensemble of the same system cannot sample the dense and sparse regions equally due to the difference in the static pressure between.

In the three dimensional system we observed a dynamic transition to an inactive, glassy phase. The inactive phase was structurally similar to the active phase with lower potential energy and longer structural relaxation times, akin to the glassy phase. These observations are consistent with the previous studies of Lennard-Jones glass-forming systems. The transition occurred at finite s^* for all systems and $s^* \sim 1/t_{\text{obs}}$ at fixed N. The critical bias in the constant-pressure ensemble is less than in the constant-volume ensemble. In the constant-pressure ensemble the transition was accompanied by an increase in system density and the value of k_{inactive} was smaller than the constant-volume ensemble.

The density of the inactive phase was $\phi = 0.58$, far from any predicted ϕ_{GCP}, the activity was even lower than an equilibrium system at equal density ($\phi = 0.58$). The increase in density is not enough to drive the dynamic transition although there is a strong correlation between activity and the average density of a trajectory.

Previous studies of dynamic transitions in atomistic glass-formers found that the inactive phase had equal vibrational energy to the equilibrium phase, but a lower inherent structure energy. This was shown in the melting profile of inactive configurations, there is no short-time thermalisation of the high-frequency vibrational modes, only a slow relaxation of the low-frequency modes. We observed a similar melting profile for the Harmonic system, a

single kink in the energy profile corresponding to structural relaxation from one inherent structure to another.

Further analysis of the vibrational modes showed that the inactive phase suppressed the stiffest and the softest modes. The suppression of the soft modes means that large-scale structural relaxation takes much longer and τ_α is much longer. The relaxing of stiff modes corresponds to an increased stability in the local structure and an increase in the compressibility.

Our jamming protocol finds the nearest zero-temperature jammed state in configuration space. The distribution of ϕ_J produced from inactive configurations was denser than the distribution of equilibrium jammed states. The densest distribution of ϕ_J was centred around $\simeq 0.665$, below any suggested maximum random packing. There is a very strong correlation between the activity of the trajectory a configuration is drawn from and the jamming density of the configuration.

In all cases there is a dynamic phase transition between systems with "normal" fluctuations in the activity and inactive systems with persistently low activity. Dynamic transitions in the s-ensemble are governed by the slowest phenomena in the system. In systems with fluctuating volumes, the barostat is the slowest mechanism in the system and fluctuations in the volume dominate the dynamic phase behaviour. There may be other ensembles that would preserve direct equivalence but that remains an open question.

The three-dimensional systems do not show ensemble inequivalence with respect to the scaling of s^*, but there is a decrease in the values of s^* in the constant-pressure ensemble. The density of the constant-pressure ensemble spontaneously increases in the inactive phase. Although the inactive phase is still more inactive than an equilibrium system at equal density. The change in density occurs at the same bias as the dynamic transition and is concomitant with the transition in activity, the change becomes sharper with increasing observation time.

7.1 Open questions

The onset of hyperuniformity in the active phase of the one-dimensional system is weaker in the constant-pressure ensemble. Changing the density of the system is more effective than changing the structure, the increase of system density occurs at smaller $|s|$ than modifying the structure of the system on the particle scale. Whether $S(q) \to 0$ as $N \to \infty$ or whether it will saturate at a finite value is unknown, furthermore the nature of the distribution of the separations is unknown. To become hyperuniform the distribution of separations must either deviate from an exponential distribution or long-range correlations between separations must arise. However as $|s|$ increases the density saturates, if $|s|$ is increased further then the structure of the system may begin to change and the suppression of small-q fluctuations may increase. The exact scaling of hyperuniformity with system size, observation time and bias, and the limiting behaviour of the active phase of the system, is unknown. There are analytic predictions that jammed packings are hyperuniform[81], we do not measure any sign of hyperuniformity in the inactive phases of the one-dimensional system. Possibly as $s \to \infty$ the systems would approach $\phi = 1$ and hyperuniform ordering would emerge. With regards to experimental work there is not a method to probe the s-ensemble, however it could be possible to measure the jamming properties of glassy colloidal systems.

We have not investigated the three-dimensional system biased to greater than equilibrium activity, nor has any other study on atomistic glass-formers. Whether the system would adopt hyperuniform structures, or whether there would be a change in the potential energy of the system is unknown. With respect to the inactive phase one could measure static correlation lengths between regions of fast dynamics.

We have not analysed the properties of the jammed configurations, it would be interesting to measure the stability of the packings to external stress and whether the inactive configurations produce more stable packings. Also measuring $S(q)$ for the jammed packings may show signs of hyperuniformity.

The low temperature limit of the harmonic potential is repulsive hard spheres, a study of the system at different temperatures could illustrate the

effect of finite temperature fluctuations in atomistic glass-formers. In KCMs it is known that softening constraints leads to a finite value for s^* and a finite temperature critical point, whether this remains true in atomistic system is unknown.

The role of hyperuniformity in systems that are subject to strong constraints is a topic of discussion and current research. Suppression of long wavelength density fluctuations appears to be a mechanism to satisfy geometric constraints while maintaining a high packing density. Whether hyperuniform ordering is a general means of satisfying dynamic constraints, and any requisite correlations between structure and dynamics is unknown.

We have demonstrated that thermodynamic ensembles are inequivalent with respect to dynamic phase transitions. The ensembles maintain a fixed value for the instantaneous volume or pressure at all times, possibly ensembles that maintain a fixed value of a dynamic observables would be equivalent. Although it would be interesting, that question is beyond the scope of this thesis.

Bibliography

[1] G. Biroli and J. P. Garrahan, J. Chem. Phys. **138**, 12A301 (2013).

[2] *Dynamical Heterogeneities in Glasses, Colloids and Granular Media* (Oxford University Press, ADDRESS, 2011).

[3] R. Mari, F. Krzakala, and J. Kurchan, Phys. Rev. Lett. **103**, 025701 (2009).

[4] L. Berthier, Am. J. Phys. **4**, (2011).

[5] A. J. Liu and S. R. Nagel, Nature **396**, 21 (1998).

[6] L. Berthier, H. Jacquin, and F. Zamponi, Phys. Rev. E **84**, 051103 (2011).

[7] L. Berthier and T. A. Witten, Europhys. Lett. **86**, 10001 (2009).

[8] C. A. Angell, Science **267**, 1924 (1995).

[9] P. G. Debenedetti and F. H. Stillinger, Nature **410**, 259 (2001).

[10] G. Brambilla *et al.*, Phys. Rev. Lett. **102**, 085703 (2009).

[11] J. P. Garrahan and D. Chandler, Phys. Rev. Lett. **89**, 035704 (2002).

[12] M. Merolle, J. P. Garrahan, and D. Chandler, PNAS **102**, 10837 (2005).

[13] L. O. Hedges, R. L. Jack, J. P. Garrahan, and D. Chandler, Science **323**, 1309 (2009).

[14] W. Kob and H. C. Andersen, Phys. Rev. Lett. **73**, 1376 (1994).

[15] E. Pitard, V. Lecomte, and F. van Wijland, Europhys. Lett. **96**, 56002 (2011).

[16] C. J. Fullerton and R. L. Jack, J. Chem. Phys. **138**, 224506 (2013).

[17] T. Speck and D. Chandler, J. Chem. Phys. **136**, 184509 (2012).

[18] T. Speck, A. Malins, and C. P. Royall, Phys. Rev. Lett. **109**, 195703 (2012).

[19] L. Berthier and T. A. Witten, Phys. Rev. E **80**, 021502 (2009).

[20] O. Cohen and D. Mukamel, Phys. Rev. E **90**, 012107 (2014).

[21] C. Appert-Rolland, B. Derrida, V. Lecomte, and F. van Wijland, Phys. Rev. E **78**, 021122 (2008).

[22] R. L. Jack, L. O. Hedges, J. P. Garrahan, and D. Chandler, Phys. Rev. Lett. **107**, 275702 (2011).

[23] F. H. Stillinger and T. A. Weber, Science **225**, 983 (1984).

[24] L. Berthier, G. Biroli, J.-P. Bouchaud, and R. L. Jack, in *Dynamical Heterogeneities in Glasses, Colloids, and Granular Media*, edited by L. Berthier *et al.* (Oxford University Press, Oxford, 2011).

[25] C. Toninelli *et al.*, Phys. Rev. E **71**, 041505 (2005).

[26] G. Biroli and J. P. Bouchaud, in *The Random First-Order Transition Theory of Glasses: a critical assessment*, edited by P. G. Wolynes and V. Lubchenko (Wiley and Sons, Oxford, 2012).

[27] U. Bengtzelius, W. Götze, and A. Sjolander, J. Phys. C **17**, 5915 (1984).

[28] S. P. Das, Rev. Mod. Phys. **76**, 785 (2004).

[29] F. C. Frank, P. R. Soc. A **215**, 43 (1952).

[30] R. L. Jack, J. P. Garrahan, and D. Chandler, J. Chem. Phys. **125**, 184509 (2006).

[31] L. O. Hedges and J. P. Garrahan, J. Phys. Condens. Mat. **19**, 205124 (2007).

[32] Y. S. Elmatad, R. L. Jack, D. Chandler, and J. P. Garrahan, PNAS **107**, 12793 (2010).

[33] D. Ruelle, *Thermodynamic Formalism*, 2 ed. (Cambridge University Press, Cambridge, 2004).

[34] A. Widmer-Cooper, P. Harrowell, and H. Fynewever, Phys. Rev. Lett. **93**, 135701 (2004).

[35] J. Comp. Phys. **254**, 27 (2013).

[36] J. Jäckle and S. Eisinger, Z. Phys. B Con. Mat. **84**, 115 (1991).

[37] J. P. Garrahan *et al.*, Phys. Rev. Lett. **98**, 195702 (2007).

[38] J. P. Garrahan *et al.*, J. Phys. A. **42**, 075007 (2009).

[39] L. Bertini *et al.*, J. Stat. Phys. **116**, 831 (2004).

[40] V. Lecomte, J. P. Garrahan, and F. van Wijland, J. Phys. A Math. Theor. **45**, 175001 (2012).

[41] R. L. Jack and P. Sollich, Prog. Theor. Phys. Supp. **184**, 304 (2010).

[42] A. A. Budini, R. M. Turner, and J. P. Garrahan, J. Stat. Mech. **2014**, P03012 (2014).

[43] D. Moroni, P. G. Bolhuis, and T. S. van Erp, Physica A **340**, 395 (2004).

[44] J. P. Garrahan, P. Sollich, and C. Toninelli, in *Dynamical Heterogeneities in Glasses, Colloids, and Granular Media*, edited by L. Berthier *et al.* (Oxford University Press, Oxford, 2011).

[45] B. Derrida, J. L. Lebowitz, and E. R. Speer, Phys. Rev. Lett. **87**, 150601 (2001).

[46] M. Plischke and M. Bergersen, *Equilibrium statistical physics*, 3 ed. (World Scientific, Singapore, 2006).

[47] L. E. Reichl, *A Modern Course in Statistical Physics*, 3 ed. (Willey VCH, Weinheim, 2011).

[48] L. J. Bain, *Introduction to probability and mathematical statistics* (Pacific Grove, Calif. : Duxbury, Pacific Grove, Calif., 1992).

[49] J. P. Garrahan and D. Chandler, PNAS **100**, 9710 (2003).

[50] C. Kittel, *Introduction to Solid State Physics*, 8 ed. (John Wiley and Sons, Hoboken, 2004).

[51] A. J. Liu and S. R. Nagel, in *Jamming and Rheology, Constrained dynamics on microscopic and macroscopic scales*, edited by A. J. Liu and S. R. Nagel (CRC Press, Boca Raton, 2001).

[52] S. Torquato and F. H. Stillinger, Rev. Mod. Phys. **82**, 2633 (2010).

[53] P. Chaudhuri, L. Berthier, and S. Sastry, Phys. Rev. Lett. **104**, 165701 (2010).

[54] Y. Jiao, F. H. Stillinger, and S. Torquato, J. Appl. Phys. **109**, 013508 (2011).

[55] H. Jacquin, L. Berthier, and F. Zamponi, Phys. Rev. Lett. **106**, 135702 (2011).

[56] L. E. Silbert, A. J. Liu, and S. R. Nagel, Phys. Rev. E **68**, 011306 (2003).

[57] A. Donev, S. Torquato, F. H. Stillinger, and R. Connelly, Phys. Rev. E **70**, 043301 (2004).

[58] L. Silbert, A. J. Liu, and S. R. Nagel, Phys. Rev. E **70**, 043302 (2004).

[59] C. E. Zachary, Y. Jiao, and S. Torquato, Phys. Rev. Lett. **106**, 178001 (2011).

[60] S. Torquato, A. Scardicchio, and C. E. Zachary, J. Stat. Mech. **2008**, P11019 (2008).

[61] R. Kurita and E. R. Weeks, Phys. Rev. E **82**, 011403 (2010).

[62] Y. Jiao *et al.*, Phys. Rev. E **89**, 022721 (2014).

[63] D. Frenkel and B. Smit, *Understanding Molecular Simulation* (Elsevier, San Diego, 2002), pp. 23–61.

[64] N. G. Van Kampen, *Stochastic processes in physics and chemistry* , 3 ed. (Elsevier, Amsterdam, 2007).

[65] A. Kolb and B. Dünweg, J. Chem. Phys. **111**, 4453 (1999).

[66] A. M. Ferrenberg and R. Swendsen, Phys. Rev. Lett. **63**, 1195 (1989).

[67] G. Caballero *et al.*, J. Phys. Condens. Mat. **17**, S2503 (2005).

[68] X. Cheng, Phys. Rev. E **81**, 031301 (2010).

[69] J. R. Shewchuk, www-2.cs.cmu.edu (1994).

[70] M. Galassi, *GNU scientific library: reference manual, 3rd Ed.* (Network Theory, Bristol, 2009).

[71] W. T. Coffey and Y. P. Kalmykov, *The Langevin equation , with applications to stochastic problems in physics, chemistry and electrical engineering*, 3 ed. (World Scientific, Hackensack, 2012).

[72] B. Lin *et al.*, Phys. Rev. Lett. **94**, 216001 (2005).

[73] L. Lizana and T. Ambjörnsson, Phys. Rev. Lett. **100**, 200601 (2008).

[74] K. Nelissen, V. R. Misko, and F. M. Peeters, Europhys. Lett. **80**, 56004 (2007).

[75] Jack, Robert L, Thompson, Ian R, and Sollich, Peter, Phys. Rev. Lett. **114**, 060601 (2015).

[76] R. Wittkowski *et al.*, Nat Comms **5**, 5351 (2014).

[77] M. C. Marchetti *et al.*, Rev. Mod. Phys. **85**, 1143 (2013).

[78] M. E. Cates and J. Tailleur, Annu. Rev. Condens. Matter Phys. **6**, 219 (2015).

[79] R. Matas-Navarro, R. Golestanian, T. B. Liverpool, and S. M. Fielding, Phys. Rev. E **90**, 032304 (2014).

[80] M. E. Cates and J. Tailleur, Europhys. Lett. **101**, 20010 (2013).

[81] S. Torquato and F. H. Stillinger, Phys. Rev. E **68**, 041113 (2003).

[82] D. Chen, Y. Jiao, and S. Torquato, J. Phys. Chem. B **118**, 7981 (2014).

[83] L. Berthier *et al.*, Phys. Rev. Lett. **106**, 120601 (2011).

[84] M. Florescu, S. Torquato, and P. J. Steinhardt, PNAS **106**, 20658 (2009).

[85] H. Spohn, J. Phys. A. **16**, 4275 (1983).

[86] G. L. Eyink, J. Stat. Phys. **61**, 533 (1990).

[87] E. de Miguel and G. Jackson, J. Chem. Phys. **125**, 164109 (2006).

[88] M. P. Allen and D. J. Tildesley, *Computer Simulation of Liquids* (Oxford University Press, Oxford, 2006).

[89] J. P. Hansen and I. R. McDonald, *The Theory of Simple Liquids* (Academic Press, London, ADDRESS, 2006).

[90] W. Kob and L. Berthier, Phys. Rev. Lett. **110**, 245702 (2013).

[91] L. Berthier and W. Kob, J. Phys. Condens. Mat. **19**, 205130 (2007).

[92] J. F. Peters, M. Muthuswamy, J. Wibowo, and A. Tordesillas, Phys. Rev. E **72**, 041307 (2005).